Morphodynamics of the Haringvliet ebb-tidal delta

Unravelling the mechanisms behind its morphological evolution

A. Colina Alonso

TU Delft Delft University of Technology

Deltares
Enabling Delta Life

Morphodynamics of the Haringvliet ebb-tidal delta

Unravelling the mechanisms behind its morphological evolution

by

A. Colina Alonso

in partial fulfillment of the requirements for the degree of

Master of Science
in Civil Engineering

at the Delft University of Technology (TU Delft)
to be defended publicly on Friday June 1st, 2018 at 11.00 AM.

Student number:	4180577	
Chair committee:	Prof. dr. ir. Z.B. Wang,	Delft University of Technology & Deltares
Committee members:	Ir. P.K. Tonnon,	Deltares
	Dr. ir. B.C. van Prooijen,	Delft University of Technology
	Dr. ir. D.J.R. Walstra,	Delft University of Technology & Deltares
	Ir. P.L.M. de Vet,	Delft University of Technology & Deltares

An electronic version of this thesis is available at `http://repository.tudelft.nl/`.

Cover: Slikken van Voorne, southwest of the Slufter. Photography by Jan Alewijn Dijkhuizen

TU Delft Delft University of Technology

Deltares Enabling Delta Life

ACKNOWLEDGEMENTS

This thesis concludes the Master of Science program in Hydraulic Engineering at Delft University of Technology. The research was conducted at the research institute Deltares and I am very grateful for the opportunity to work on my thesis in its inspiring and open environment. I could not have thought of a better working space and learning environment for the past eight months.

This study would not be possible without the support of my graduation committee. Therefore, I would like to thank the committee members, Zheng Bing Wang, Pieter Koen Tonnon, Bram van Prooijen, Dirk-Jan Walstra and Lodewijk de Vet for their guidance during the entire project. My sincere gratitude goes to Zheng Bing Wang for giving me the opportunity to work on this topic and for the valuable comments and fruitful discussions during our meetings. Pieter Koen, I am very grateful for your continuous support with Delft3D and for always making time whenever I had a question or needed advice. Bram, thank you for your enthusiasm and critical feedback. You were always full of ideas and our meetings were often eye-openers for me. I am also very grateful for the opportunity you provided with the NCK-days. Dirk-Jan, many thanks for being critical while also reminding me not to get lost in the (model)details and to look at the bigger picture. Lodewijk, many thanks for the time you invested in me. Your close involvement in the project, positive mindset, constructive feedback and advice on the graduation process are very much appreciated.

Furthermore, I would like to thank my temporary colleagues and fellow graduate students at Deltares for their interest, great advice and especially for the enjoyable times during the coffee-breaks. You were great sparring partners as well as a very welcome distraction whenever I needed it.

Last but certainly not least, this achievement would not have been possible without the support of my family and friends, for which I am very grateful. To my parents, Alberto and Yolanda, and my sister María: thank you for always believing in me, for your unconditional support and for your trust. René, I am so glad we were in this together. Thank you for being you, for believing in me and for making the past years unforgettably fun.

Ana Colina Alonso
Delft, May 2018

SUMMARY

KEY POINTS

- While the formation of the intertidal shoal Hinderplaat was a direct consequence of a human intervention, its degradation was a natural response of the system to frequent hydrodynamic forcing conditions
- Tidal currents push the Hinderplaat in offshore direction, but this is counteracted by waves: these generate cross-shore and longshore currents on the shoal, inducing its landward migration and southward spreading
- Extreme discharge events provide a significant contribution to channel formation on the Hinderplaat by generating initial local breaches that are enhanced by regular tidal flows

---

EXECUTIVE SUMMARY

Ebb-tidal deltas (ETDs) evolve constantly under the influence of natural processes and anthropogenic activities. The Haringvliet ETD in the Southwest of the Netherlands is an extreme example of the latter: closing off the estuary in 1970 triggered a regime shift, completely altering the evolution of the ETD. Initially, the coast-normal sandy shoals evolved towards a narrow coast-parallel intertidal spit: the Hinderplaat. Subsequently, this tidal flat breached around 1995. Thereafter, the flat eroded continuously while sediment was transported from the flat towards the coast.

Previous research with the aim to understand the morphological development of the Haringvliet ETD, has provided insights into the processes that are responsible for the large morphological changes directly after the construction of the Haringvliet Barrier. The processes driving the observed ongoing erosion and flattening of the Hinderplaat are however still poorly studied and understood. Therefore in this research, the underlying mechanisms are investigated and linked with anthropogenic interferences and meteorological events.

To this end, a combination of data analysis and numerical simulations is applied. In an analysis of single-beam bathymetry measurements (gathered in the Vaklodingen dataset), the development of the subtidal shoreface and the intertidal area of the Hinderplaat was explored. In general, the degradation of the Hinderplaat can be divided into three developments: (1) a landward migration since its formation, (2) a lowering since 1992 after a period of significant heightening and (3) a breach and channel formation in 1995, after which the shoal spread and merged with other shoals.

A depth-averaged (2DH) Delft3D model is used to explore the mechanisms behind these developments and to reveal the relative importance of the tidal-, river discharge-, wind-, surge- and wave-forcing driving the flow and sediment transport in the ETD. The first two developments (landward migration and lowering) occurred gradually, hence they were possibly a response of the system to the regular hydrodynamic forcing. Various simulations with a wide range of forcing-scenarios are performed to evaluate this. The third development (breaching) was observed in the same year an extreme discharge had occurred. A morphodynamic hindcast is performed to study the link between the two.

Model results indicate that the landward migration of the Hinderplaat was induced by regular wave action from WNW to NNE direction. Such wave conditions generate cross-shore transport over the shoal in eastern direction. This counteracts the effect of the tide, that enhances (much smaller) residual transport rates in seaward direction. Furthermore, breaking waves generate longshore transport along the Hinderplaat, with the highest transport rates at its southern end. This resulted in its spreading in southern direction and lowering of the highest part of the shoal. In addition, a correlation is found between the sudden increase in height of the Hinderplaat before the degradation and the construction of the Slufter. Considering the abundant transport

rates from the Slufterdam towards the shoal, it is concluded that the port extension served as an important sediment source directly after construction. However, the sediment supply might have decreased in subsequent years. The hindcast simulation confirms that breaching of the shoal was a direct consequence of the high discharge event of February 1995: the strong offshore directed currents created an initial channel which was later on maintained by the tide.

Wind-driven currents are very effective in generating residual flow patterns at the shoreface in front of the Hinderplaat. Besides, both the wind and surge act as important amplifiers for the sediment transport rates on top of the shoal. However, waves are indispensable for the morphological changes of the study area as the other hydrodynamic drivers are hardly capable of generating sediment transport by themselves.

Concluding, it is undoubted that the formation and thereby existence of the Hinderplaat is a direct consequence of the man-made closure of the Haringvliet estuary. However, its degradation (lowering, landward migration, breaching and further spreading) is a response of the system to the natural hydrodynamic forcing. Therefore, this evolution can be considered as part of the intrinsic behaviour of the shoal that is independent of human interventions in the former estuary.

SAMENVATTING

KERNPUNTEN

- Hoewel het ontstaan van de intergetijde Hinderplaat een direct gevolg was van een menselijke ingreep, is het verdwijnen ervan onderdeel van het natuurlijke gedrag onder invloed van reguliere hydrodynamische condities
- De Hinderplaat zou onder invloed van het getij in zeewaartse richting moeten verplaatsen, maar dit wordt tegengewerkt door de golfwerking: golven genereren dwars- en langsstromingen over de plaat, die zorgen voor de landwaartse migratie en het verspreiden in zuidelijke richting
- Extreme afvoeren dragen aanzienlijk bij aan de geulvorming op de Hinderplaat, gezien ze voor initiële doorbraken zorgen die later worden versterkt door het getij

---

SAMENVATTING

Buitendelta's ontwikkelen zich voortdurend onder invloed van zowel natuurlijke processen als menselijke ingrepen. De buitendelta van het Haringvliet in het zuidwesten van Nederland is hier een sterk voorbeeld van: het afdammen van het estuarium in 1970 veroorzaakte een verschuiving van het hydrodynamisch regime, waardoor de evolutie van de buitendelta volledig transformeerde. Aanvankelijk ontwikkelden de voormalig kustdwarse zandbanken zich tot een lange kustlangse intergetijdebank. Later ontstond een doorbraakgeul rond 1995. Hierna erodeerde de plaat, waarbij het sediment landinwaarts werd verplaatst.

Voorgaande onderzoeken met als doel de morfologische ontwikkelingen van de buitendelta te begrijpen, hebben inzicht gegeven in de processen achter de initiële transformatie na het aanleggen van de Haringvlietdam. De processen die verantwoordelijke zijn voor de voortdurende erosie en het afvlakken van de Hinderplaat worden echter nog onvoldoende begrepen. In dit onderzoek worden de onderliggende mechanismen achterhaald, waarna ze in relatie worden gebracht tot voorgaande menselijke ingrepen en extreme meteorologische gebeurtenissen.

De toegepaste methode bestaat uit een combinatie van data analyses en numerieke simulaties. De ontwikkelingen van de vooroever en het intergetijde gebied van de Hinderplaat zijn onderzocht met een analyse van singlebeam echolood dieptemetingen (verzameld in de Vaklodingen dataset). Over het algemeen kan de afbraak van de Hinderplaat in drie ontwikkelingen worden verdeeld: (1) een landwaartse verplaatsing sinds het ontstaan van de plaat, (2) een verlaging ervan sinds 1992, na een periode van significante groei en (3) een doorbraak en geulvorming in 1995, waarna de bank verspreidde over de buitendelta en samensmolt met andere zandplaten.

Een dieptegemiddeld (2DH) Delft3D model is gebruikt om de mechanismen achter deze ontwikkelingen te onderzoeken en om het relatieve belang van het getij, de rivierafvoer, de wind, de golven en stormvloeden op de stroming en de sedimenttransporten te onthullen. De eerste twee ontwikkelingen vonden geleidelijk plaats, waardoor ze mogelijk deel uitmaakten van het inherente gedrag van de buitendelta onder reguliere hydrodynamische condities. Om dit te toetsen zijn meerdere simulaties met een breed scala aan forceringen uitgevoerd. De derde ontwikkeling is geobserveerd in een jaar waarin ook een periode van extreme rivierafvoeren plaatsvond. Er is een morfodynamische hindcast uitgevoerd om de link tussen deze twee gebeurtenissen te onderzoeken.

De modelresultaten tonen aan dat de landwaartse verplaatsing van de Hinderplaat veroorzaakt werd door de reguliere golven uit WNW tot NNO richting. Deze golfcondities genereren dwarstransporten over de plaat in oostelijke richting. Dit werkt de effecten van het getij tegen, dat (veel kleinere) zeewaartse netto transporten tot stand brengt. Bovendien veroorzaken brekende golven langstransporten over de Hinderplaat, die

het sterkst zijn bij het zuidelijke uiteinde. Deze zorgen voor zowel het verspreiden van de plaat in zuidelijke richting, als voor het afnemen van de maximale hoogte. Verder is een correlatie gevonden tussen de plotselinge toename in hoogte van de plaat voor haar afbraak en de bouw van de Slufter. Gezien de overvloedige sedimenttransporten vanuit de Slufterdam richting de Hinderplaat, is geconcludeerd dat de havenuitbreiding een belangrijke sedimentbron is geweest direct na de constructie ervan. De toevoer van sediment is waarschijnlijk afgenomen in de opeenvolgende jaren. Een hindcast simulatie heeft bevestigd dat de doorbraak van de plaat een direct gevolg was van de hoge rivierafvoeren in februari 1995: de sterke stromingen creëerden een initiële doorbraak die later werd versterkt door het getij.

Windgedreven stromingen zijn zeer effectief in het genereren van residuele stromingen op de vooroever voor de Hinderplaat. Bovendien versterken wind en stormopzetten de transporten over de plaat. Golven zijn echter essentieel voor de morfologische veranderingen, gezien de andere hydrodynamische actoren niet in staat zijn om op zichzelf sedimenttransporten teweeg te brengen.

De vorming, en daarmee het bestaan van de Hinderplaat is een direct gevolg van de kunstmatige afsluiting van het Haringvliet estuarium. Niettemin kunnen we concluderen dat haar afbraak (verlagen, landwaartse verplaatsing, doorbraak en verspreiden) onderdeel was van het gedrag onder invloed van de natuurlijke hydrodynamische condities. Daarom kan dit deel van de evolutie van de Hinderplaat worden beschouwd als inherent gedrag van de plaat, dat los staat van menselijke ingrepen in het voormalig estuarium.

CONTENTS

1

INTRODUCTION

1.1. BACKGROUND

Estuaries, tidal lagoons and tidal bays, collectively called *tidal basins*, interrupt coastlines all over the world with their inlets. They have a great socio-economic value enabling recreation, port and harbour related industry, resource exploitation and inland waterways (Stive and Wang, 2003). Moreover, their morphology provides ecological opportunities for marine flora and fauna, granting ecosystem services that are of fundamental importance to human well-being (Costanza et al., 1997, Jeuken et al., 2003, Millennium Ecosystem Assessment, 2005, Murray et al., 2015). Tidal basins generally consist of three main morphologic elements: the tidal inlet, the ebb-tidal delta and the tidal basin itself. These elements interact with each other under the effect of meteorological and hydrodynamic forces and strive to gain or maintain in (dynamic) equilibrium individually and collectively (Elias, 2006). Their morphology evolves constantly under the influence of natural processes as well as anthropogenic activities. When an equilibrium is disturbed by the affecting forces, the initial response of the system is to redistribute the sediment within the elements. For larger scale permanent distortions, sediment exchange may take place between the tidal basins and the adjacent coastlines (Kragtwijk et al., 2004). Depending on the history, the geology and the shape of the basin amongst others, it can act as either a source or a sink of sediment for adjacent coastlines (Eelkema et al., 2013). Long-term import or export of sediments, i.e. drowning or accretion of the basin, may threaten its valuable properties (Jeuken et al., 2003).

This research treats the case of the Haringvliet in the Dutch Voordelta. The Haringvliet used to be a meso-tidal estuary connecting the Rhine and Meuse rivers to the North Sea, see Figure 1.1. After the flooding disaster of 1953, the estuary was dammed in 1970 as a part of the Delta Project. The goal was to improve safety against flooding and to create fresh water basins for agriculture. Later, sluices were built in the Haringvliet Barrier to regulate the upstream river discharge (Paalvast et al., 1998).

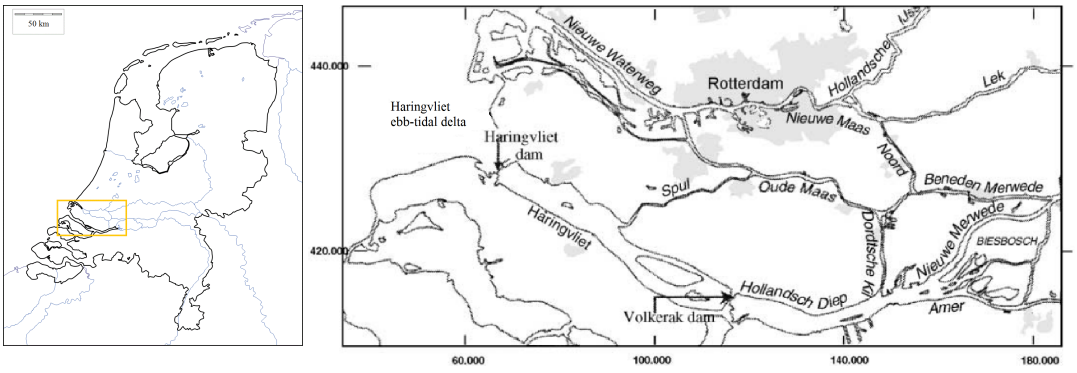

Figure 1.1: Overview of the Haringvliet estuary before closure. Adjusted by Tönis et al. (2002) from Bol and Kraak (1998).

Before the closures, the Voordelta already was an area with great morphological activity by nature, which was initially enhanced after the interventions of the Delta Project (Aarninkhof and van Kessel, 1999). Closing off the Haringvliet estuary triggered a regime shift, completely altering the evolution of the former ebb-tidal delta (Elias and Van der Spek, 2014), as shown in Figure 1.2. First, the coast-normal sandy shoals evolved towards a narrow coast-parallel intertidal spit, the Hinderplaat. This sandy shoal provided great opportunities for ecology. Subsequently, it breached around 1995; since then continuous erosion has been taking place, while ongoing sediment transport from the flat towards the coast has been observed. The morphological changes of the Hinderplaat have continuously affected its ecological value (Rijkswaterstaat, 2014).

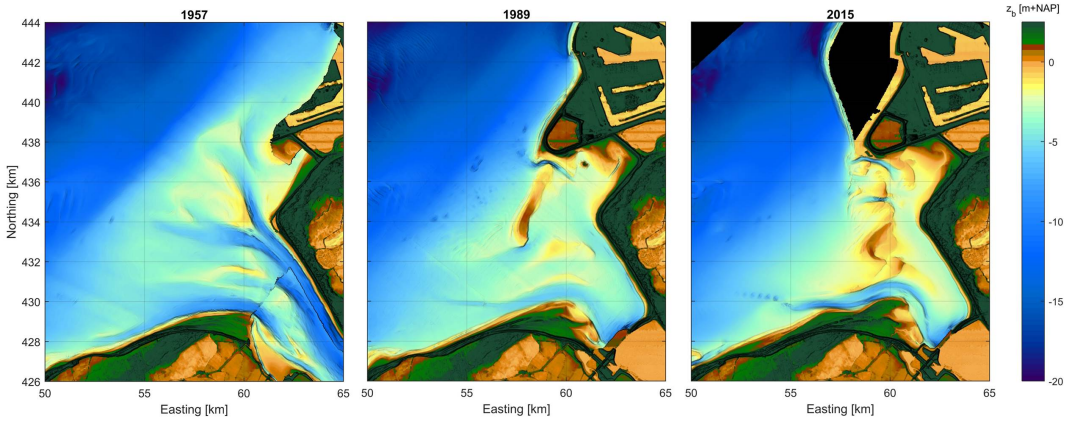

Figure 1.2: Different stages of the evolution of the Haringvliet outer delta, based on the Vaklodingen data

A similar evolution has taken place in the Grevelingen ebb-tidal delta, located south of the Haringvliet. The Grevelingen estuary was entirely closed-off by the Brouwersdam in 1971, whereafter the shoreface started to erode and large volumes of sand were transported landwards creating the Bollen van den Ooster (Kohsiek, 1988). However, this intertidal sandbar is still present and even growing.

1.2. RELEVANCE OF THE RESEARCH

Previous studies have been carried out to understand and predict the morphological behaviour of the Haringvliet ebb-tidal delta. Initially, they used to have a descriptive character based on data analyses, although for the last 20 years also process-based morphodynamic models have been used for this purpose. Van Holland (1997) developed a numerical Delft3D model together with Roelvink et al. (1998) to analyse the response of the outer delta to different designs of Maasvlakte 2 and policies for the Haringvliet Sluices. The model has been adapted by Steijn et al. (2001) and De Vries (2007) showing promising results, although it is concluded that its predictive capabilities regarding the morphological development of the ebb-tidal delta could and should be improved.

The Haringvliet outer delta is a complex case where both coastal and estuarine processes have played a role, which makes it challenging for morphodynamic modelling. Therefore, it is highly important to understand the system, apart from developing models that can predict its behaviour. The morphological development is the result of the interaction between the physical processes of water movement, sediment transport and bottom changes (Wang et al., 2012). Compared to the morphodynamic behaviour of uninterrupted coastlines and rivers, the morphodynamic response of tidal basins is a degree more complicated and less well understood (Stive and Wang, 2003). However, knowledge of the physical processes driving the morphology is essential to facilitate an efficient and sustainable development. Considering the ecological value of tidal flats like the Hinderplaat, it is crucial to gain insight into the processes causing their (de)formation. This knowledge can be used when deciding on future interventions, but also when considering their maintenance policy.

The impact of anthropogenic interventions on morphological processes in intertidal areas can be related to changes in physical processes. Previous research with the aim to understand the morphological development of the Haringvliet ebb-tidal delta has provided insights into the processes causing the large morphological

changes directly after the construction of the Haringvliet Barrier. The processes driving the observed ongoing erosion and flattening of the Hinderplaat are however still poorly studied. It is essential to obtain this knowledge to enable well thought-out decision making on possible future interventions in the Haringvliet environment. Moreover, gained knowledge on the processes in the Haringvliet could be used to understand the evolution of the shoal Bollen van den Ooster and similar systems worldwide.

This research is part of the project *KPP B&O kust*, standing for *Knowledge on Primary Processes regarding Management and Maintenance of the Dutch coast*, by Rijkswaterstaat and Deltares. The project focusses on data analyses, large-scale system understanding and on the development of numerical models. Its main goals are to gain a better understanding of the workings of the Dutch coastal system and to improve the coastal policy maintenance by sand nourishments. Knowledge on the effects of anthropogenic interventions on the Dutch Delta is used by Rijkswaterstaat to increase the efficiency of the coastal zone management.

1.3. OBJECTIVE AND RESEARCH QUESTIONS

This study aims to reveal the physical processes that are responsible for the morphological evolution of the Hinderplaat in the Haringvliet ebb-tidal delta. In this context physical processes are defined as the interaction between water movement, sediment transport and changes in morphology. The mechanisms may be related to either human-interventions or (meteorological) events, or they may be a part of the intrinsic behaviour of the intertidal sandbar under regular conditions. It is most likely that a combination of the latter causes the evolution. As previously mentioned, the Haringvliet case is complex as the governing processes have constantly been changing with the constructed interventions. On the other hand, this makes it possible to study the impact of such human activities. Besides, Rijkswaterstaat has collected a large amount of bathymetry data of this location over the years, that provides the means to study the morphological evolution in detail. The primary focus of this research is on the degradation of the Hinderplaat, as this is the least understood.

The general research question is therefore formulated as follows:

What was the main cause of the degradation of the Hinderplaat?

The following sub-questions have been specified to find an answer to this question:

1. What has been the morphological development of the Hinderplaat since the construction of the Delta Works in the Haringvliet estuary?
2. What interventions have taken place in and around the Haringvliet outer delta and what meteorological events have occurred since the first closure?
3. What are the characteristics of the water motion and which mechanisms are most dominant?
4. What are the characteristics of the sediment transports, which mechanisms are most dominant and how does this contribute to the observed morphological evolution of the Hinderplaat?
5. How are the mechanisms behind the degradation of the Hinderplaat related to the human interventions and meteorological events?

1.4. RESEARCH APPROACH AND THESIS OUTLINE

In order to reach the objective and find the answers to the research questions, the research has been divided into four stages:

- **Literature review**
  This study starts with a literature research consisting of two parts: a part that treats the theoretical background and a part that contains the necessary background information on the study area. The theoretical background is studied to identify important processes of tidal basin and ebb-tidal delta morphodynamics. Previous findings on the (morphological) evolution and the hydrodynamics of the study area are discussed and knowledge gaps in the current state of research are identified. The theoretical background is summarised in Chapter 2 and the literature review on the study area is captured in Chapter 3.

- **Data analysis**
  Subsequently, a data analysis is performed on the morphological evolution of the Haringvliet outer delta. The bathymetric analysis is based on echo soundings made by Rijkswaterstaat, collected in the *Vaklodingen* dataset. With the measured bed levels, it is possible to study the bathymetric changes, as well as erosion/sedimentation patterns and volume changes. These findings are also discussed in Chapter 3.

- **Modelling study**
  Based on the outcomes of the literature review and the data analysis several hypotheses are formulated regarding the evolution of the Hinderplaat. These are presented in Chapter 4. A 2DH Delft3D model is used to test the hypotheses and reveal the relative importance of the tidal-, river discharge-, wind-, surge- and wave-forcing driving the flow and sediment transport in the outer delta. Previous studies, e.g. Elias (2006), Lesser (2009) and Eelkema (2013), have shown that process-based numerical models are very useful in increasing the spatial and temporal resolution of field measurements. These models can be applied as a tool to interpolate behaviour that is observed in a limited number of points in space at a limited number of moments in time (Eelkema et al., 2013). It is not the aim to reproduce the exact morphological development of the delta, rather than to determine how currents, waves and river discharges might have led to the degradation of the Hinderplaat. The model setup is summarized in Chapter 5. Modelling results of various simulations with a range of different forcings are elaborated in Chapter 6.

- **Conceptual model**
  Based on the findings of this study, a conceptual model is presented in Chapter 7. It visualises the conclusions and provides information on the observed evolution and the governing processes behind the morphological changes since the closure of the Haringvliet estuary.

2

THEORETICAL BACKGROUND

2.1. INTRODUCTION

In this chapter general background information is provided on tidal basins and their morphological units. This contributes to an understanding of the methods and theoretical concepts in this report. The classification of coastal systems is treated in Section 2.2, after which theoretical background on tidal basin classification, features and morphodynamics is given Section 2.3. Import and export sediment transport relations are explained in Section 2.4. Finally the concepts of adaptation towards a (new) equilibrium and adaptation timescales are treated in Section 2.5.

2.2. CLASSIFICATION OF COASTAL SYSTEMS

Many types of classifications can be used to describe and analyse the range of coastal systems all over the world. These may be based on tectonic controls, material, hydraulic processes, etc. This report follows the process-based classification on the relative importance of wave- and tidal energy and sediment transport for prograding and transgressive coasts, as shown in Figure 2.1. The top triangle of this figure has separately been described by Galloway (1975). He recognized the relative influence of waves, tides and rivers as the three major factors affecting delta development on the morphological structure. This classification is depicted in Figure 2.2, showing a triangular diagram that distinguishes wave-dominated, tide-dominated and river-dominated deltas. The colors of the diagram represent the relative influence of the forces that drive the morphology. A delta may become *abandoned* when its deterioration is induced by a reduction in sediment supply. This is usually a consequence of delta lobe switching, river damming, sand mining or sea level rise (Nienhuis et al., 2013).

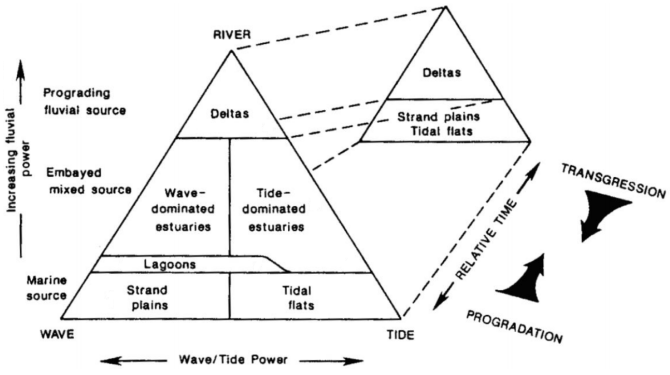

Figure 2.1: Ternary shoreline classification diagram (Boyd et al., 1992, Dalrymple et al., 1992)

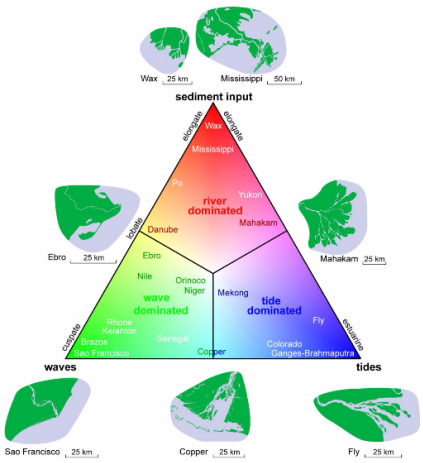

Figure 2.2: Delta classification diagram by Galloway (1975), adjusted by Bosboom and Stive (2013)

2.3. TIDAL BASINS AND COASTAL INLETS

Tidal inlets are openings in the shoreline, such as two barrier islands, that connect bays or lagoons to the open ocean (Bosboom and Stive, 2013). Tidal currents maintain the inlets and prevent them from closing. From a morphological point of view these systems have a highly dynamic behaviour, which often intervenes with human utilization.

2.3.1. BASIN CLASSIFICATION

Based on the entrance characteristics and the importance of fresh-water run-off three distinct types of tidal basins can be discerned (Carter, 1988):

- *Tidal lagoons* are basins that are enclosed by wave-shaped barrier islands or spits. The presence of the barriers limits the wave penetration, while water flows in and out through passes or inlets in between. The fresh water run-off is typically limited. A typical example of a tidal lagoon is the Dutch Wadden Sea.
- *Tidal bays* are more open to the deep water of the ocean or sea due to the absence of barrier islands. Also in this case the fresh-water run-off is limited. Although waves can enter the bay unhindered, they usually loose their energy close to the entrance due to depth-limited breaking and bottom friction (Bosboom and Stive, 2013). A good example is the Baie of St. Michel in France.
- Unlike the first two types, *estuaries* experience a fresh water run-off. The interaction of the salt- and fresh water is a fundamental characteristic of estuaries. Depending on the degree of mixing between the two water bodies, they can be classified as stratified, partially mixed or mixed. Unlike river mouths, estuaries tend to be tide-dominated. Wave effects near the mouth can result in entrance constrictions by the development of spits, shoals or barriers. An example of an estuary is the Western Scheldt.

2.3.2. INLET CLASSIFICATION

Although tidal basins are evidently tide-dominated environments, in their tide-maintained entrance areas the wave and tidal influences are combined (Bosboom and Stive, 2013). Hayes (1979) came up with a classification based on the tidal range outside the inlet and the seaward generated wave conditions, distinguishing five inlet classes. As both parameters are independent of the inlet systems configuration, they are both suitable for a process-based classification (Bosboom and Stive, 2013). The classification considers the relative effect of waves and tides rather than the absolute values, as shown in Figure 2.3.

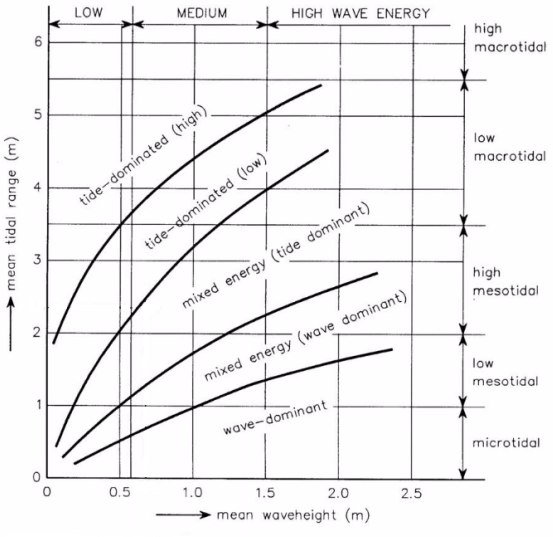

Figure 2.3: Hydrodynamical classification according to the method of Davis and Hayes (1984). Retrieved from Bosboom and Stive (2013)

2.3.3. TIDAL DELTAS

Due to large discharges and velocities in an inlet or estuary mouth, a strong sediment exchange is enhanced between the basin and the outside area (Bosboom and Stive, 2013). In the divergent ebb-tidal flow the flow velocities decrease, leading to sediment deposition creating the *ebb-tidal delta* (also referred to as the *outer delta*). Likewise, the *flood-tidal delta* is created by sediment deposition by the incoming flood currents.

The overall morphology of the deltas is largely determined by the combined action of waves and tides. While tidal currents induce a net offshore sediment flux building up the outer delta, wave action acts as bulldozer moving sediment onshore and limiting the area over which it can spread (Hageman, 1969). Meanwhile the flood-tidal delta benefits from the onshore flux. Consequently, tide-dominated inlets tend to have relatively large ebb-tidal deltas compared to the flood-tidal delta, while for wave-dominated inlets the flood-tidal deltas are well developed and the outer deltas tend to be small. In relatively small basins with an abundant sediment supply, the flood-tidal delta may span the entire basin area. An example is the Wadden Sea: as the flood-tidal deposits are found everywhere in the basin, we only speak of the outer delta and the basin. The flood-tidal delta is no longer considered to be a distinct morphological unit (Bosboom and Stive, 2013).

2.3.4. HYDRODYNAMIC FORCING AT THE EBB-TIDAL DELTA

The currents in the vicinity of an inlet are partly tidal, partly wave-driven and partly wind driven (Bosboom and Stive, 2013). in the case of estuaries also density driven currents play a role. As waves encounter a complex topography in the outer delta, they refract, diffract and reflect, causing complex wave patterns in the outer delta. While tidal currents are mainly concentrated in the main channels, the wave-driven currents are found in the shallow areas where waves break (Bosboom and Stive, 2013). This section treats the most relevant points of consideration regarding the hydrodynamic forcing at the outer delta.

- **Wave patterns**
  In case of normal-incident waves, both the delta edge (consisting of side lobes) and the gorge are exposed to the wave energy. However, due to refraction the waves turn towards the depth contours, concentrating the energy in the central front edge of the outer delta. When considering obliquely incident waves, one of the two lobes (depending on the wave-angle)is fully exposed while the other is sheltered.

  Although barrier islands provide a shelter to the tidal basin, wave energy can still penetrate through the inlet. This is however still partly sheltered by the ebb-tidal delta: so the wave-energy reaching the inlet is much less than offshore. The wave-energy penetrating from the open sea into the basin is rather small and restricted to the area just behind the gorge. Wave-energy found further into the basin usually originates from locally generated waves.

- **Tidal residual currents**
  There is a variety of mechanisms that lead to tidal residual currents, causing residual sediment transport. Examples are residual flow patterns due to acceleration near the inlet, Stokes' drift and curvature-induced flow. For shallow areas like tidal inlets it is therefore incorrect to represent the tide as a small-amplitude wave (Bosboom and Stive, 2013).

- **Wave-induced currents**
  Horizontal variations in the transport of momentum by waves, i.e. horizontal variations in the radiation stress, may affect the mean sea level and generate currents, particularly in the surf zone (Holthuijsen, 2007). Due to the complex topography of tidal deltas the alongshore and cross-shore momentum equations need to be resolved in two horizontal directions. In tidal inlets these currents can even dominate the tidal residual currents (Bosboom and Stive, 2013).

- **Wind-induced currents**
  Wind forcing acts as a shear stress on the water surface generating wind-driven currents, which is more effective when acting on shallow water bodies. Due to the complex topography of tidal inlets, the wind-driven current fields show a significant variation in space. Probably more important that the direct wind-induced currents is the effect of the wind-induced water level set-up during a severe storm (Bosboom and Stive, 2013): when stresses are directed on a water surface for a longer period, this can cause a water level set-up. Even though the peak wind velocities usually last a few hours, the effects of the generated set-up can last much longer, sometimes even suppressing the ebb current for over a day. Great

amounts of water have to be squeezed through the inlet during severe storms, which can influence the morphology considerably as new inlets and channels are generally created under these conditions.

- **Estuarine circulation**
  In estuaries with large fresh water run-off, density differences arise between the saline water from the sea and the fresh water coming from the river upstream. The horizontal density gradient can induce density-driven estuarine circulation (also referred to as gravitational circulation), which is known as a major mechanism for generating turbidity maxima in tidal estuaries (Burchard and Baumert, 1998). Moreover, tidal straining can also cause estuarine circulation: this is the asymmetry in tidal mixing caused by the interaction between tidal shear and horizontal density gradients (Wang et al., 2012). It has the consequence of vertical mixing of tracers (e.g. salinity and suspended sediment) and momentum during flood, while this mixing is suppressed during ebb. Consequently, more onshore momentum is transported down to the bottom during flood, than offshore momentum during ebb, resulting in estuarine circulation

- **Wave-current interaction**
  As both the tidal and wave-driven current patterns are concentrated for a large part in deeper channels of the outer delta, currents may affect the wave propagation. Currents can even be so strong that they prevent waves from entering certain areas.

2.3.5. SEDIMENT VOLUME OF THE OUTER DELTA

The volume of the ebb-tidal delta is defined based on the no-inlet bathymetry of which the coastal slope is assumed to be undisturbed and similar to the adjacent coasts (Walton and Adams, 1977). Hence, the morphological boundary of the outer delta is located where there are negligible differences between the actual and the no-inlet bathymetry, as shown in Figure 2.4 (Dissanayake, 2011). As earlier stated, the sediment volume of the outer delta is larger for large tidal forces and low onshore directed wave energy, so that the outer delta can extend further seawards with the absence of a distinct terminal lobe. The following empirical relation was found by Walton and Adams (1977) for the total sediment volume stored in the outer delta:

$$V_{od} = C_{od} P^{1.23} \tag{2.1}$$

In which:

V_{od}	sand volume stored in the outer delta	$[m^3]$
C_{od}	empirical coefficient	$[m^{-0.69}]$
P	tidal prism	$[m^3]$

The coefficient C_{od} is dependent on the wave climate, such that for the same P, V_{od} is the same for a more energetic wave climate (Bosboom and Stive, 2013). When an increase in the volume of the outer delta is enhanced, e.g. by increasing the tidal prism, the required sediment may originate from three sources: the adjacent barrier coast, the basin or from offshore. It is most possible that it will be a combination of the three sources. Conversely, when the tidal prism is decreased, the ebb-tidal delta will be too large and erosion will take place until the system adapts itself to the a equilibrium state.

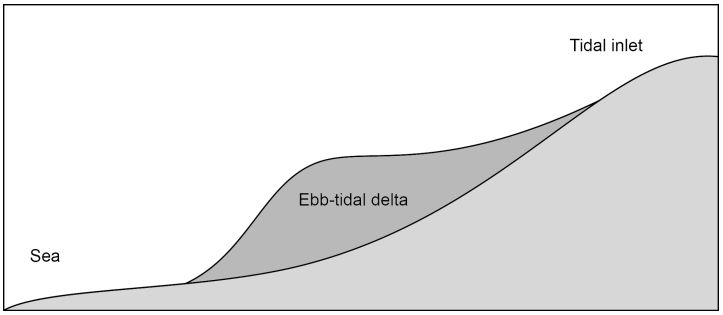

Figure 2.4: Cross-section showing the definition of the outer delta relative to a no-inlet bathymetry.
Adapted from Dissanayake (2011)

2.3.6. THE INNER BASIN

Various empirical relations have been found that describe the stability of the morphological units of the channels and flats inside the tidal basin. These relations link the geometric properties of the units to the hydraulic boundary conditions. The correlation between tidal prism and inlet cross-sectional area was first recognized a century ago by LeConte (1905) and later modified by O'Brien (1931, 1969). The following relation was established:

$$A_{eq} = CP^q \tag{2.2}$$

In which:

A_{eq}	minimum equilibrium cross-section of the entrance channel, measured below MSL	$[m^2]$
P	(spring) tidal prism	$[m^3]$
q, C	coefficients	$[-], [m^{2-3q}]$

This relation is valid for large estuary mouths, as well as for tidal bays and lagoons. The coefficient q is order of magnitude 1, while C is in the range 10^{-4} to 10^{-5}. Later it appeared that not only at the entrance, but also along a channel the flow area was related to the tidal prism passing through the cross-section. So, the general relations reads:

$$A_{MSL} = C_A P_{AB} \tag{2.3}$$

In which:

A_{MSL}	minimum equilibrium flow area in a cross-section of the basin, measured below MSL	$[m^2]$
P_{AB}	(spring) tidal prism landward of the cross-section under consideration (AB)	$[m^3]$
C_A	coefficient	$[m^{2-3q}]$

If the flood-tidal delta spans the entire basin area, which is often the case for small basins as explained in Section 2.3.3, the following relationship holds for the total basin channel volume (Eysink, 1990):

$$V_C = C_V P^{3/2} \tag{2.4}$$

In which:

V_C	equilibrium total channel volume, below MSL	$[m^3]$
P	tidal prism landward	$[m^3]$
C_V	coefficient	$[m^{-3/2}]$

From the relation given by equation 2.4 it is possible to deduce a relationship between the area of the tidal flats and the total basin area:

$$A_f = A_b - A_{ch} = A_b - \frac{V_c}{D_c} \approx A_b - \alpha \frac{P\sqrt{A_b}}{D_c} \approx A_b - \beta \frac{H_m}{D_c} A_b^{3/2} \tag{2.5}$$

In which:

A_f	flats area (the area above MSL	$[m^2]$
A_{ch}	horizontal area covered by the channels	$[m^2]$
α, β	constants of proportionality	$[m^{-1}]$
D_c	characteristic channel depth	$[m]$
H_m	mean tidal range	$[m]$

2.4. NET SEDIMENT TRANSPORT

As a tidal wave reaches the shallow delta front of a basin, it is strongly deformed by bottom friction and other effects associated with the local morphology. This distortion may strengthen or weaken the maximum flood and ebb velocities. It might also cause an asymmetry in the acceleration of the tidal flow (*acceleration asymmetry* or *slack water asymmetry*). Both phenomena may enhance net sediment transport, thus intervene in the morphological evolution of the tidal basin. If we ignore external conditions as storm surges and sediment availability we can say that in a way the tidal basin determines its own evolution (Bosboom and Stive, 2013).

Coarse sediments (e.g. sand) are mainly transported as bed load. For this, the difference between the flood- and ebb-currents are most important, as bed load transport is assumed to be proportional to u^n, in which u is the current speed and n is a factor between 3 and 5 (Wang et al., 2012). A system is called *flood-dominant* when the flood velocities are higher than the ebb velocities. The difference in the magnitude of the currents during flood and ebb may be induced by:

- the presence of a mean net current, caused by either tide-topography interactions, wind effects of density currents,
- the deformation of the tidal wave when propagating through a shallow basin, as the propagation speed differs for high and low water. A higher propagation speed during high water causes faster rising tide and therefore stronger flood currents.

Flood-dominance causes a larger influx than outflux of sediment leading to a net landward directed near-bed transport of coarse sediment. Vice versa, *ebb-dominant* systems enhance seaward directed transport, flushing the coarse sediment away from the basin. A basin geometry with shallow channels and a limited intertidal storage area enhances flood-dominance, whereas basins with deep channels and large intertidal storage volumes enhance ebb-dominance. The type of geometry can be depicted in hypsometric curves, as shown in Figure 2.5: these curves give information about the channel depth and the extent of the tidal flats.

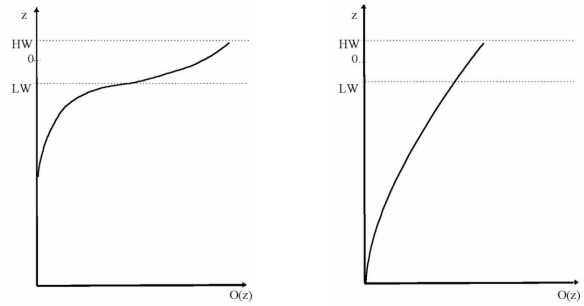

Figure 2.5: Hypsometric curves for two types of basin: the left figure represents a situation with shallow channels ans large intertidal storage areas, the right represents a basin with deep channels and small intertidal areas. From Bosboom and Stive (2013)

Fine sediment is generally transported as suspended load. This does not only depend on the local instantaneous flow velocity, but also on the flow conditions upstream and in the past (Bosboom and Stive, 2013). Since sediment particles sink to the bottom around slack tide, differences in the currents around slack water after the flood and ebb periods cause net sediment transport. Figure 2.6 shows a case for which the high water slack is longer than the low water slack. The red dotted line shows that fines need time to respond to a new hydrodynamic forcing, as the adaptation timescale for sedimentation T_a is inversely proportional to the settling velocity w_s. The result is a higher sediment concentration during the flood period, thus a residual sediment transport in flood-direction. For coarse sediment an asymmetry in slack water duration does not matter, since the sedimentation timescale is much shorter.

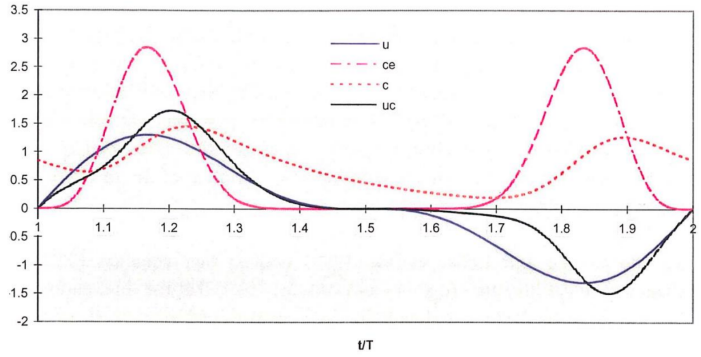

Figure 2.6: The result of lag effects on net fine sediment transport. From Wang et al. (1999)

2.5. EQUILIBRIUM STATE AND ADAPTATION TIMESCALES

The behaviour of coastal systems is dynamic on both time and spatial scales. In this case the timescale ,T, is interpreted as the period of time required for significant morphological developments to take place. Dronkers (2016) suggests that both scales are closely coupled: the larger the spatial scale of a feature, the larger the timescale in which significant changes occur. De Vriend (1991) specified this for tidal inlets, as shown in Figure 2.7. In this relation he also included the respective forcing conditions.

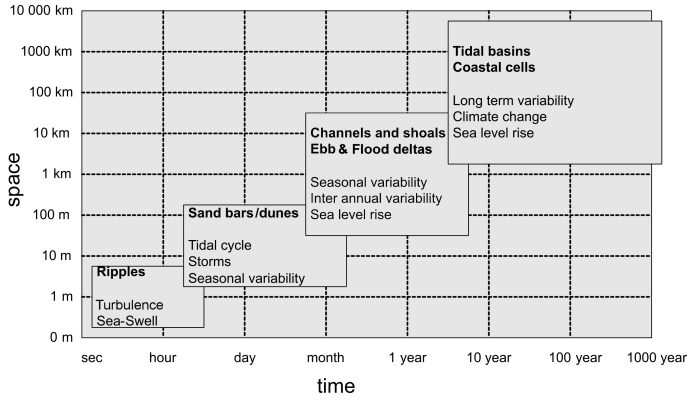

Figure 2.7: Components of tidal inlets and their respective forces in temporal and spatial scales. After Tung (2011) based on De Vriend (1991)

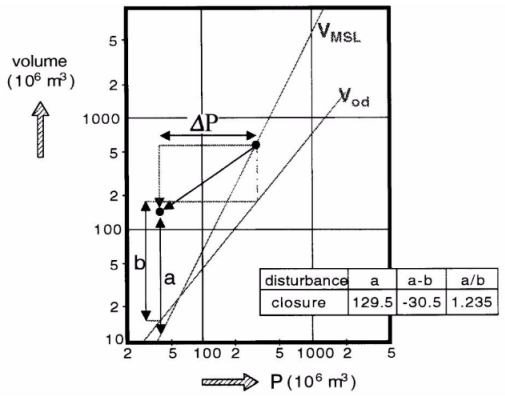

Figure 2.8: Effect of closure of a part of the basin on the morphological units. From Bosboom and Stive (2013)

In the equilibrium condition, the geometry of a tidal basin is such that the durations of flood and ebb are approximately equal. A basin is considered to be in *dynamic equilibrium* if its overall planform shape and size and hypsometry undergo little to no changes due to a balance between the input and output of marine and riverine sediment under the prevailing boundary conditions (de Haas et al., 2017). This equilibrium state can be maintained when the estuary or tidal embayment alternates between flood-dominant and ebb-dominant conditions, resulting in no net sediment import or export when averaged over a certain timescale. However, bars and channels may form, disappear and migrate over timescales of decades, as long as the basin as a whole has balanced sediment import and export.

When a morphological system is not in equilibrium with the hydrodynamic forcing, morphological adjustments take place immediately until the system adapts itself towards a new equilibrium state. The rate of adjustment depends on the magnitude of the still remaining disruption (Bosboom and Stive, 2013). The process of the response is usually fast at first and decelerates (often exponentially) as the new equilibrium is nearly reached.

This research treats the morphological adaptation of the Haringvlietmouth after damming the estuary and thus reducing the basin area. Therefore, an example is given of the changes in dynamic equilibrium when closing off a part of a tidal basin, from a theoretical point of view: the closure results in a reduction of the total channel volume V_C (V_{MSL} in Figure 2.8) and of the tidal prism P. This figure shows that for the new situation the channel volume is $a\,m^3$ too big and the outer delta sediment volume $b\,m^3$ too big. The surplus of sediment of the outer delta is available to adapt the channels. If this is not enough ($a - b > 0$) the rest is supplied from outside, causing erosion of the downdrift coast. The figure also shows that a change in the tidal prism has a larger effect on the equilibrium channel volume than on the equilibrium volume of the outer delta V_{od}.

2.6. SUMMARY

This chapter explained general theory on tidal basins, their morphological units and (potential) evolution in time in terms of sediment transport and morphological units. It is shown that these coastal systems strive towards a new equilibrium state when disturbed by, for instance, human interventions. This thesis treats the case of the Haringvliet outer delta, whose channels and shoals have undergone a major transformation after damming the Haringvliet estuary. This is explained in the next chapter.

3

THE STUDY AREA

3.1. INTRODUCTION

This chapter discusses the study area of this research, based on a literature review and on several data analyses. First, the study area is introduced in Section 3.2. Subsequently, Section 3.3 discusses the human interventions in the Haringvliet. Section 3.4.1 gives an overview of the datasets used for the analyses of this chapter. The results of the data analysis on the morphodynamic development are presented in Section 3.4. The local hydrodynamics and bed composition properties are discussed in Sections 3.5 and 3.6.

3.2. THE DUTCH DELTA AND ITS VOORDELTA

The coastal system of the Southwest Netherlands consists of a series of (former) estuaries, from north to south: the Brielse Maas, Haringvliet, Grevelingen, Eastern Scheldt and Western Scheldt. These distributaries of the rivers Rhine, Meuse and Scheldt are together known as the Dutch Delta, see Figure 3.1. Their ebb-tidal deltas form a relatively shallow area in front of the Netherlands, stretching from Hoek van Holland to Zeebrugge and reaching a width of 10 km. This area is also known as the *Voordelta* (Elias and van der Spek, 2016). The Western Scheldt and Eastern Scheldt have remained open tidal basins, whereas the Grevelingen, Haringvliet and Brielse Maas were closed off as apart of the *Delta Works*. Going from south to north, the depth of the Voordelta decreases, the channels become smaller and the surface area of intertidal shoals increases. The sediment of the Voordelta mainly consists of fine to medium sand (Terwindt, 1973), although local mud deposits have formed in closed-off channels with small flow velocities and waves (Piekhaar and Kort, 1983).

The morphological development of deltas is largely determined by tide- and wave-induced sediment transport processes. Both types of processes are present in the Voordelta. However, a large difference can be observed in the two southern open estuaries compared to the northern closed ones. The tide in the Western and Eastern Scheldt exists of the tidal flow in longshore direction in the North Sea and the tidal flow in cross-shore direction going in and out of the estuaries. The latter is also referred to as the estuary-driven tide. In the outer deltas of the Grevelingen and Haringvliet only the longshore tidal flow remained present after damming the estuaries. Even though this can also cause local circulation currents, these are significantly smaller than the ones caused by the estuary-driven tide. Due to the reduced tidal influence, the wave-driven transports have become relatively more important in the northern estuaries(Elias and Van der Spek, 2014).

This research focuses on the Haringvliet ebb-tidal delta, that was originally connected to the tidal inlets of the Brielse Maas and the Haringvliet. Their closures, in 1950 and 1970 respectively, triggered a regime shift leading to a large-scale adaptation of the ebb-tidal delta. This evolution is treated in Section 3.3 and 3.4. The main focus of this research is on the biggest tidal flat of the Haringvliet delta, *the Hinderplaat*, which has shown a highly dynamic evolution over the years. This shoal developed towards an elongated sandy spit, with a part that was located above mean high water (MHW). Later, its height gradually decreased. Figure 3.2 shows the names of the main channels and shoals in the Haringvliet based on the bathymetric measurements of 2010 and 2011.

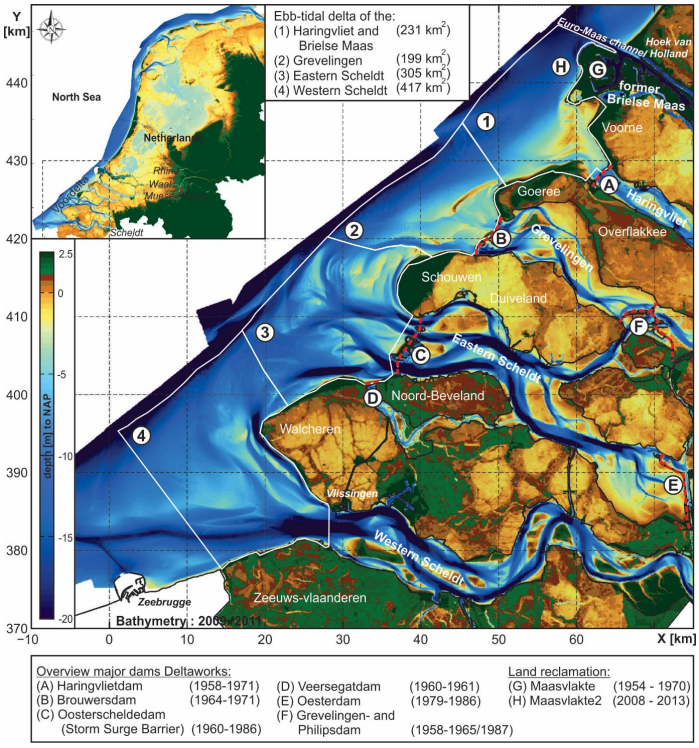

Figure 3.1: Overview of the Dutch Delta and the Deltaworks, based on the Vaklodingen bathymetry of 2009-2011 (Elias et al., 2015)

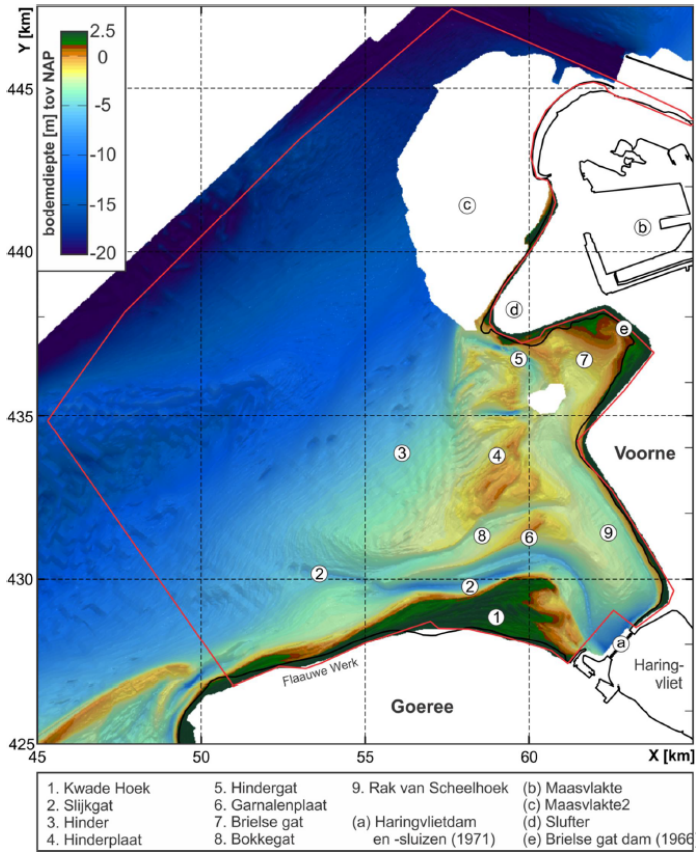

Figure 3.2: Overview of the channels and shoals in the Haringvlietmouth in 2010-2011 (Elias and Van der Spek, 2014)

3.3. ANTHROPOGENIC INTERFERENCES IN THE HARINGVLIET

The Haringvliet estuary has been influenced by several human interventions in the past, altering its morphological development. An overview of the main human interventions as described in this section is shown in table 3.1. An elaborated overview of the historical evolution of the Voordelta and its recent developments can be found in the paper about the Voordelta of Elias et al. (2015).

Table 3.1: Overview main interventions around the Haringvliet estuary

Closure works	
1950	Damming Brielse Maas, creating the Brielse Lake
1957-1970	Construction of the Haringvlietdam
1966	Second closure of the Brielse Gat, creating the Oostvoorne Lake
1971	Closure by the Brouwersdam
Extension Port of Rotterdam	
1964-1966	Construction of Europoort
1967-1976	Construction of Maasvlakte 1
1986-1987	Dredging operations Hindergat and construction of the Slufter(dam)
2008-2013	Construction of Maasvlakte 2
Maintenance dredging operations & nourishments	
1969-1985	Sand nourishments to strengthen the coast of Goerree
1973-1993	Sand nourishments to strengthen the coastline and dunes of Voorne
1983-now	Maintenance dredging Slijkgat channel
1991-2005	Slufterdam sand nourishments
1991	Dynamic Maintenance policy Voorne and Goerree
Haringvliet sluices policy	
1970-2018	Enabling river discharge regulation. Sluice capacity: 25.000 m^3/s
2018	Kierbesluit: partly open sluices, creating a brackish water zone in the Haringvliet

3.3.1. CLOSURE WORKS

Before its closure, the Haringvliet was a large river mouth just south of the Port of Rotterdam, forming an open connection with the Hollandsch Diep and the Biesbosch (Tönis et al., 2002). In the 14^{th} century dykes were built along the river, causing a decrease in the estuary area (Van Vessem, 1998). These hard structures had to be constructed to counteract chronic erosion. However, these changes were relatively small compared to the impact of the Delta Works. In 1953 the southern part of The Netherlands was flooded after a storm surge. As a reaction to this disaster, an earlier formulated flood safety plan, the Delta Project, was implemented. A part of this plan consisted in (partly) closing some of the tidal inlets in the southwest to shorten the coastline and reduce the risk of flooding due to storm surges. From 1957 until 1970 the closure works in the Haringvliet took place, disconnecting the basin from the rivers Rhine and Meuse and slowly creating a fresh water zone landwards of the Haringvliet Barrier. The dam was implemented with sluices, to enable control of the river discharge with a maximum capacity of $25.000 m^3/s$. The closure work significantly reduced the area of the remaining estuary.

3.3.2. LAND RECLAMATIONS

From 1967 to 1976 another major human intervention took place when the Port of Rotterdam was extended by Maasvlakte 1, north of the Haringvliet delta. A smaller land reclamation was completed in 1986, when the Slufter was built as an additional extension. This land reclamation, that served as storage basin for contaminated sediments dredged from the harbour, covered the northern part of the Hinderplaat. In 2013 the most recent extension of the port was completed: Maasvlakte 2. Between 2008 and 2013, $240 * 10^6 m^3$ were deposited to create this last port extension, of which the main part ($210 * 10^6 m^3$) was dredged from the North

Sea. The remaining part originates from dredging the port basins (Giardino et al., 2014). Maasvlakte 2 extends further west than the ebb-tidal delta ever had, sheltering the Haringvliet outer delta from NW waves (Elias and van der Spek, 2016).

3.3.3. MAINTENANCE DREDGING OPERATIONS

In the SE part of the estuary the channel Slijkgat is located, connecting the harbour of Stellendam to the North Sea. After the closure by the Haringvliet Barrier, the tidal prism of the fresh water discharge decreased causing the Slijkgat to become smaller. As its navigability had to be maintained, this channel has been dredged since 1983. The initial policy was to maintain a width of $200m$ at a depth of $NAP-4m$. In 2000 a new policy was adapted for a channel of 100m wide with a depth of $NAP-5m$. Over the past 20 years, a yearly average volume of $250*10^3m^3$ has been dredged to meet the requirements (Wegman, 2015).

3.3.4. NOURISHMENTS

The sand dam of the Slufter has been maintained with sand nourishments on the beach as well as on the shoreface adding nearly $12*10^6m^3$ of sand between 1991 and 2005. The coastline of Goerree was strengthened by means of sand nourishment from 1969 until 1985. Also the dunes at the tip of Voorne have been strengthened, adding $9.7*10^6m^3$ of sand in 20 years (Steijn et al., 2001). As part of the *Dynamic Maintenance Policy* the coastlines of Voorne and Goeree are currently evaluated yearly and nourished if necessary (Elias and van der Spek, 2016).

3.3.5. HARINGVLIET SLUICES POLICY

The Haringvliet Sluices allow fresh water run-off from the Haringvliet Lake into the North Sea during low water. Detailed information on the discharges through the Haringvliet Sluices in the past is given in Section 3.5.4. For many years the effects of implementation of different policies at the Haringvliet Sluices have been studied. In 2018 the new policy, *Kierbesluit,* will be implemented. This policy consists of almost permanently partly opening the sluices, causing saline water to enter the fresh water basin and creating a gradual transition zone. Only in case of very low river discharges, they will be completely closed (Rijkswaterstaat, 2017a).

3.4. MORPHOLOGICAL EVOLUTION

Morphological developments in the Voordelta are determined by a combination of the autonomous morphodynamics caused by the tide and waves, current changes of interventions of the past, current interventions and altering natural circumstances (e.g. sea level, climate) (Rijksinstituut voor Kust en Zee, 2007). This section gives a description of the morphodynamic evolution of the Haringvliet delta since the first closure. For previous developments is referred to Elias et al. (2015) and Elias and Van der Spek (2014).

3.4.1. DATASETS

Various previous studies have been carried out regarding the morphodynamics in the Haringvliet since 1950. In the past, this research was mainly conducted with bathymetry measurements and data analyses exploring trends and patterns of the morphology (Wegman et al., 2017). The RIKZ and RIZA execute monitoring programs to gather information used for deciding about national policies for the Dutch waters. These measurements are used for coastal zone management as well as for projects regarding the flood safety of the Netherlands (Wiegmann et al., 2005).

For the period after 1957, single-beam bathymetry measurements have been executed by Rijkswaterstaat. The obtained data is gathered in the *Vaklodingen* dataset. This dataset covers the entire Haringvlietmouth and its ebb-tidal delta up to the seaward $-20m$ contour, with a grid resolution of $20m$. Although measurements of the Dutch Delta are performed on yearly basis, the measured area may vary every year. The accuracy of the Vaklodingen data has been estimated between $0.11m$ and $0.40m$ (Perluka et al., 2006, Wiegmann et al., 2005). According to Marijs and Parée (2004) the total error of the data originates from three sources: (1) stochastic errors due to individual data outlines, which have been reduced from $0.48m$ (1969) to $0.36m$ (present). (2) Secondly, systematic errors are introduced by the measuring instruments. (3) The final source is variable systematic errors consisting of user errors in measuring and handling the data. All bathymetric data analyses conducted in these research are based on the Vaklodingen dataset.

3.4.2. LARGE-SCALE MORPHOLOGICAL DEVELOPMENTS OF CHARACTERISTIC PERIODS

This subsection describes the morphological evolution divided into characteristic periods. Figure 3.3 shows bathymetry maps of the Haringvliet ebb-tidal delta for the period of 1957-2015. It must be noted that the bed levels of the Haringvliet Lake and the Maasvlakte basins are not included in the plots.

1950-1964: BEFORE THE CLOSURES AND DIRECTLY AFTER DAMMING THE BRIELSE MAAS

Before its closure, the Haringvlietmouth showed typical characteristics of an ebb-tidal delta. The east-west driven currents created several deep channels surrounded by sandy shoals in the outer delta. The changes in the period of 1950-1964 have been described as follows: "A seaward extension in which the intertidal area approximately doubles. After closing the Brielse Maas the flats of the mouth evolved into a single flat, the Westplaat, while sedimentation took place in the channels. The height of the Westplaat increased from $NAP + 0.5m$ to $NAP + 0.9m$. Most changes took place north of the channel Gat van de Hawk, while the channel itself remained stable" (Van der Spek, 1987).

1964-1970: DAMMING THE BRIELSE GAT AND HARINGVLIET

In the period of 1965-1970, the remaining part of Brielse Gat and Haringvliet were both closed and the construction of Maasvlakte 1 started. This port extension was partly constructed on top of the Westplaat. The remaining part of the shoal grew towards the south and eventually merged with the coast of Voorne. Within a few years, the ebb-tidal delta experienced major changes when its channels filled in with mud while their orientation changed from shore-normal to shore-parallel. The Brielse Gat experienced severe sedimentation as a consequence of its closure. Changes in the orientation of the shoals were already observed before finalizing the closure of the Haringvliet in 1970: the former shore-normal Zeehondenplaat had changed into the shore-parallel Hinderplaat (Elias and van der Spek, 2016).

1970-1986: THE SUDDEN SHIFT AFTER THE CLOSURES

With the closure of the Haringvliet the tidal flow in cross-shore direction disappeared, causing a reduction of the tidal prism. This resulted in a decrease of sand supply by the ebb current, increasing the relative importance of wave-driven transport (Van der Spek, 1987). According to the theory, this should cause net sediment transport in landward direction and erosion of the delta front, which perfectly matches the observed morphological behaviour: after completing the closure of the Haringvliet in 1970, the long spit-shaped Hinderplaat grew rapidly in both length and height, creating a stable state sheltering the back-barrier area. In the meantime, the seaward edge of the ebb-tidal delta eroded (Elias et al., 2015). As a consequence of the decrease in current velocities, the channels siltated filling in with predominantly mud, except for the Gat van de Hawk that scoured as its discharge increased due to the new tidal current patterns (Rijkswaterstaat, 1973). Erosion of the Grevelingen ebb-tidal delta and sand nourishments on the coast of Goeree created a significant sediment supply from the SW. This resulted in accretion of the coast of Goeree, as well as an expansion of the spits of Kwade Hoek (Elias and van der Spek, 2016).

1986-1992: CONTINUOUS GROWTH OF THE HINDERPLAAT

During the construction of the Slufter the channel Gat van de Hawk disappeared and the new channel Hindergat was dredged. The Slufter covered the northern part of the Hinderplaat. Wave action remained to push the ebb-tidal delta landward, as the erosion of the front continued while the area behind Hinderplaat encountered siltation. The highly dynamic Hinderplaat still increased in height and length, although its width decreased as can be observed in Figure 3.3.

1992-PRESENT: DISAPPEARING OF THE HINDERPLAAT

The Hinderplaat started to decrease in height in 1992, although the southern part temporarily showed local sedimentation again around 1996. In 1993 the sandbar breached, creating the channel Gat van de Deur and slowly transforming the Hinderplaat into a new dynamic system with several small inlets. Since then ongoing sediment transport from the Hinderplaat towards the coast has been observed. At this moment the Hinderplaat is no longer a distinct bar, as it has spread out to the east forming a tidal-flat-like area (Elias et al., 2015). According to De Winter (2008) and Elias and van der Spek (2016) it is expected that the northern part of the Hinderplaat will continue spreading towards the north, eventually merging with the Slufter coast. The most recent land reclamation of the Port of Rotterdam, Maasvlakte 2, has provided even more shelter for the Haringvliet mouth from NW waves. This is likely to have a considerable impact on the morphology, although the exact consequences are still unknown.

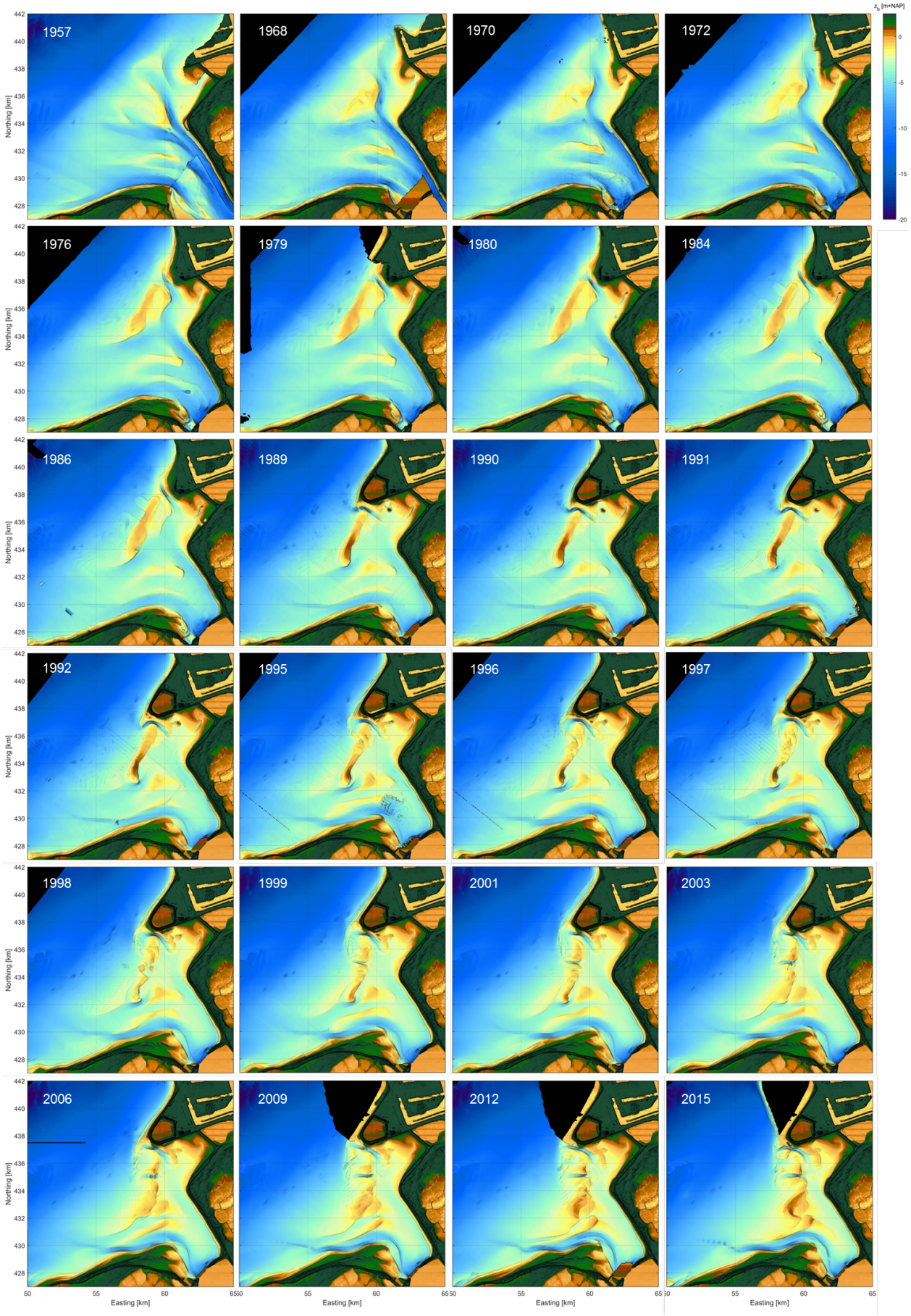

Figure 3.3: Ebb-tidal delta bathymetry from 1957 to 2015, based on the Vaklodingen dataset. Complete maps have been compiled by filling in missing data with measurement data of the nearest years available.

3.4.3. ORIENTATION OF THE HINDERPLAAT

Since the closure of the Haringvliet, the orientation of the Hinderplaat is characterised by an alignment that follows the orientation of the northern coast. This was first observed in 1976 and has lasted until the shoal breached and spread over the northern part of the outer delta (1995-2006). Remarkably, the orientation of the merged shoal at the current situation again seems to coincide with the orientation of Maasvlakte 2. Moreover, it is noteworthy that this also holds for the Bollen van den Ooster shoal in the Grevelingen outer delta, as shown in Figure 3.1. The correspondence between the alignment of the shoals and the orientation of the adjacent northern coastlines insinuates that longshore sediment transport rates induced by northern conditions play a key role in the existence of the shoals.

3.4.4. HYPSOMETRY

Figure 3.4 shows the cumulative hypsometric curve for the area of the Haringvliet outer delta. This area is defined in Figure 3.3 by the red outline. A hypsometric curve is a cumulative distribution function of elevations in a geographical area. It shows the proportion of land area at various elevations by plotting relative area against relative height. As the data do not cover the analysed area completely for every year, missing data has been completed with interpolation between the values of the nearest years for which data is available.

By analysing Figure 3.4 several trends can be observed in the ebb-tidal delta for the period of 1964-2012. The area of around $70 * 10^6 m^2$ with the highest elevation level (above $NAP - 5m$) has become higher over the years, while the part with the lowest elevation level has become even lower when comparing the curve of 1964 with the most recent one (2012). This matches the observed erosion of the lower shoreface. An exception is noticed for the period between 1980 and 1990: during this period the lower part of the curve shows an increase in height. However, it is more accurate to state that the total area of depth classes of $NAP - 20m$ until $NAP - 5m$ has increased, whereas the relative area of depth classes $NAP - 5m$ to $NAP + 15m$ has decreased. On the other hand, the intertidal area, between mean low water (MLW) and mean high water (MHW) around 0m NAP, has increased over the years as the basin has become more shallow. This is also indicated in Figure 3.5: when plotting the hypsometric data in time, while the colours indicate the depth classes, the change in distance between the lines shows how the area between the depth classes has changed.

The increase of intertidal area corresponds with the theory of Dronkers (2016), who states that at equilibrium deep tidal basins with a small relative tidal amplitude have a small intertidal area, while shallow basins have a relatively large intertidal area. This can have the consequence that shallow tidal basins with small tidal flats tend to import sediment, except for the case of strong negative asymmetry at the mouth. This analysis shows a transition zone between the two trends around $NAP - 5m$ height and $80 * 10^6 m^2$ area, yet this is strongly correlated with the chosen polygon. One should take into account that the turning point may change when also deeper stretches are included in the analysis. Overall the trend resulted in a steepening of the hypsometric curves over the years, except for the part around high water and low water.

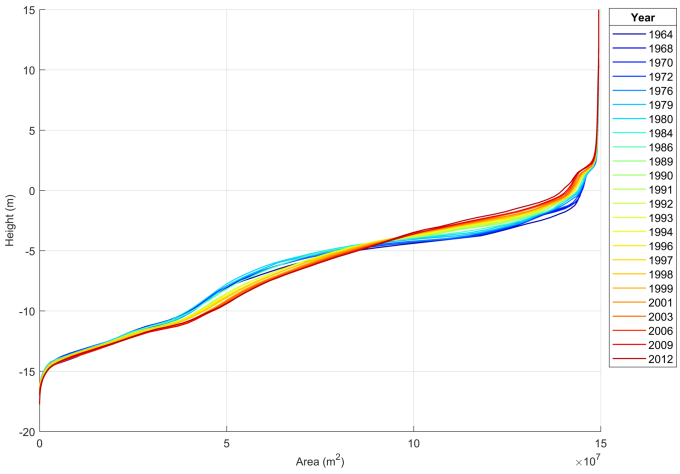

Figure 3.4: Hypsometric curve for the Haringvliet estuary, based on the Vaklodingen dataset. Heights are given in metres relative to NAP

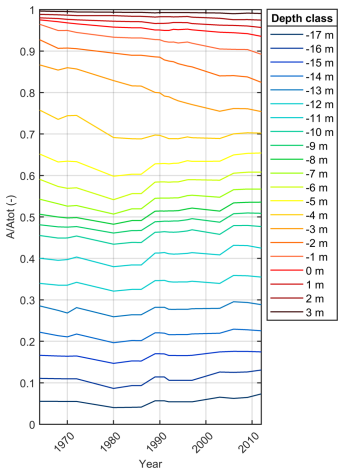

Figure 3.5: Hypsometric data plotted in time, depth classes are in metres relative to NAP

3.4.5. CROSS-SECTIONAL ANALYSES

HARINGVLIET EBB-TIDAL DELTA

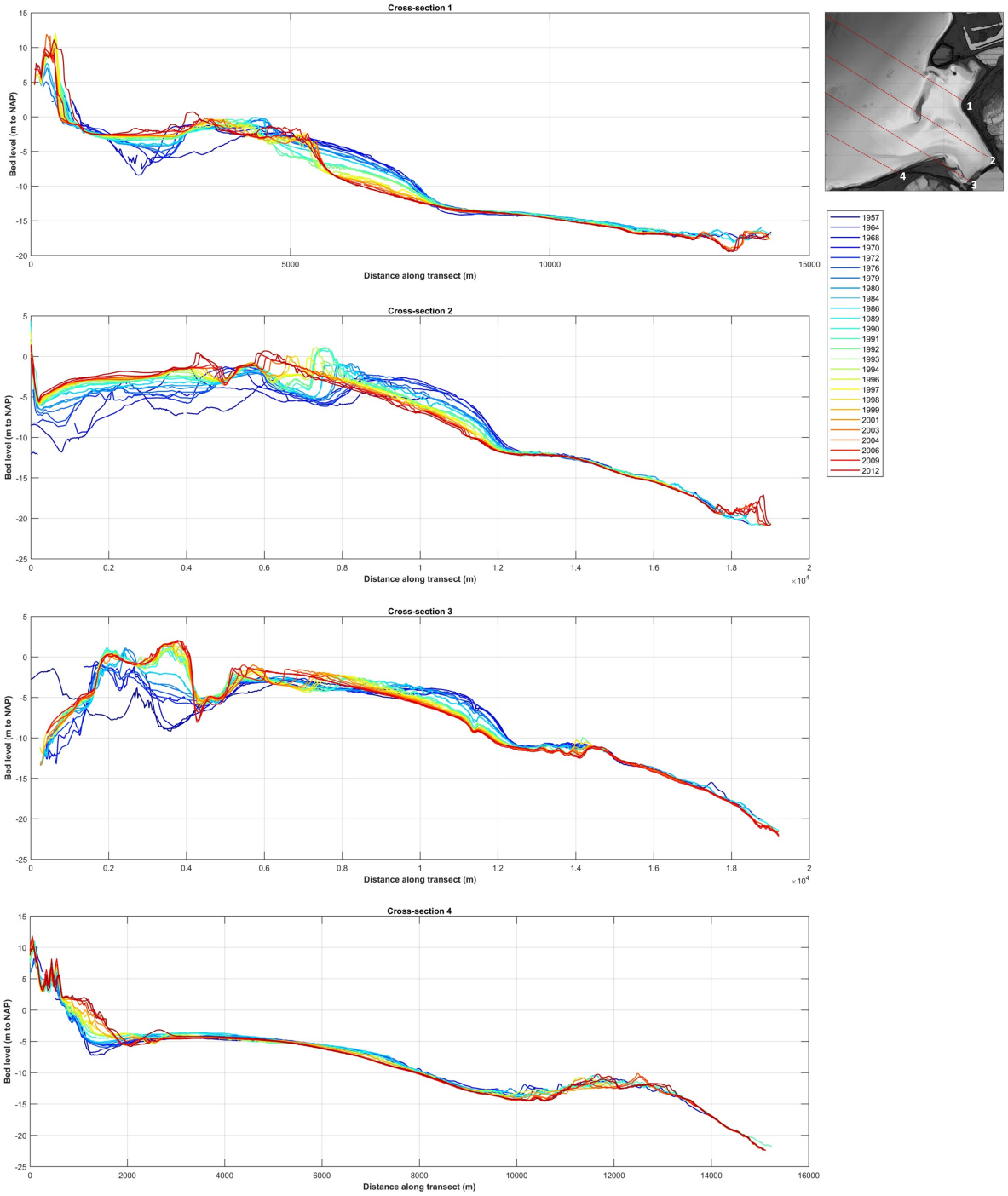

Figure 3.6: Cross-sectional evolution of the Haringvliet for the period 1957-2012, based on the Vaklodingen dataset

Figure 3.6 shows the development of four representative cross-sections of the Haringvliet. The first three cross-sections show a highly dynamic development over the years, whereas the fourth remains relatively stable. However, the topography below $NAP - 12m$, remains stable for all sections. Erosion of the delta front is clearly visible: this is a consequence of the decrease of the sediment supply by the ebb current and the relative increase in wave-driven sand transport (Elias and van der Spek, 2016). Landward directed sediment transport has led to a general accretion of the landward part of the outer delta as shown by the first three

cross-sections. A clear correlation is found, showing that the height decrease of the Hinderplaat started when the shoreface stopped eroding, around 1992. Cross-section 3 also shows the infilling of tidal channels around 1000 and 2500m distance. Besides, the expansion of the recurved spits of Kwade Hoek can also be recognized in this picture, as well as in Figure 3.3.

As previously stated, cross-section 4 has remained remarkably stable over the years compared to the other cross-sections. However, accretion of the shoreface and coast of Goeree can be observed, as a result of a large sediment supply from the southwest. This supply was fed by the erosion of the delta front of Grevelingen ebb-tidal delta and the sand nourishments on the coast (Elias and van der Spek, 2016).

HINDERPLAAT

To explore the evolution of the Hinderplaat into greater detail, the bathymetry changes of three cross-sections of this shoal and its back area are shown in Figure 3.7. Phenomena that stand out in all three cross-sections are the creation of the sandbar after 1970, its increase in height between 1985 and 1992, the decrease afterwards and its gradual landward migration in time. The peak height of the Hinderplaat (over $NAP - 1m$) is reached in its most southern part around 1992, as shown in cross-section 1. This cross-section also shows a fast infilling of the Rak van Scheelhoek channel after construction of the Haringvlietdam. A similar phenomenon is depicted by the first cross-section, showing rapid sedimentation in both the Brielse Gat and the Gat van de Hawk after damming of the Brielse Maas and during the construction of the Haringvliet Barrier. The landward sedimentation continued, filling the area behind the Hinderplaat over the years. Meanwhile, erosion of upper shoreface seawards of the Hinderplaat has taken place since the closures up until this moment, whereas erosion of the lower shoreface stopped when the height of the Hinderplaat stopped increasing.

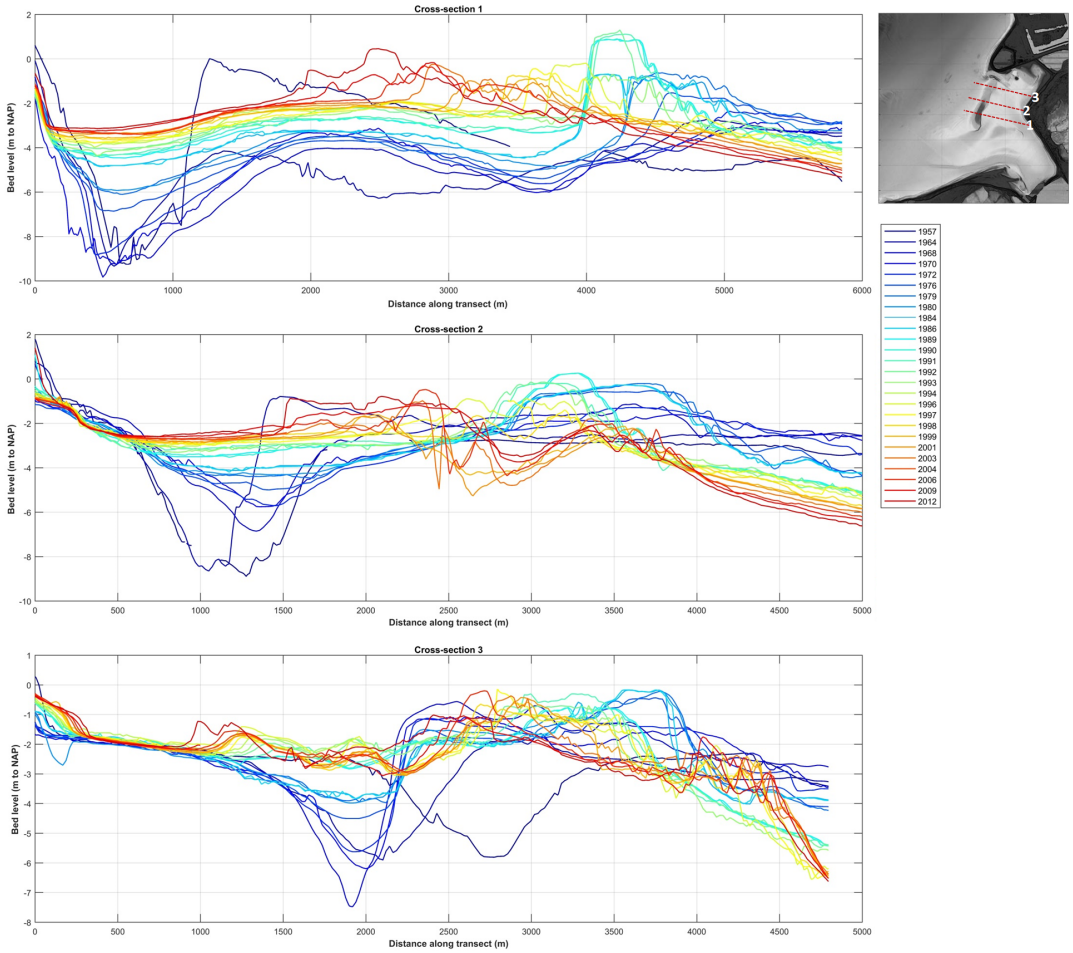

Figure 3.7: Cross-sectional evolution of the Hinderplaat and the sheltered back area for 1957-2012, based on the Vaklodingen dataset

HINDERGAT CHANNEL

After construction of the Slufter on top of the former Gat van de Hawk, the Hindergat channel was dredged in between the Hinderplaat and the dam. A main difference between these channels is their orientation: while the Gat van de Hawk curved in NW direction, the Hindergat was dredged with an orientation towards the SW at the seaward side. After construction the channel migrated towards the north until 2003, showing a displacement of more than 200m in less than 20 years, see Figure 3.8. Meanwhile, its depth remained similar during this period of time. Since 2003 the Hindergat has migrated to the south and it has become significantly more shallow. This corresponds with the moment when the Hinderplaat was largely spread over the northern part of the former ebb-tidal delta and had merged with the Garnalenplaat.

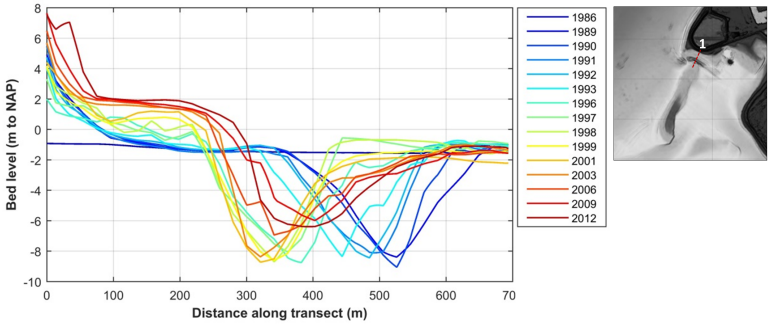

Figure 3.8: Cross-sectional evolution of the Hindergat channel for 1986-2012, based on the Vaklodingen dataset

3.4.6. PHASES OF THE EVOLUTION

A distinction has been made by Elias and van der Spek (2016) in three stages of development of the Haringvliet ebb-tidal delta for the adaptation period to the human interventions since the closure of the Haringvliet:

- *Phase 1* consists of the *dynamic equilibrium* prior to the closure, characterized by shore-perpendicular tidal flats and channels. During this phase dynamic channel migration could be observed, sometimes resulting in channel abandonment and infilling.

- *Phase 2* can be seen as the *distorted state* after damming the Haringvliet and Grevelingen estuaries. The reduction of the cross-shore tidal flow caused a regime shift, from a mixed-energy to a wave-dominated state. The decrease in tidal prism caused a decrease in the equilibrium ebb-tidal delta volume. Ebb currents were reduced and the relatively predominant wave energy moved sand onshore. While the shoreface eroded, sediment deposition took place in the landward part of the delta, see Figure 3.9a. An abundant supply of sediment caused the development of a long and narrow sandbar in coast-parallel direction: the Hinderplaat. This bar, that acted as a coastal barrier, provided shelter for the landward part of the Haringvliet outer delta. According to (Elias and van der Spek, 2016) the tidal system evolved from an ebb-tidal delta into a small-scale tidal inlet-tidal basin system.

- In *Phase 3 breaching and erosion* of the Hinderplaat took place. A new (dynamic) equilibrium between tides and waves-driven sediment transport had not been reached. Erosion of the shoreface and the Hinderplaat continued. As the sheltered landward part still contained accommodation space in the form of relatively deep channels, this caused rapid infilling by deposition of both sand and silt. Around 1995 the Hinderplaat breached, after which several small-scale inlets were formed. As the tidal exchange through these inlets is limited, they are likely to be closed by wave action. Storm events can form new breaches, (re)forming the tidal inlets in the Haringvlietmouth (Elias and van der Spek, 2016).

  In this research, the last phase is considered to be two-parted. In phase 3A most erosion of the Hinderplaat took place although it could still be considered as a distinct bar, whereas in phase 3B the former spit-shape can no longer be recognized. An analysis of the sedimentation-erosion patterns as shown in Figure 3.9, confirms that the evolution can be divided into the above-mentioned phases. The first phase has not been visualized since no digital bathymetry data are available for that period of time.

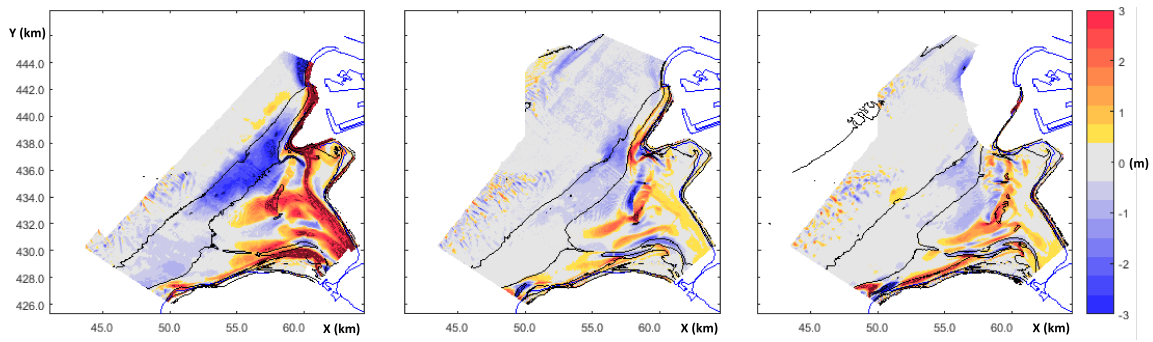

(a) Phase 2: 1968-1992 (b) Phase 3A: 1992-2001 (c) Phase 3B: 2001-2012

Figure 3.9: Initial bed level changes for the evolution-phases. Red indicates sedimentations an blue stands for erosion.

3.4.7. SEDIMENT BUDGET

The total sediment budget of the Haringvliet is determined by natural erosion/sedimentation processes and by dredging, dumping, sand mining and nourishment operations. The sediment budget of the Haringvliet has been explored in several studies in the past. Elias and van der Spek (2016) have presented a re-evaluation of the volume changes of the Haringvliet ebb-tidal delta, taking the development of the individual morphological units into account. The studied area is defined by the red polygon of Figure 3.2. The analysis is based on the Vaklodingen database. Since these data are not suitable for detailed analyses of beaches and dunes, these areas have been excluded from the results.

In the period of 1964-1976 the outer delta experienced a great increase in volume, see Figure 3.10. Although large morphology changes have been observed since then, the total volume change of the period afterwards is a lot smaller. According to Elias and van der Spek (2016) this is because the sediments can no longer be transported into the estuary and they are mainly redistributed instead. This redistribution is mainly caused by the natural shift of channels (Slijkgat, Bokkegat and Hindergat) and the Hinderplaat (Van Vessem, 1998). Note that although the net volume change is relatively small, the gross volume changes of the period 1976-2000 are significantly large. The large sedimentation rate between 1965 and 1980 might have been a result of the formation of the Hinderplaat. The created shelter for the back area made it possible for sediment to settle behind this sandbar. Since 1980 sediment losses of approximately $1 * 10^6 m^3/year$ have occurred. This volume decrease could be due to the consolidation of mud deposits in Rak van Scheelhoek (Elias and van der Spek, 2016). Lately, sediment losses have decreased again and the total volume of the Haringvliet outer delta has remained nearly constant since 2000.

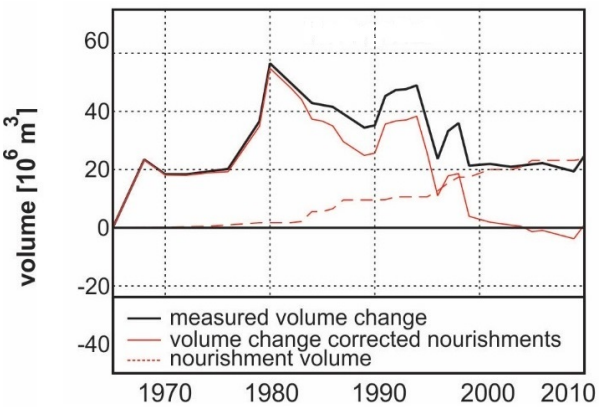

Figure 3.10: Cumulative volume changes of the Haringvliet ebb-tidal delta, retrieved from Elias and van der Spek (2016)

3.4.8. ADAPTATION TIMESCALE

It is difficult to determine the adaptation timescale of the Haringvliet and to predict the new (dynamic) equilibrium state. Morphological adaptations processes after major human interventions are very complex and different opinions have been given in previous research on this topic. While Van Vessem (1998) concluded that 40-80% of the morphological changes had occurred at that time, Tönis et al. (2002) stated that this should be even 93% by the year 2000. They based this conclusion on their derivation of the adaptation timescale of the Haringvliet. According to the calculations, the adaptation timescale of the largest homogeneous part of the estuary was only $T = 11 years$, although internal adaptations of small areas are still likely. However, this timescale may seem too small when considering the relation between time and spatial scales of coastal phenomena, as presented in Figure 2.7. Considering the sedimentation-erosion patterns of Figures 3.9a, 3.9b and 3.9c and the volumetric changes presented in Figure 3.10, it seems likely that the Haringvlietmouth is approaching its new equilibrium state. According to Elias and van der Spek (2016) it is expected that the ebb-tidal delta deposits will fill the tidal basin completely, merging with the coast and extending the coastal plain. However, implementation of the Kierbesluit policy may disturb this new equilibrium. This would again induce changes of the morphological units, forcing the outer delta towards a different state.

3.5. HYDRODYNAMIC FORCING

The morphology of deltas is largely determined by the local hydrodynamics. Four main driving forces affect the water levels and flow patterns in the Haringvliet: the tide, waves, wind and river discharge. This section discusses the driving forces and the regime shift that has taken place in the hydrodynamic classification of the Haringvliet after damming the estuary. Hydraulic data (waves, tides, water levels, etc) used for this research consist of public online data, based on long-term measurements provided by Rijkswaterstaat (2017b, 2018). The discharge data through the Haringvliet Sluices are based on daily averaged values, which are yearly computed with a numerical model.

3.5.1. TIDAL REGIME

The semi-diurnal North Sea tide travels from north to south along the Dutch coast. The amplitude along the coast varies to a large extent due to the topography of the North Sea basin (Dronkers, 1998): along the west coast it decreases from south to north, with values of $3.8m$ at Vlissingen, $2.1m$ at the Haringvliet and $1.4m$ in den Helder (De Vries, 2007). The tidal signal just seawards of the Haringvliet outer delta for January and February 2018 is depicted in Figure 3.11. This signal shows significant spring-neap variations and a daily inequality, which is mainly present during spring-tide. Note that the tidal levels on the right are an indication based on the tide of these two months and may vary when analysing the tidal signal for a longer period.

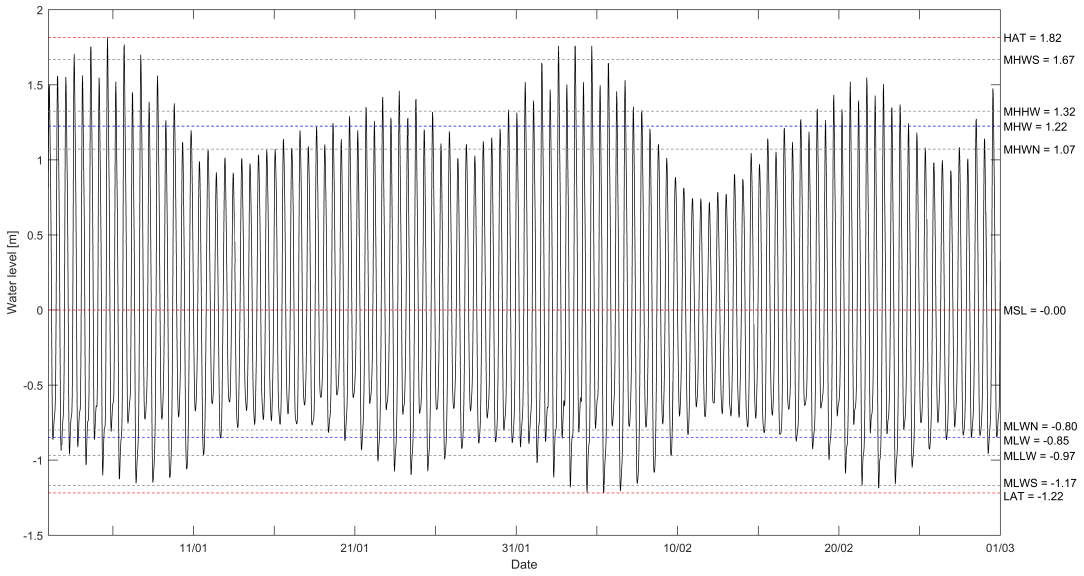

Figure 3.11: Tidal signal containing four spring-neap tidal cycles in front of the Haringvliet outer delta. Retrieved from *Delft Dashboard* measuring station: Xtide Tidal Station Haringvliet 10

Before the closure, the Haringvliet was a long basin, causing a phase difference between tidal velocities inside the estuary and the longshore tidal velocities offshore, see Figure 3.12a (Sha and Van den Berg, 1993). A four phase cycle could be observed in the Haringvliet mouth, as depicted in Figure 3.12b. The phases were described as follows:

1. At high tide flood currents occur both outside and inside of the estuary.
2. Approximately 3 hours after high tide the current outside of the estuary is in flood direction and the current inside is in ebb direction. This causes water to flow from the estuary into the North Sea.
3. At low tide ebb currents occur both outside and inside of the estuary.
4. Approximately 3 hours after the first low tide the current outside of the estuary is in ebb direction and the current inside is in flood direction. This causes water to enter the landward part of the estuary.

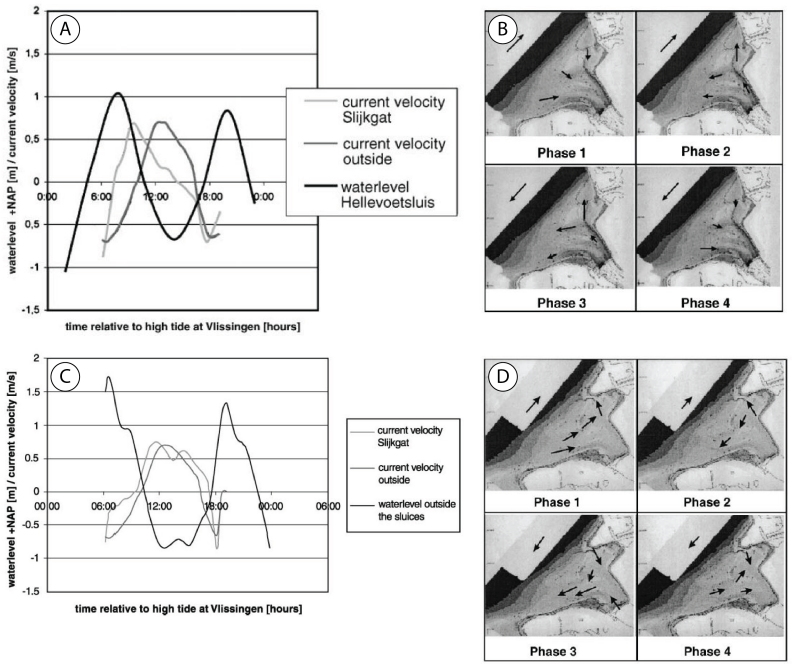

Figure 3.12: Propagation of the tide in the outer delta before and after construction of the Haringvliet Barrier. A: Current velocities and water level before closure, B: Current patterns in the Haringvliet before closure, C: Current velocities and water level after closure, D: Current patterns in the Haringvliet after closure (Tönis et al., 2002)

Because of the Haringvlietdam, the tide could no longer enter the landward part of the estuary. The estuary changed into a short tidal basin, with currents leading the water level by 90°. A reduction of tidal prism caused a decrease in current velocities. The current patterns changed in the new situation showing a circular character. Again four phases could be recognized during a tidal cycle, see Figure 3.12d. Tönis et al. (2002) described them as follows:

1. At high tide the water enters the Haringvliet at the south side and leaves at the north side.
2. Approximately 3 hours after high tide the current inside of the estuary is in ebb direction, while the current outside is in flood direction.
3. At low tide the water enters the estuary at the north side and leaves at the south side.
4. Approximately 3 hours after low tide the current outside of the estuary is in ebb direction and the current insidenumerate

Damming the Haringvliet caused a reduction in flow velocities of 35-80%. Furthermore, the maximum flow velocities during flood have become larger than the maximum ebb-flow velocities. This phenomenon is also known as a *peak-flow asymmetry* called *flood dominance*. This results in a net current related sediment transport in landward direction, which matches the observed morphological behaviour of the Haringvliet. This sediment transport mechanism is further elaborated in Section 2.4.

3.5.2. WAVE CLIMATE

The Voordelta is a mixed-energy environment which combines the influence of tidal and wave processes. Its wave climate mainly consists of wind waves, locally generated in the North Sea basin. Figure 3.13 gives an overview of the wave climate in the Haringvliet outer delta. Wave energy fluxes from southwest to west direction generally dominate on the Hinderplaat, although northwesterly waves with longer periods arrive on regular basis at the Haringvliet.

As waves approach the Haringvliet, the bathymetry becomes shallower and the waves tend to deform due to shoaling, refraction and wave breaking. The accretion that has been taking place since the damming of the Haringvliet, has caused waves to break more seaward (Tönis et al., 2002). This increase in energy dissipation has reduced the influence of waves in the vicinity of the dam (Rijkswaterstaat, 1973). At this location mostly the tidal influence is noticed: waves generally do not arrive here since the largest amount of wave-energy is dissipated on the flats in the front. In the western part of the estuary waves are most dominant, as this location is most exposed to wave action. This is a well known phenomenon: in tidal inlets, the wave-driven currents around the shoals on the outer delta can be so strong that they dominate the tidal residual currents (Bosboom and Stive, 2013).

The effect of northwesterly waves inside the Haringvliet decreased due to the land reclamations of Maasvlakte 1 and the Slufter (Tönis et al., 2002). Because of the land reclamation of Maasvlakte 2, the influence of northwesterly waves has decreased even more.

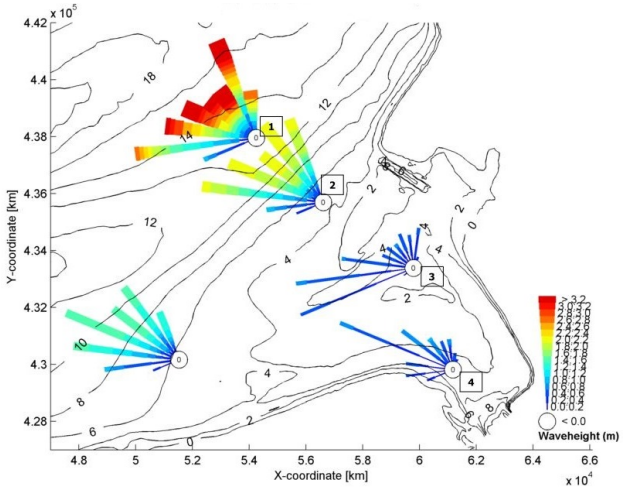

Figure 3.13: Waveclimate at the Haringvliet ETD. Retrieved from De Winter (2008)

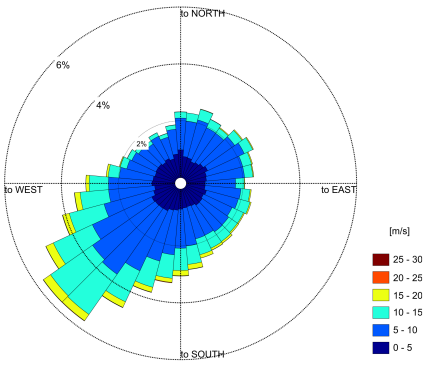

Figure 3.14: Windclimate at Europlatform. Data retrieved from Rijkswaterstaat (2018)

3.5.3. WIND FORCING

Wind-driven currents are an often forgotten type of currents in tidal basins, while wind-driven flow is likely to provide a significant contribution to residual currents and thereby also net sediment transport in shallow areas, as described in Section 2.3.4 (Wang et al., 2012). The wind at the Haringvliet is typically southwesterly (see Figure 3.14), with mean wind speeds of $7.5 m/s$ measured at the windstations *Europlatform* and *Lichteiland Goeree* (Rijkswaterstaat, 2017b). However, mainly winds from the northwest cause set-up, since this is the direction with the largest fetch. This set-up can reach values of $1.5 m$ (De Winter, 2008). An extreme storm in the Southwest Netherlands occurred on January 25^{th} 1990, with wind speeds of $30 m/s$ generating waves of over 6m height at Europlatform (Rijkswaterstaat, 2018).

3.5.4. DISCHARGE THROUGH THE HARINGVLIET SLUICES

The fresh water run-off from the Haringvliet Lake influences the hydrodynamics in the Haringvlietmouth. Water run-off is only permitted around low water: the locks are opened 3.5 hours before low water and closed 3.5 hours after (De Vries, 2007). Usually discharge through the locks occurs every tide, although a large variation in released volume can be observed throughout the year (De Winter, 2008).

The sluices have a maximum capacity of $25,000 m^3/s$, although on average only during 1.3% of the year, the discharge exceeds $4000 m^3/s$ (Rijkswaterstaat, 2017b). When the discharge is smaller than $2000 m^3$, which occurs 89.9% of the time, the water flows into the sea through the Slijkgat. Only small velocities of less than $0.2 m/s$ are induced by the fresh water run-off. In case of discharges between $2000 m^3$ and $4000 m^3$, occurring in the remaining 8.8% of the time, a small part also flows through Rak van Scheelhoek, the Hindergat and over the Garnalenplaat. In this case the discharge induced flow velocities upto $0.4 m/s$ near the sluices. A discharge larger than $4000 m^3$ covers the entire Haringvlietmouth (De Vries, 2007). Since under regular circumstances most of the discharge reaches the sea through the Slijkgat, it is likely that this will mainly affect the dynamics of this channel (De Winter, 2008). Nevertheless, De Vries (2007) concluded that prescribing a high river discharge at the sluices can lead to large morphological changes to the Hinderplaat: various connecting channels can be formed on the flat, as a result of large water level gradients. Moreover, when great volumes of fresh water flow over the seawater a landward directed undertow is generated and consequently sediment transport is enhanced in landward direction. The correlation between high discharges and wave and wind conditions was studied in a previous study: it was found that high river discharges hardly ever go together with storm conditions (Steijn et al., 2001).

Figure 3.15 shows an analysis of the discharge volumes since 1971. The mean yearly discharge lies around $1000 - 2000 m^3/s$ for the entire period, without showing rarely high values in any year. Yet, the results of the maximum discharge per year (which is based on a daily averaged value) show exceptionally low values for the years 1976 and 1985 as well as above average values for 1993 and 1995. The largest computed daily discharge was reached in February 2^{nd} 1995 (during the 1995 flooding in the Southeast Netherlands), when the fresh water run-off reached an average value of $9015 m^3/s$. A period of extremely high discharges has been observed around that day: during 8 days the average discharge through the sluices exceeded $7000 m^3/s$.

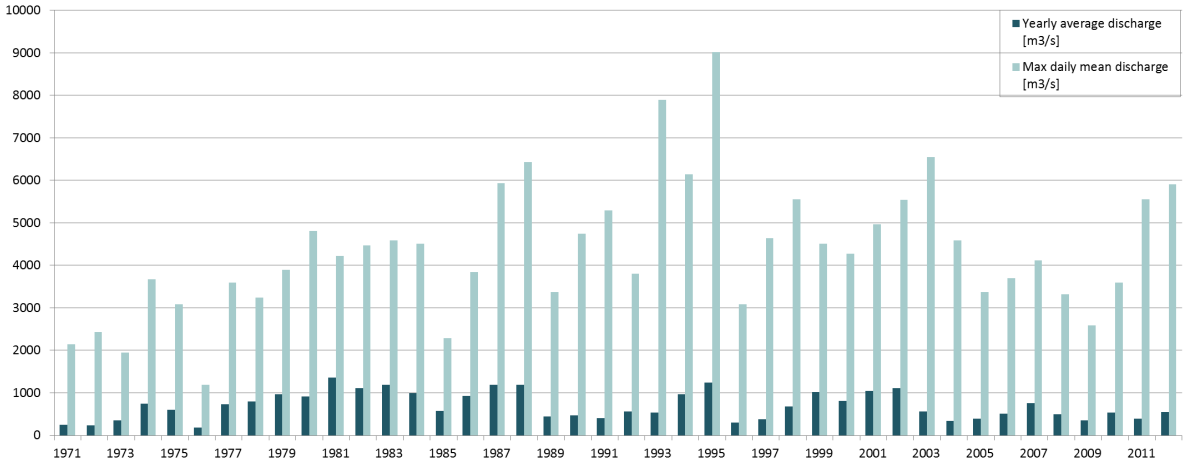

Figure 3.15: Discharge data of the Haringvliet Sluices for 1971-2012. Data retrieved from Rijkswaterstaat (2017b)

3.5.5. HYDRODYNAMIC CLASSIFICATION

The four main hydrodynamic drivers do not influence the Haringvliet equally, as for every location some processes may be more dominant that others. According to the classification of Davis and Hayes (1984) (modified after Hayes (1979)), the inlet of the Haringvliet would qualify as mixed-energy before the closure. Damming the estuary resulted in a regime shift towards a wave dominated area (Cleveringa, 2008). De Winter (2008) determined the hydrodynamic classification for the following locations of the Haringvliet: (1) the northern part of the shoreface, (2) west of the Hinderplaat, (3) north of the Granalenplaat and (4) near the dam. The exact locations are shown in Figure 3.13. To determine the classification the mean wave height for each of the locations was determined by SWAN calculations. The tidal range is based on the work of Steijn et al. (2001). The results of the classification are shown in Figure 3.16. The outcome for the first two locations correspond with the statement of (Cleveringa, 2008). The latter two are classified as tide-dominated, since the mean wave height is a lot smaller in the shallow and sheltered landward side of the basin.

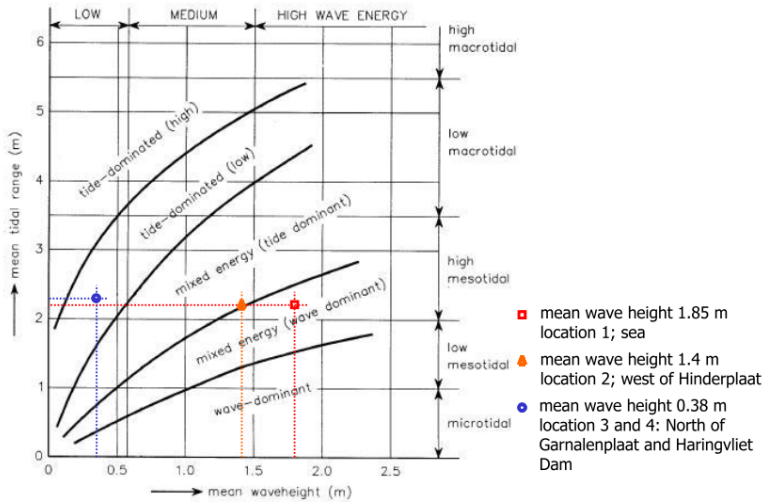

Figure 3.16: Hydrodynamic classification of four locations in the Haringvliet. Location numbers correspond with numbers in Figure 3.13. Based on Hayes (1980) from De Winter (2008)

3.6. BED COMPOSITION

Most of the sediment in the Haringvlietmouth was disposed in the outer delta during the formation of the estuary. Only a small part originates from the Rhine and Meuse (Van Vessem, 1998). After the closure most sediment supply came from the southern coast of Goerree, the Bollen van de Ooster tidal flat and the seaward edge with the North Sea. A very small amount, which mainly consists of mud, originates from the deeper parts of the Northsea.

Figure 3.17 shows measurement results of the median grainsize and the mud percentage in the Haringvliet. The first 2 years after the construction of the Slufter, the median grainsize decreased. However, in the period after 1987, this value increased again. The increase in grain size was clearly found at the seaward end of the ebb-tidal delta, at the Hinderplaat and at the sheltered landward part of it. Van Vessem (1998) relates this to a supply of coarser sediment from the North Sea and from Bollen van de Ooster. The increase in grainsize at the Hindarplaat is probably also a consequence of the construction of the Slufter and the dredging activities at the coast of Voorne.

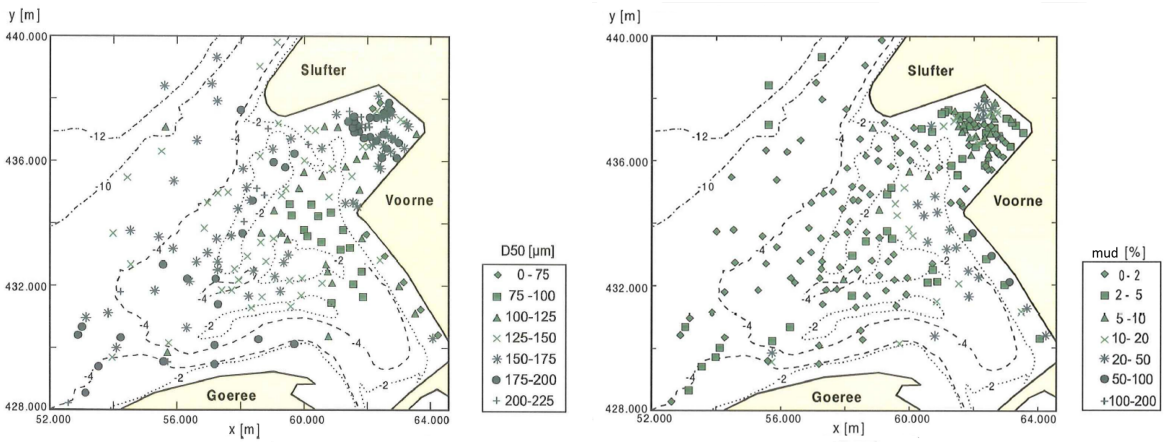

(a) Median grainsize

(b) Mud-percentage

Figure 3.17: Sediment properties in the Haringvliet ebb-tidal delta. From Van Vessem (1998)

3.7. SYNTHESIS

Based on the information presented in this chapter, conclusions are defined to answer the first two research questions. Before the closure of the Haringvliet estuary, the ebb-tidal delta was in dynamic equilibrium, characterized by shore-normal shoals and flats, maintained by a combination of the tidal force in long- and cross-shore direction and the wave action (phase 1 of the evolution). Since 1968 the shore-normal Zeehondenplaat started to alter its orientation, eventually changing into the shore-parallel Hinderplaat, whose pronounced spit-shaped geometry was obtained around 1976. This is defined as phase 2 of the evolution, also referred to as the distorted state of the ebb-tidal delta after damming the estuary. Subsequently, the shoal migrated landwards and grew both in length as in height. This went on until 1992, when its degradation started. The period of degradation and breach of the Hinderplaat is defined as phase 3 of the evolution: in phase 3A the shoal eroded while still travelling landwards. In phase 3B the shoal spread and merged with the Garnalenplaat and the coast of Voorne.

In general, the degradation of the Hinderplaat can be divided in the following developments: a landward migration since its formation, general lowering since 1992 and breaching and channel formation in 1995. Moreover erosion of the lower shoreface was observed approximately until the moment when the Hinderplaat started to decrease in height, although the upper shoreface on the seaward side of the Hinderplaat continued eroding. Additionally, a northward migration of the adjacent channel Hindergat took place until 2003.

The Haringvliet has been subject to several human interventions in the past. In the 14^{th} century dykes were built along the river, which caused a decrease in the estuary area. However, these changes were relatively small compared to the implemented the Delta Works. Between 1950 and 1970 the Brielse Maas and the Haringvliet were dammed. A year later also the Brouwersdam was constructed. Moreover, the Port of Rotterdam has been extended several times, with the construction of Maasvlakte 1 & 2 and the Slufter. The coasts of Voorne and Goerree and the Slufterdam have been nourished regurlarly since 1969, whereas the Slijkgat has been dredged to maintain its navigability.

The two most relevant types of extreme events are considered in this analysis, namely extremely high discharges through the Haringvliet Sluices and exceptionally strong storm events. Both in 1993 and 1995 exceptionally high daily values were observed for the water run-off through the sluices. The highest discharge, observed on February 2^{nd} 1995, exceeded the value of $9000 m^3/s$. An extreme storm event in the Southwest Netherlands occurred on January 25^{th} 1990, with wind speeds of $30 m/s$ generating waves of over $6 m$ height at Europlatform (Rijkswaterstaat, 2018). Conclusions regarding the general hydrodynamic forcing and sediment properties (Sections 3.5 and 3.6) do not directly give answers for the research questions, but provide information for the setup of the numerical model. Therefore, they are not treated here.

4

HYPOTHESES AND MODELLING METHODOLOGY

4.1. INTRODUCTION

The literature review and data analysis presented in Chapter 3 provide insights into the processes that have led to the formation of the Hinderplaat. The processes driving the observed ongoing degradation of the Hinderplaat are however still poorly understood. A 2DH Delft3D model is used to investigate the underlying mechanisms and to explore their link with former anthropogenic interferences and meteorological events. Based on the results of the literature review and data analysis, hypotheses are formulated regarding the degradation of the Hinderplaat; these are presented in this chapter (Section 4.2), followed by the modelling methodology to test them (Section 4.3).

4.2. HYPOTHESES

The degradation of the Hinderplaat can be divided in three main separate developments, as described in Section 3.7. The processes that are responsible for the morphological evolution of an outer delta may be related to *human interventions* or *extreme meteorological events*, or they may be a part of the *intrinsic behaviour* of the intertidal shoal under regular conditions. The proposed hypotheses are therefore divided into these three categories.

4.2.1. HUMAN INTERVENTION-RELATED

As shown in Section 3.4 the degradation of the Hinderplaat started around 1992: until that moment the Hinderplaat had become longer and higher, but in 1992 its height started to decrease while its landward migration continued. This deformation of the Hinderplaat could be linked to the extensions of the Port of Rotterdam. Maasvlakte 1 was constructed between 1967 and 1976. After this period sedimentation of the Hinderplaat took place, for which it is unlikely that this intervention caused the degradation. The same holds for the Slufter: after completing the construction the Hinderplaat still increased in height. Moreover, it gained its pronounced spit-formed shape, remarkably following the orientation of the Slufter. It is erroneous to link the degradation of the Hinderplaat to the construction of Maasvlakte 2: the degradation started 20 years before this intervention took place. So, while the formation of the Hinderplaat is proven to be a consequence of human interventions in the study area, based on the knowledge gathered in Chapter 3 we can state that it is unlikely that its degradation had a similar cause.

4.2.2. EXTREME EVENT-RELATED

The evolution could be a consequence of events as storms or an unlikely high discharge through the sluices, since severe (meteorological) events can have an irreversible impact on the delta morphology (De Vries, 2007). An extreme storm in the Southwest Netherlands occurred on January 25^{th} 1990, with wind speeds of $30 m/s$ generating waves of over $6m$ height at Europlatform (Rijkswaterstaat, 2018, Van der Kruif, 2017). Yet, it is highly unlikely that such a storm was the cause of the lowering and landward migration of the Hinderplaat,

as this has been a gradually ongoing process since 1992 instead of an abrupt change of the development.

In 1993 and 1995 extremely high river discharges were measured at the Haringvliet Sluices, as shown in Figure 3.15. The most extreme fresh water run-off was detected on February 2^{nd} 1995. Previous research has shown that high river discharges cause large water level gradients, possibly enhancing the creation of channels on the Hinderplaat (De Vries, 2007). Therefore it is plausible that the breach that is visible in the bathymetry map of 1995, has been a consequence of the high river discharge in February. This cannot be verified by merely using the bathymetry data as only yearly data is available.

4.2.3. INTRINSIC BEHAVIOUR

The degradation of the Hinderplaat might also be the intrinsic behaviour of the shoal, without having a link with human interventions nor extreme events. It seems possible that the sedimentation of the shoal was meant to stop when the erosion of the foreshore finalized. It is however poorly understood which mechanisms (e.g. tide, wave conditions, wind and density driven currents) are responsible for which part of the development.

4.2.4. FORMULATED HYPOTHESES

With the conclusions of the previous chapter and the reasoning of the previous subsections, the following hypotheses have been formulated:

1. *Current patterns in the Haringvliet ebb-tidal delta are strongly influenced by the wind forcing, considering the limited depth of the area.*
2. *Wind effects are of major importance for the morphological evolution of the Hinderplaat and its surrounding channels.*
3. *The landward migration of the Hinderplaat is part of its intrinsic behaviour under regular conditions, rather than a consequence of human activities and sporadic events.*
4. *A reduction of the sediment availability of the foreshore combined with ongoing landward directed sediment transport in the back-barrier area caused the shift from an increase to a decrease in the height of the Hinderplaat in 1992.*
5. *Longshore sediment transport rates induced by northern conditions play a key role in the existence of the Hinderplaat.*
6. *Breaching of the Hinderplaat was a consequence of the high discharge event of February 1995.*

4.3. METHODOLOGY

To test the hypotheses, a modelling study with a Delft3D model has been performed. The complex bathymetry of the study area causes a spatial variability in flow patterns and sediment transport. The use of a process-based model is required to solve the flow and sediment transport rather than using a semi-empirical or conceptual model. Delft3D is a process-based model that describes waves, currents, sediment transport and bed level changes via a set of mathematical equations based on physical principles (De Vriend and Ribberink, 1996). Data sets are only used for calibration and validation purposes. It is not the aim to reproduce the exact morphological development of the outer delta, but to determine how the forcing mechanisms have influenced the evolution of the Hinderplaat.

Since the first five hypotheses are related to the natural behaviour of the system, numerical simulations serve to investigate the relative importance of tidal-, discharge-, surge-, wind- and wave-driven flow for the hydrodynamics and the sediment transport in the study area. To test hypothesis number six, a morphodynamic hindcast is performed.

All simulations are done in 2DH mode, which corresponds to solving the depth-averaged non-linear shallow water equations. Three-dimensional morphological simulations over a long period are not feasible, because of the excessive computation times involved.

4.3.1. MODELLING THE INTRINSIC BEHAVIOUR UNDER REGULAR CONDITIONS

The Delft3D model is used to obtain insight in the physics behind the observed morphodynamic changes of the ebb-tidal delta and to identify the relevance of the governing processes and mechanisms. This is done by running the model with varying imposed forcing and determining its initial sedimentation/erosion (ISE) response. Simulations are performed with different conditions for the tide, river discharge, surge, wind and waves. In Table 4.1 an overview is given of the performed simulation scenarios and their forcing. The last row shows which simulations have to be compared to evaluate the corresponding process. Due to model limitations, the schematisation of the surge levels is limited to water level changes, imposed over the entire offshore boundary: water level gradients are not accounted for (see Section 5.4). One should therefore keep in mind that the identification of the contribution of surge-forcing is far from complete, as especially the gradients are likely to have an impact on the morphodynamics.

Table 4.1: Overview of the simulations scenarios and forcing processes. The last row shows which simulations have to be compared to evaluate the corresponding process. Surge level gradients along the offshore boundary are not accounted for, therefore the quasi-real time simulations are not completely realistic (marked grey).

			Process		
Simulation	***Tide***	***Discharge***	***Wind***	***Waves***	***Surge***
A. Tidal forcing only	yes	no	no	no	no
B. Tide and Q_{river} forcing	yes	yes	no	no	no
C. No wind forcing	yes	yes	no	yes	no
D. No wave forcing	yes	yes	yes	no	no
E. All processes	yes	yes	yes	yes	no
F. Quasi-real-time	yes	yes	yes	yes	yes
Process definition	A	A-B	C-E	D-E	E-F

The wave and wind climate at the study area is split into a large number of conditions, to examine the individual impact of each of them. Each condition is run for a simulation period of over two weeks, containing constant values for the wind speed, direction, the wave height and direction and the surge levels. This is not realistic, but it does give a clear indication of the effect of the imposed forcing. Once again, one should keep in mind that it is not the aim to reproduce the exact morphological development of the outer delta, but to determine how the forcing mechanisms have influenced the evolution of the Hinderplaat.

Sediment transport computations are initiated after a 1488 minutes hydrodynamic spin-up time (two tidal cycles). Then, the model is run for a simulation period of 30 tidal cycles to dissipate the errors induced by the discrepancy between boundary conditions and the initial state of the bed levels (morphological spin-up time). To reduce the computational time only 6 tides are simulated with a morphological acceleration factor (MorFac) of 5 (see Lesser, 2009, for more information on this parameter). Subsequently, two tidal cycles are simulated with a MorFac of 0.1, which is small enough to represent a morphostatic simulation. In morphostatic simulations the bottom is assumed to be fixed, which is valid under the assumption that significant changes in the bottom morphology occur on much larger timescales than the timescales involved with the adaptation of the flow and transports. This is the case as the simulation period is too short to simulate real morphological feedback between morphology and hydraulic forcing. However, it is long enough to show the differences in sediment transport between the modelled scenarios. The model results are obtained from the results of the two final tidal cycles.

4.3.2. HINDCASTING THE 1995 DISCHARGE EVENT

To determine whether breaching of the Hinderplaat occurred during the extreme discharge event of February 1995, a hindcast run is performed in which the forcing conditions are simulated as realistic as possible. During eight consecutive days, the daily mean discharge exceeded $7000 m^3/s$. This period is simulated with a MorFac of 1, after a spin-up time of two tidal cycles. The processed time series of the river discharge through the sluices and the measured wind and wave climate are provided by Rijkswaterstaat. A major part of the event took place during spring-tide. This is reproduced by multiplying the morphological tide by a factor of 1.28 (see Section A.2).

5

MODEL SETUP

5.1. INTRODUCTION

This chapter treats the setup of the Haringvlietmodel in Delft3D, building on the proposed methodology of the previous chapter. The grid and bathymetry schematisation are shown in Section 5.2. Subsequently, the FLOW- and WAVE-modules and their settings are described in Section 5.3, after which with the derivation of the imposed boundary conditions is described in Section 5.4. Model calibration and validation has been carried out in previous research, which is summarised in Section 5.5.

5.2. GRID AND BED SCHEMATISATION

Delft3D makes use of curvilinear staggered grids, which form the base of the numerical scheme on which the equations are computed. In a staggered grid not all quantities, such as the water level, the depth, the velocity components or concentration of substances, are defined at the same location in the numerical grid (Deltares, 2014a). The depth points are defined at the center of the grid cells, while velocity points are computed for the center of the grid cell sides and water levels at the grid cell corners. A computational grid must be large enough to prevent that boundary disturbances enter the area of interest. However, it is preferable to limit the number of grid points to reduce the computational time. Moreover, the resolution of the grid should be higher in the areas of interest. Keeping these requirements in mind, an optimal computational grid has been constructed in previous studies (Steijn et al., 2001, Van Holland, 1997).

The model makes use of three grids: one used by the FLOW-module and two used within the WAVE-module. The FLOW-grid covers the area between *Noordwijk* (northern boundary) and *Nieuw Haamstede* (southern boundary). The larger grid used in the WAVE-module covers a part of the North Sea, whereas the second grid only covers the Haringvliet delta with a higher resolution: the size of the grid cells within the outer delta is in the order of $50x50m^2$, while the size of the cells covering the North Sea is in the order of $600x600m^2$. The small WAVE-grid is nested in the larger one and combined the two WAVE-grids cover the entire FLOW-grid. At the southern boundary the large WAVE-grid even extends the FLOW-grid, since boundary disturbances due to the waves are too eminent in this part. By extending the WAVE-grid one ensures that waves are fully developed once they enter the FLOW-grid (De Vries, 2007). Figure 5.1 shows the grids of the Haringvlietmodel.

Data from the Vaklodingen set of 1992 have been used to schematise the bathymetry. Depending on the resolution of available observations, depth measurements have been triangularly interpolated or grid-cell averaged to the curvilinear grid. The obtained bathymetry has been smoothened to reduce the small-scale disturbances. In previous studies two sediment fractions were implemented in the model to model both sand and mud transport. Measurements had shown where the most mud was present in the Haringvliet delta; this was represented in the model by placing layers of mud on several parts of the bathymetry. In this study the sediment schematisation is limited to only sand with a median grain size of $160\mu m$. This is done for two reasons: first of all the research focus is on the Hinderplaat area, where practically only sand is present (see Figure 3.17b). Besides, to add mud transport first information on the initial mud deposits is needed for the simulated period and this information is not available for the simulated period.

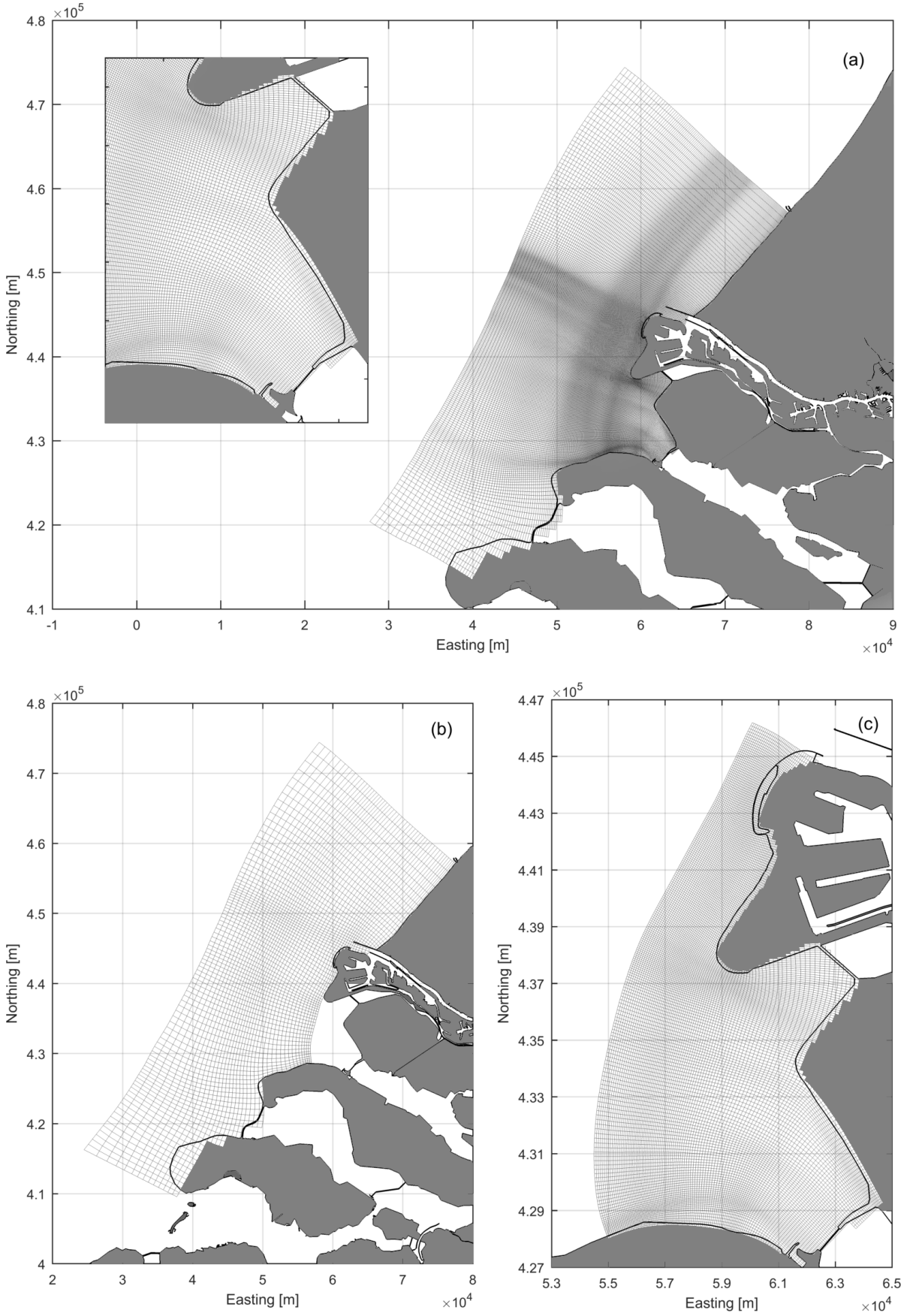

Figure 5.1: Delft3D model grids for (a) flow, the insert on the left shows details of the grid at the Haringvlietmouth, (b) large-scale wave grid at the North Sea and (c) detailed wave grid

5.3. MODULES SETUP

The hydrodynamic module of Delft3D, Delft3D-FLOW, solves the Navier-Stokes equations for an incompressible fluid, under the shallow water and the Boussinesq assumptions. The unsteady shallow water equations can be solved either 3D or in depth averaged mode. For this research the model is used in 2DH mode, so the vertical momentum equation is reduced to the hydrostatic pressure relation. This is possible as vertical accelerations are assumed to be small compared to the gravitational acceleration. The equations are solved with the Alternating Direction Implicit method in the horizontal direction. Since the solution is implicit, the numerical stability is not restricted by the time step Δt or the grid size Δx. Nevertheless, the accuracy of the flow computations decreases with an increasing Δt. A time step of $\Delta t = 30\,s$ is chosen, as it is small enough not to affect the results compared to computations with smaller time steps.

Waves are computed in the module Delft3D-WAVE which uses SWAN to simulate the evolution of random, short-crested waves (Deltares, 2014b). SWAN is a third generation numerical wave model that is based on a discrete balance of action density: waves are described by using the 2D wave action density spectrum. The numerical scheme used to compute wave propagation is implicit, making it unconditionally stable regardless of the water depth. The online WAVE module accounts for wind generation, dissipation by wave breaking, white-capping and bottom friction, non-linear wave-wave interaction and wave propagation through obstacles. In this study the JONSWAP type of density spectrum is applied as a boundary condition. To consider the effect of waves on currents and vice versa the WAVE and FLOW modules are coupled by imposing a dynamic interaction between the modules.

Sediment transport is calculated simultaneously with the flow calculations by the online sediment version of Delft3D-FLOW. Bed load transport of sand is computed with the *Van Rijn 2007* formula, for a detailed description see van Rijn and Walstra (2003). In depth averaged mode suspended sand transport is calculated according to the *Galappatti approximation*, see Galappatti and Vreugdenhil (1985). Table 5.1 summarizes the main parameter settings.

For a more detailed description of Delft3D and its application for coastal morphological modelling is referred to Deltares (2014a), Deltares (2014b) and Lesser (2009).

5.4. BOUNDARY CONDITIONS

To solve the non-linear shallow water equations of the FLOW-module, boundary conditions have to be provided at all open boundaries. Also the WAVE-module needs incident wave conditions at the water-water boundaries of the large computational grid. The smaller grid, which only covers the Haringvlietmouth, automatically obtains its boundary conditions from the large grid. This section treats the derivation of the boundary conditions for both modules.

5.4.1. FLOW BOUNDARY CONDITIONS

Three types of boundary conditions have been prescribed at the open boundaries of the FLOW-module, namely: water level, Neumann and discharge conditions. These conditions have been derived and validated in previous studies (De Vries, 2007, Roelvink, 1999, Steijn et al., 2001).

For the alongshore boundaries water level boundary conditions have been applied. The water level is determined by the amplitude of the tidal components and the water level setup. The following equation describes the water level at the open boundaries:

$$\xi(t) = A_0 + \sum_{i=1}^{n} A_i cos(2\pi f_i t - \varphi_i) \tag{5.1}$$

In which:

$\xi(t)$	water level elevation at the boundary at moment t
A_0	mean water level over a certain period
A_i	local tidal amplitude of harmonic component i
f_i	frequency of harmonic component i
φ_i	phase of harmonic component i

Table 5.1: Summary of the main model parameter settings

Module	*Parameter*	*Value*	*Description*
Flow	Δt	30	Computational time step [s]
	ρ_w	1025	Density of water [kg/m^3]
	ρ_a	1.25	Air density [kg/m^3]
	Roumet	C, Chezy	Type of bottom friction formulation [-]
	Ccofu	60.0	Uniform bottom roughness in u-dir [$m^{1/2}/s$]]
	Ccofv	60.0	Uniform bottom roughness in v-dir [$m^{1/2}/s$]]
	Vicouv	1.0	Uniform horizontal eddy viscosity [m^2/s]
	Dicouv	0.5	Uniform horizontal eddy diffusivity [m^2/s]
	ROUwav	FR84, Fredsoe	Bottom stress formulation due to wave action [-]
	Dryflc	0.1	Threshold depth for drying and flooding [m]
	CSTbnd	yes	Boundary condition [-]
Wave	Spectrum	JONSWAP	Shape of the wave spectrum [m]
	PeakEnhancFac	3.3	Peak enhancement factor in case of jonswap spectrum [-]
	Setup	false	No wave related setup [-]
	WaveForces	dissipation 3d	Method of wave force computation [-]
	GenModePhys	3	Generation mode of physics [-]
	Breaking	true	Include wave breaking, B&J model [-]
	BreakAlpha	1	Alpha coefficient for wave breaking [-]
	BreakGamma	0.73	Gamma coefficient for wave breaking [-]
	Triads	false	Include triads [-]
	BedFriction	JONSWAP	Bed friction type [-]
	BedFricCoef	0.067	Bed friction coefficient [-]
	Diffraction	false	Include diffraction [-]
	WindGrowth	true	Include wind growth [-]
	WhiteCapping	Komen	Formulation for white capping [-]
	Quadruplets	true	Include quadruplets [-]
	Refraction	true	Include refraction [-]
	FreqShift	true	Include frequency shifting in frequency space [-]
Transport	MorFac	0.1/1/5	Morphological scale factor [-]
	MorStt	1.488e+003	Spin-up interval for start of morphological changes [min]
	MorUpd	true	Update bathymetry during FLOW simulation [-]
	EqmBc	true	Equilibrium concentration profile at inflow boundaries [-]
	DensIn	false	Include effect of concentration on fluid density [-]
	D_{50}	160	Median grain diameter [μ m]
	TraFrn	vanrijn07	Sediment transport formula [-]
	Gammax	0.8	Cut-off criterion, represents the ratio wave height/water [-]

To schematise the tide as a cyclic morphological tide, its signal has been schematised by a harmonic analysis. The representative tide is derived from a tidal cycle from the time series that has a tidal range of $1.91m$, which is 1.1 times the mean tidal range (Roelvink, 1999, Steijn et al., 2001). The morphological tide is implemented as a harmonic boundary condition consisting of eight tidal components. The amplitude of the mean water level is determined by the surge level. This is determined for each wave condition, as it depends on the corresponding wind speed and direction.

Along the cross-shore southern and northern boundaries of the model Neumann boundary conditions are prescribed: instead of a fixed water level, alongshore water level gradients are imposed to overcome difficulties of determining water levels in the cross-shore sections. As the cross-section extent is limited, one can assume the alongshore gradient to be constant the entire length of the boundaries. This gradient only varies in time as a result of the tidal wave propagating along the coast. The water level gradients have to be determined for each tidal component. The Neumann boundary conditions have been derived in a previous study by De Vries (2007). For further elaboration on the used method is referred to that thesis.

At the boundaries of the Nieuwe Waterweg and the Haringvliet Sluices dicharges are prescribed. These discharges are known from calculated data from Rijkswaterstaat (2018). Preceding studies categorised in a high discharge regime, a normal discharge regime and a low discharge regime, as shown in Table 5.2 (De Vries, 2007, Roelvink, 1999, Steijn et al., 2001). Simulations to investigate the gradual changes of the Hinderplaat are performed with the Normal discharge scenario, since data analysis results have shown that these changes are not a consequence of extreme (high or low) discharge events. The extreme event of 1995 is modelled with a time series that represents the exact discharge values that were measured at that time, as presented in table 5.3.

Table 5.2: Discharge regimes for the Haringvliet Sluices and Nieuwe Waterweg as prescribed by Steijn et al. (2001) and De Vries (2007)

Regime -	***Occurence*** [%]	$Q_{Haringvliet}$ $[m^3/s]$	$Q_{NieuweWaterweg}$ $[m^3/s]$
High	2.9	5045	1695
Normal	51.1	897	1695
Low	46	41	1103
Mean	100	624	1431

Table 5.3: Discharge data during the modelled extreme event

Date -	$Q_{Haringvliet}$ $[m^3/s]$
29-01-1995	7226
30-01-1995	7898
31-01-1995	8475
01-02-1995	7167
02-02-1995	9015
03-02-1995	8065
04-02-1995	7276
05-02-1995	7408

At the open inflow boundaries it is also necessary to specify boundary conditions for the sediment concentration. Neumann boundaries have been prescribed for the sand concentration. With this, one sets a zero concentration gradient at the boundaries, determining that the concentration is equal to the concentration just inside the model domain.

5.4.2. WAVE BOUNDARY CONDITIONS

5.4.2.1. WAVE CLIMATE DATASET

To schematise the wave-climate, wave data has been gathered from the measurement station *Europlatform* (3.28°E, 52.00°N). Although this measurement station is located beyond the model area, it is better to use data from this station rather than using the data measured at stations *Goeree* or *Eurogeul 3* which are located within the model domain. The reason for this is that datasets from *Europlatform* are most complete, containing additional information on wave- and wind directions.

Two datasets of *Europlatform* were available for the wave schematisation: one of the period 1979-2001 and one of 2006-2012. Both sets have been compared to determine which one was most appropriate for the schematisation and whether the sets had to be combined. Figure 5.2 shows the schematisations for both wave climates in directional and wave height bins. Both figures show the same pattern, which is logical considering that they both represent the wave climate of the same location. A comparison of parameters such as the mean, maximum and minimum measured wave height showed that both climates are quite similar, without containing significant differences. Therefore it has been concluded that using one of the two climates is probably sufficient for the wave schematisation. It was found that the climate of 1979-2001 contained

wind-data obtained at *Europlatform*, while for the period of 2006-2012 only wind data from station *Goeree* is available. When schematising the wave climate it is important to link the wave conditions to the corresponding wind conditions. Furthermore, the first dataset contains more data points, as it covers a longer period in time. For these reasons it has been decided to use the climate from 1979-2001 for the wave schematisation.

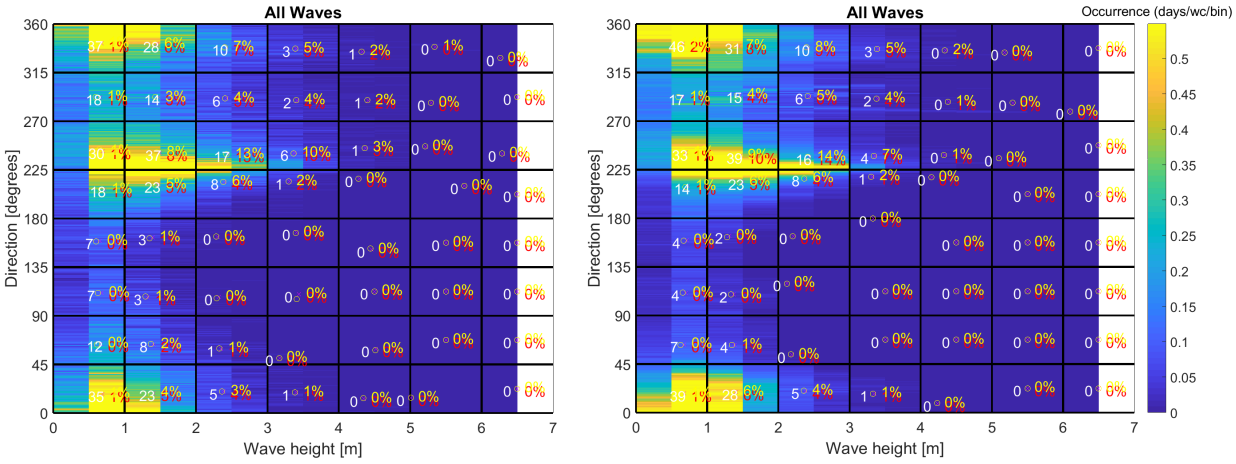

(a) 1979-2001 (b) 2006-2012

Figure 5.2: Wave climate schematisation for two different periods in time. Red numbers indicate the days of occurrence per year, yellow the morphological impact and red the total morphological scatter. The red cross shows the weighted centroid of each ave class.

5.4.2.2. SELECTION REPRESENTATIVE SET OF WAVE CONDITIONS

To schematise the wave climate, measured waves from the chosen dataset are sorted into sectors, which are formed by bins. Each bin represents a wave height and peak wave direction class with respective class sizes of $\Delta H_s = 0.5m$ and $\Delta D_p = 45°$. Each wave condition is assigned into one of the 56 sectors according to the measured height and direction. For all bins it is checked how many measured wave conditions it contains. By dividing this with the total number of wave conditions the probability of occurrence of wave properties within that class can be specified. To obtain the schematised wave climate only the bins that have a probability of occurrence that is larger than 0 are selected. For each bin the mean significant wave height is determined by calculating the wave height that corresponds to the mean sediment transport caused by the wave conditions in the corresponding bin. To that end, data points are weighted proportional to $H_s^{2.5}$ as this roughly corresponds with the CERC formula for longshore transport and is frequently used to estimate the morphological impact of waves (Lesser, 2009). Thereafter the wave direction and peak period that correspond to the mean wave height are computed. Moreover, the matching wind conditions are calculated for each bin. The resulting wave climate is shown in table 5.4.

The morphological impact per wave condition of Table 5.4 and Figure 5.2 is estimated according to:

$$M_c = p_c H_{s,rep}^{2.5} = \frac{\sum_{i=1}^{N_c} H_{s,i}^{2.5}}{N_s} \tag{5.2}$$

and the morphological scatter per bin according to:

$$\Delta_m = M_c \frac{\sum_{i=1}^{N_c} \sqrt{(|\, H_{s,i} - H_{s,rep}\,|^{2.5})^2 + (D_{p,i} - D_{p,res})^2}}{N_c} \tag{5.3}$$

In which:

p_c	probability of occurrence per wave condition
N_s	total number of wave records
N_c	number of wave records per class
$H_{s,i}$	individual significant wave height
$D_{p,i}$	individual significant wave direction
$H_{s,res}$	representative significant wave height
$D_{p,res}$	representative significant wave direction

Since every wave-condition is also combined with varying forcing conditions (wind-forcing on/off, surge levels, etc.) this leads to a large amount of output data. To obtain a manageable output, the wave climate is schematised to determine which conditions should be analysed first. This is elaborated in Appendix A.

The wind- and wave conditions during the extreme discharge event of 1995 have been measured by Rijkswaterstaat. This time series, which contains data for every three hours, has been processed to simulate the event realistically. Tables A.2 and A.3 provide an overview of the imposed conditions.

5.5. CALIBRATION AND VALIDATION

Calibration is the tuning of a numerical model by adjusting parameter settings in order to reproduce physical phenomena as closely as possible (Van Maren, 2004). Validation consists of proving that the model accurately describes the physical phenomena using an additional dataset. Initially, the model was setup in a study by Van Holland (1997) without calibration. However, the hydrodynamic and morphodynamic results were validated and a sensitivity analysis was performed. Reasonable results were obtained for the computed water levels, current velocities and wave propagation. Nevertheless, the morphodynamic results showed several deviations from the observed bathymetries. Subsequently, an extensive sensitivity analysis of the model was performed by Roelvink (1999). A few years later, the model was once again calibrated and validated by Steijn et al. (2001), when it was used to predict the effects of Maasvlakte 2 and a new policy for the sluices. In 2007 a sensitivity analysis was performed with the improved model by De Vries (2007). The results have been taken into account in this research.

Prior research has provided several recommendations to improve the morphodynamic predictive performance of the Haringvliet-Delft3D model (De Vries, 2007). Many are not followed in this study, as it is not a goal to improve the (long-term) morphodynamic predictions of the model. However, they are considered to be noteworthy, especially for future studies with the model. Regarding the wave climate optimization procedure, the representative wave conditions should be derived using the new transport formulation TR2004 of Van Rijn 2007. The roller effect of waves can be implemented by using the roller model in Delft3D-FLOW and applying different sediment fractions might improve the representation of erosion patterns. Mud transport was previously calculated in a simplified form of a depth-average approach; this can be improved by modelling mud using the advection-diffusion equation. Furthermore, the sand mud interaction should be implemented in the model. This is however still very difficult to achieve in Delft3D. Finally, the simulations could be carried out in 3D mode to include baroclinic effects due to the density differences over the water column in case of high discharges.

Although improving the morphodynamic performance is not within the scope of this project, a brief study has been conducted on the predictions at the shoreface. The behaviour of the morphology in this area is likely to have an impact on the evolution of the Hinderplaat (see Section 3.4.5) and the model predictions obtained in previous studies show significant differences with the observed behaviour: model results showed sedimentation in the shoreface in front of the Hinderplaat, while the Vaklodingen data show erosion patterns (De Vries, 2007, Van Holland, 1997). By running the model with a wide range of forcings it is found that the model always predicts sedimentation of this area, except when run with north-easterly wind forcing. This is a very infrequent condition: therefore it is concluded that it is unlikely that erosion only takes place under this condition. Calibration of several parameters has been performed to evaluate the model predictions in the lower shoreface. This is discussed in Appendix B.

Table 5.4: List of wave and wind conditions and their corresponding surge levels, probability of occurrence and morphological impact

$Type$ [-]	$N°$ [-]	H_s [m]	T_p [s]	D_p [°]	U_{wind} [m/s]	Dir_{wind} [°]	$Surge$ [m]	p_c [-]	M_c [$m^{2.5}$]
Calm	1	0.69	4.19	18 (N)	5.36	99	-0.09	0.0962	1.1
	2	0.67	3.87	64 (ENE)	6.27	97	-0.13	0.0340	0.4
	3	0.68	3.61	111 (E)	6.78	123	-0.15	0.0188	0.2
	4	0.65	3.56	159 (SSE)	6.51	146	-0.10	0.0192	0.2
	5	0.71	3.63	207 (SSW)	6.57	187	-0.04	0.0497	0.6
	6	0.69	3.78	242 (WSW)	6.03	225	0.01	0.0809	1.0
	7	0.66	3.95	292 (WNW)	5.18	246	0.01	0.0488	0.5
	8	0.67	4.47	342 (NNW)	4.20	231	-0.04	0.1014	1.1
Regular	9	1.40	4.77	18 (N)	8.11	86	0.09	0.0626	4.4
	10	1.41	4.53	64 (ENE)	9.27	84	-0.25	0.0213	1.5
	11	1.33	4.20	107 (E)	9.43	117	-0.29	0.0094	0.6
	12	1.39	4.18	163 (SSE)	9.70	153	-0.14	0.0079	0.5
	13	1.48	4.35	211 (SSW)	10.22	196	-0.03	0.0637	5.1
	14	1.49	4.47	241 (WSW)	9.58	236	0.09	0.1001	8.1
	15	1.47	4.57	292 (WNW)	8.29	269	0.15	0.0382	3.0
	16	1.46	4.96	341 (NNW)	6.86	275	0.05	0.0776	6.0
Medium	17	2.39	5.48	20 (N)	11.69	82	-0.11	0.0124	3.3
	18	2.35	5.28	60 (ENE)	12.86	74	-0.37	0.0038	1.0
	19	2.32	5.03	107 (E)	12.47	128	-0.32	0.0006	0.2
	20	2.30	4.94	163 (SSE)	11.82	151	-0.13	0.0008	0.2
	21	2.40	5.05	214 (SSW)	13.70	198	-0.05	0.0210	5.6
	22	2.45	5.23	240 (WSW)	13.03	237	0.16	0.0466	13.1
	23	2.43	5.28	291 (WNW)	11.61	278	0.35	0.0157	4.4
	24	2.42	5.57	338 (NNW)	10.43	302	0.25	0.0260	7.2
Medium-strong	25	3.40	6.24	19 (N)	14.45	62	-0.04	0.0019	1.3
	26	3.17	5.95	51 (NE)	13.27	62	-0.26	0.0003	0.1
	27	3.44	5.65	110 (E)	14.13	135	0.50	2.98E-05	0.0
	28	3.41	5.79	167 (SSE)	13.76	202	0.20	0.0002	0.1
	29	3.31	5.66	214 (SSW)	16.16	201	-0.05	0.0036	2.2
	30	3.38	5.86	241 (WSW)	15.91	240	0.27	0.0155	9.8
	31	3.42	5.95	289 (WNW)	14.54	282	0.63	0.0056	3.6
	32	3.40	6.20	337 (NNW)	13.40	299	0.51	0.0076	4.9
Strong	33	4.35	6.80	13 (N)	16.63	42	0.16	0.0003	0.3
	34	4.52	6.50	59 (ENE)	19.61	24	0.23	2.98E-05	0.0
	35	4.45	6.84	151 (SSE)	14.24	120	0.58	4.46E-05	0.1
	36	4.29	6.35	217 (SSW)	20.62	199	-0.11	0.0002	0.3
	37	4.38	6.48	245 (WSW)	18.78	248	0.39	0.0021	2.5
	38	4.41	6.54	289 (WNW)	17.29	290	0.85	0.0015	1.8
	39	4.33	6.81	334 (NNW)	15.87	295	0.83	0.0017	2.0
Extreme	40	5.01	7.10	14 (N)	16.70	40	0.04	1.49E-05	0.0
	41	5.76	6.80	210 (SSW)	25.60	200	0.43	1.49E-05	0.0
	42	5.21	6.84	247 (WSW)	20.95	247	0.42	0.0002	0.3
	43	5.30	6.84	287 (WNW)	19.63	286	0.95	0.0002	0.3
	44	5.35	7.38	339 (NNW)	17.62	320	1.17	0.0003	0.7
	45	6.29	7.40	240 (WSW)	28.34	225	0.38	2.98E-05	0.1
	46	6.26	7.90	328 (NNW)	20.71	326	1.27	4.46E-05	0.1

6

MODEL RESULTS

6.1. INTRODUCTION

Six model experiments with each various simulations and an event hindcast simulation have been performed to determine the mechanisms behind the evolution of the Hinderplaat. This has resulted in over 900 gigabytes of model data providing an extensive amount of results. This chapter presents the most relevant results, that eventually lead to the conceptual model presented in Chapter 7. An overview of the simulation scenarios is repeated in Table 6.1.

Table 6.1: Overview of the simulations scenarios and forcing processes. The last row shows which simulations have to be compared to evaluate the corresponding process. Surge level gradients along the offshore boundary are not accounted for (marked grey).

	Process				
Simulation	***Tide***	***Discharge***	***Wind***	***Waves***	***Surge***
A. Tidal forcing only	yes	no	no	no	no
B. Tide and Q_{river} forcing	yes	yes	no	no	no
C. No wind forcing	yes	yes	no	yes	no
D. No wave forcing	yes	yes	yes	no	no
E. All processes	yes	yes	yes	yes	no
F. Quasi-real-time	yes	yes	yes	yes	yes
Process definition	A	A-B	C-E	D-E	E-F

First, Section 6.2 presents an analysis of the flow patterns under various conditions, to understand the influence of the tidal forcing and river discharge on the flow and the contribution of wind- and wave-driven currents from different directions. Section 6.3 focusses on the morphodynamics by analysing the initial bed level changes and the underlying sediment transport patterns under varying conditions. Both sections contain results in the form of tide-averaged values. In addition, relevant snap-shots of flow and sediment transport fields are presented in detail to interpret the net results correctly.

6.2. FLOW PATTERNS

6.2.1. FLOW PATTERNS DURING A TIDAL CYCLE

As explained in Section 3.5, the tidal flow patterns in the Haringvliet outer delta completely changed after damming the estuary, because the cross-shore tidal flow almost disappeared and mainly the longshore tide remained. Flow patterns on the outer delta are complex due to the interaction of the longshore propagating tide, the river discharge flowing through the main channels and the complex delta topography. The current patterns during a tidal cycle have been studied for the different stages as defined in Section 3.5. To that end, simulations with tidal forcing and a normal discharge through the sluices are performed, since the regular current patterns are likely to be determined by both the tide, and the freshwater run-off during low water.

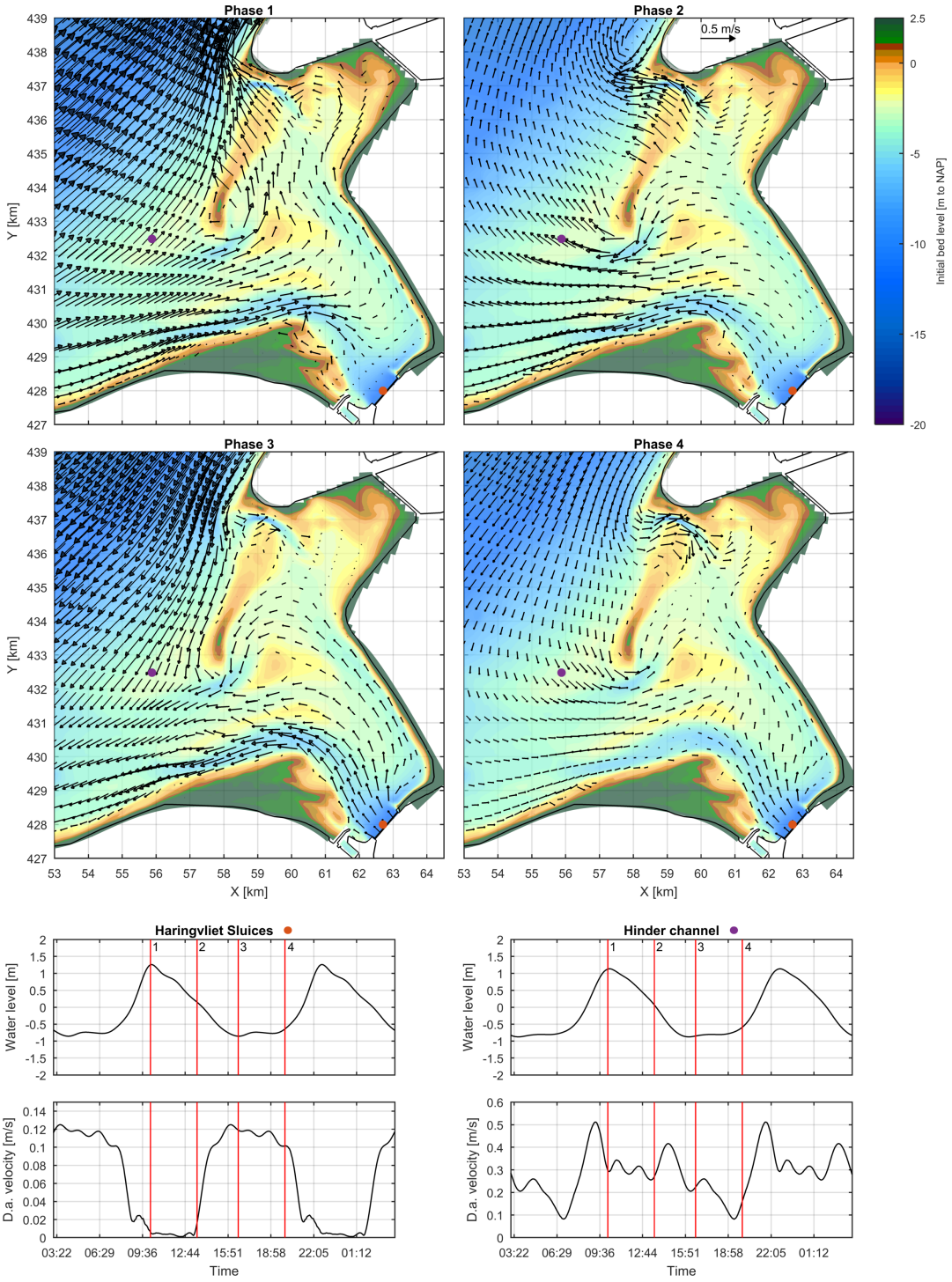

Figure 6.1: Tidal flow patterns for four stages of the tidal cycle, simulated with only tide- and discharge forcing. The arrows indicate the instantaneous flow velocities. The four lower plots show the water levels and flow velocities of the indicated time series. The red lines indicate the moments of the snap-shots. The coloured dots show the locations of the observation points.

Snap-shots of the flow patterns during the representative moments are shown in Figure 6.1. These moments are marked with red lines in the plots below the snap-shots, which show the water levels and depth-averaged flow velocities for the representative morphological tide at two locations: the Haringvliet Sluices and Hinder channel (which is located on the seaward side of the Hinderplaat). The flow velocities at the sluices are mostly influenced by water run-off from the Haringvliet Lake, which is only released during low water. A small phase difference between the horizontal and vertical tide in a time series of Hinder channel illustrates the mixed standing-progressive tide. The influence of the fresh-water outflow through the sluices is especially noticeable in the increase in flow velocities around the first low water. The size of the black arrows of the snap-shots indicates the flow velocity magnitude and the colours indicate the bathymetry. The simulated flow patterns are compared with the findings of Tönis et al. (2002), which have been discussed in Section 3.5.1.

At high water (*phase 1*) the flow is in flood direction, both inside and outside the estuary mouth. The water enters the Haringvliet at the south and leaves at the north, flowing through the main channels as well as over the shoals. The Hinderplaat is completely submerged and the flow over the flats is stronger than suggested by Tönis et al. (2002). A circulation flow around the southern end of the Hinderplaat is visible.

Three hours later the currents in the North Sea are still in flood direction, while the tide inside the basin is in ebb direction (*phase 2*). Flow velocities and water levels outside the basin have decreased significantly. Water flows out of the basin through the channels Slijkgat, Bokkegat and Hindergat and partly also over the still submerged Hinderplaat, while flow velocities at Rak van Scheelhoek are minimal.

During the first low tide at the sluices (*phase 3*) ebb currents occur outside the basin, entering the basin at the north side through the Hindergat channel and leaving at the south side. The released water from the sluices is mainly discharged through the Slijkgat channel. As the Hinderplaat is exposed, water that is piled up behind it has to leave the basin through Bokkegat and Hinder channel.

Because of the agger in the tidal signal, the water levels shortly increase after which they decrease again during the second low water. Just after the second low water (*phase 4*) offshore currents are in ebb direction and velocities have significantly reduced again. As the currents along the Hinderplaat curl around the most southern end, they disperse and enter through Bokkegat channel. The northern part of the Hinderplaat has submerged again and water flows over it, into the basin. River discharge flows mainly through Slijkgat, although partly also through Rak van Scheelhoek.

As stated, current patterns in the channels are strongly influenced by the river discharge during low water. A simulation without river discharge has been performed to prove this. The results are presented in Appendix C. A comparison between Figure 6.1 and Figure C.1 shows that the river discharge mainly influences the flow direction at the channels Slijkgat, Bokkegat and Rak van Scheelhoek during ebb flow. The river discharge partly fills in the outer delta with water, for which less water enters the delta through the offshore boundaries.

6.2.2. RESIDUAL CURRENTS DUE TO THE TIDE AND RIVER DISCHARGE

The presented overview of instantaneous flow velocities contributes to an understanding of the flow patterns in the Haringvliet ebb-tidal delta. However, to explore the morphological development not only the gross water motion is important, but also the residual flow. The residual currents are calculated by averaging the Eulerian velocities over a tidal cycle. Note that since simulations are performed with a representative morphological tide, averaging the currents over one tidal cycle gives the same results as executing the calculation over more tidal cycles. The mean current is obtained by averaging the values at each time step ($\Delta t = 30s$) through a Fourier analysis performed during the Delft3D calculation.

Figure 6.2a shows the residual currents at the ebb-tidal delta due to tidal forcing only. The residual flow is partly generated by the asymmetry of the imposed offshore tide, and partly locally generated. Residual currents due to the tide are small, with an overall order of magnitude of around 0.02 to $0.05 m/s$. They are strongest at the Hinderplaat and Hindergat channel, where they reach values of over $0.15 m/s$. At the northern part of the Hinderplaat, offshore directed net currents are generated by the tide. An isolated residual eddy characterises the currents on the southern part of the shoal. At the lower shoreface in front of the Hinderplaat, a dominance of larger ebb-flows can be distinguished. Most channels of the delta area are considered to be flood-dominant, except for the Hindergat, where large offshore-directed net currents are found at the inlet.

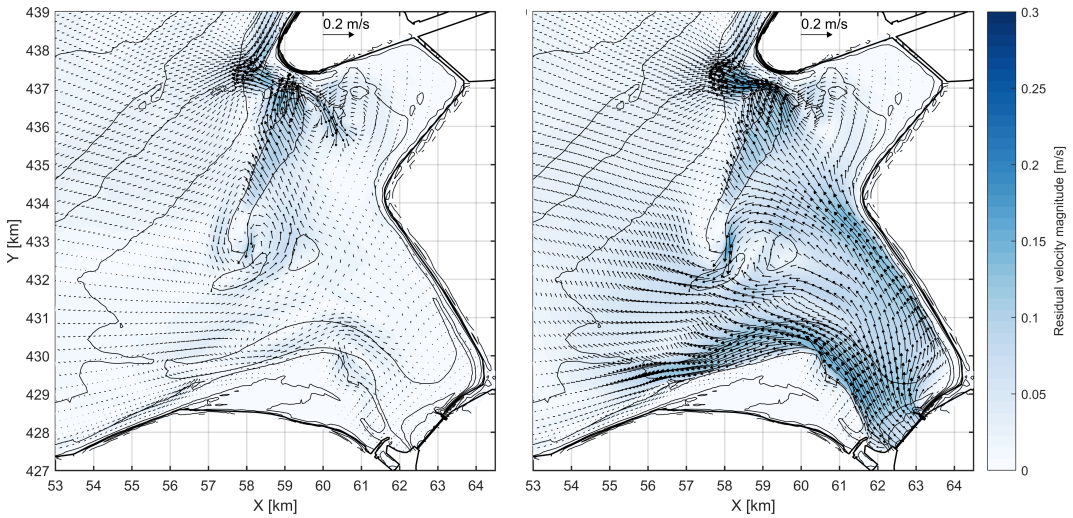

(a) Tidal forcing only (b) Tide and Q_{river} forcing

Figure 6.2: Vector representation of the residual tidal flow patterns and magnitudes for different processes included

Net currents significantly change when the effect of the discharge through the sluices is accounted for, as shown in Figure 6.2b (simulated with tidal and Q_{river} forcing, as defined in Table 4.1). Net current velocities considerably increase and have a pronounced offshore direction in the channels Slijkgat, Rak van Scheelhoek and Hindergat due to the freshwater run-off. This is in correspondence with the findings of Van Holland (1997). While net currents are in the same order of magnitude for the Slijkgat channel and Rak van Scheelhoek, the discharge through these channels differs: due to the limited depth of the latter, most of the river outflow is discharged through the former. Also in this scenario, a circulation cell at the southern end of the Hinderplaat is generated, although it is less pronounced than for the tide-only scenario.

6.2.3. THE FORCING MECHANISMS BEHIND THE FLOW

As shown in the previous section, the river discharge has a significant contribution to the residual flow. However, model results have shown that wind- and wave-generated currents can alter these patterns substantially, both in magnitude and direction.

During *calm conditions* ($H_s = 0-1m$ and $U_{wind} \approx 6m/s$, see Table 5.4 for the exact wave conditions) the flow patterns during the distinguished phases of the tidal cycle remain nearly identical: only small velocity magnitude deviations are detected during the second low water for a calm condition with NNW orientation. For the current patterns is referred to Appendix C. However, directly after low water, the current patterns at the shoreface are significantly changed for *regular conditions* ($H_s = 1-2m$ and $U_{wind} \approx 9.5m/s$) and more energetic ones. Note that when we speak about the conditions, we mean the imposed conditions at the offshore boundary of the model, from which the local wave conditions may vary due to wave propagation and transformation. This holds for both the wave height and the direction.

Figure 6.3 shows the flow patterns after the second low water (*phase 4* of the tidal cycle) for simulations with regular conditions of NW and SW directions. From a comparison with Figure 6.1, it is evident that mainly the patterns at the shoreface are affected by the imposed forcing. Forcing from SW direction is capable of changing the instantaneous current directions at the shoreface in front of the Hinderplaat during low water. Regular forcing from NW direction reduces the velocities in that area, although it is not strong enough to completely alter the flow pathways.

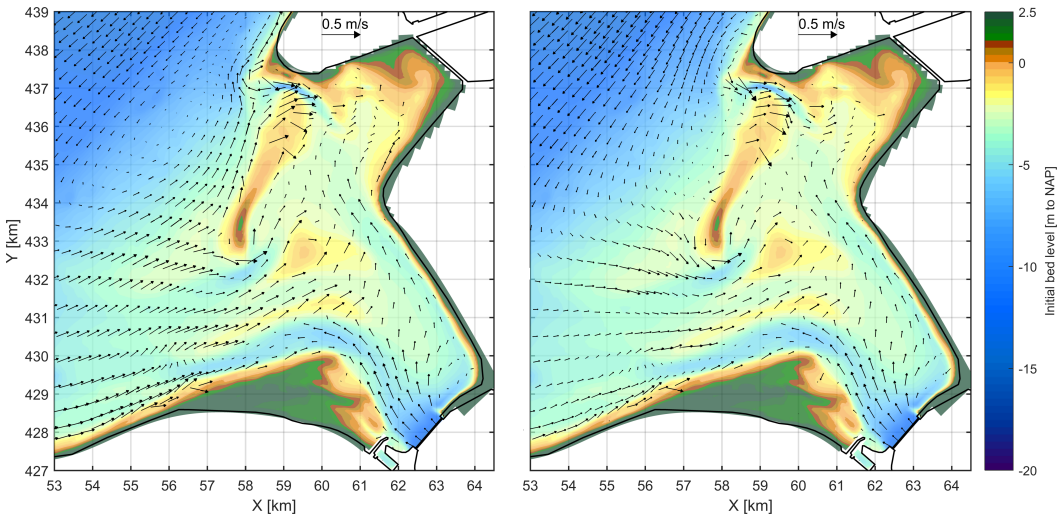

(a) Regular WSW condition (b) Regular NNW condition

Figure 6.3: Current patterns at phase 4 of the tidal cycle for regular forcing (E. all processes) of SWW and NNW direction

6.2.3.1. WIND-DRIVEN FLOWS

To determine the cause of the strikingly altered flow patterns in the shoreface, the results of Figure 6.3 are compared to flow patterns of simulations where either the wind or the wave forcing is omitted. These results are presented in Figure 6.4, which shows the flow patterns at the second low water for a simulation without wind forcing (a) and wave forcing (b). Apparently, the change of the patterns is mainly a wind-driven phenomenon. Wave-induced currents only contribute to this phenomenon to some extent by slightly reducing the velocities. It is concluded that regular wind speeds of $9.6 m/s$ and SW direction are already very effective in changing the instantaneous current pathways in front of the Hinderplaat during low water. These may cause a tidal flow reversion in areas up to 6 metres deep.

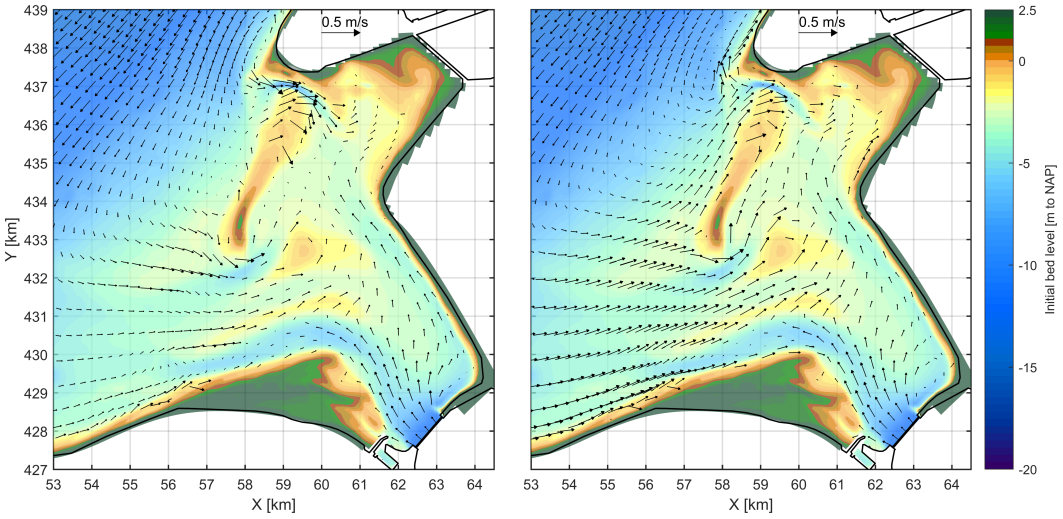

(a) Regular WSW condition, without wind forcing (b) Regular WSW condition, without wave forcing

Figure 6.4: Current patterns at phase 4 of the tidal cycle for regular SWW forcing

So far, it seems like the wind force is the main mechanism to determine the flow direction at the upper shoreface (seawards of the Hinderplaat). However, this is based on the considered snap-shots and the results may be different when considering the net (integrated) currents over a tidal cycle. To determine which mechanisms are most effective in changing the residual flow patterns, the net currents due to different forc-

ing scenarios of *regular strength* (see Table 5.4) are plotted in Figure 6.5. The orientation of the boundary forcing of the plots is WSW, which is the most frequent wave- and wind direction at the offshore boundary.

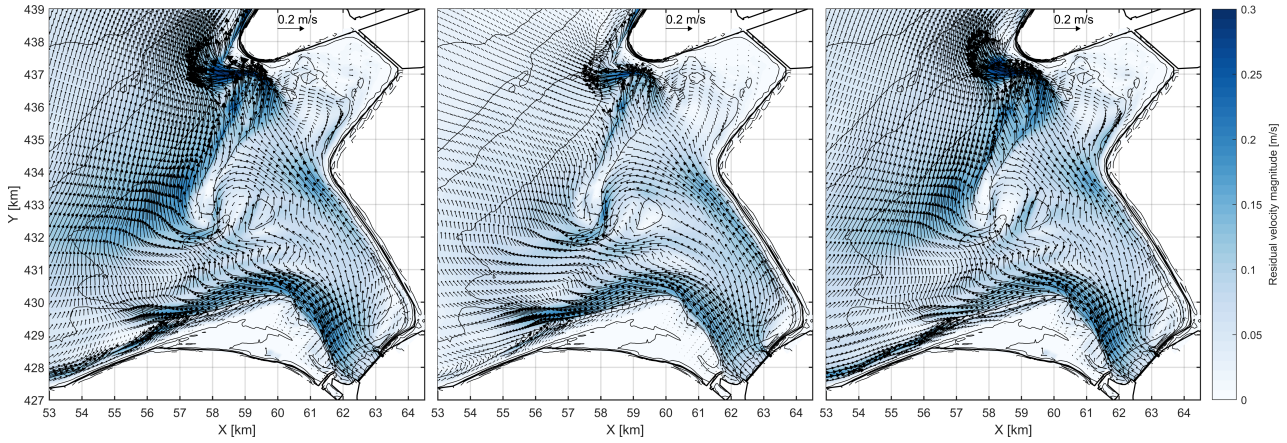

(a) All processes (b) No wind forcing (c) No wave forcing

Figure 6.5: Residual currents in the Haringvliet ebb-tidal delta for different forcing scenarios

The results show that under regular conditions, the residual flow is mainly determined by the wind-driven currents, especially on the seaward side of the outer delta. These currents are not only stronger than the wave-induced currents, but they also overrule the tidal residual flow, as seems from a comparison of Figures 6.2a and 6.5c. The direction of the wind forcing is the primary driver for the direction of the residual flow at the upper shoreface in front of the Hinderplaat. Depending on the imposed forcing, the resulting currents may be in NE or SW direction. Several simulations with slightly varying wind directions are performed to investigate the so-called *turning points* of the wind forcing, see Figure 6.6. This analysis covers both the impact of the imposed direction, as well as the depth-reach at which the forcing (largely) determines the flow patterns.

As expected, the turning point for the effect of the wind on the shoreface is found for forcing that is approximately perpendicular to the shoal. Wind directions of $260° - 275°$ induce a northward directed residual flow field at the lower and upper shoreface. From a comparison of Figure 6.6 with Figure 6.2b, it seems that the flow direction on top of Hinderplaat is much less affected, although the velocities are slightly enhanced by the wind forcing. The southern end of the shoals seems unaffected by the forcing. For the simulation with a wind direction of 300° the wind forcing is more or less perpendicular to the Hinderplaat. The net flow patterns for this situation look almost similar to the patterns for the tidal and Q_{river} forcing-scenario, as depicted in Figure 6.2b. Hence, we can conclude that perpendicular wind directions with regular speeds that are little above the mean value merely influence the residual flow patterns generated by the tidal forcing and the river discharge.

At first sight, the results of the simulation with a wind direction of 315° only show a limited influence on the shoreface, as the patterns are only slightly different from the patterns of Figure 6.6c. Yet this scenario does influence the flow on top of the Hinderplaat, as the velocities on the shoal are reduced. Moreover, the patterns on the seaward edge of the shoal are now directed towards the south, showing an increase in velocities when going from north to south which was the other way around for the previous scenarios. Likewise, wind directions of $330° - 345°$ show the same increase in velocities towards the south. Besides, for these scenarios, the flow on the shoreface is in SW direction. Note that the patterns on the Garnalenplaat are also largely influenced by the wind forcing. The development of this shoal is however out of the scope of this thesis.

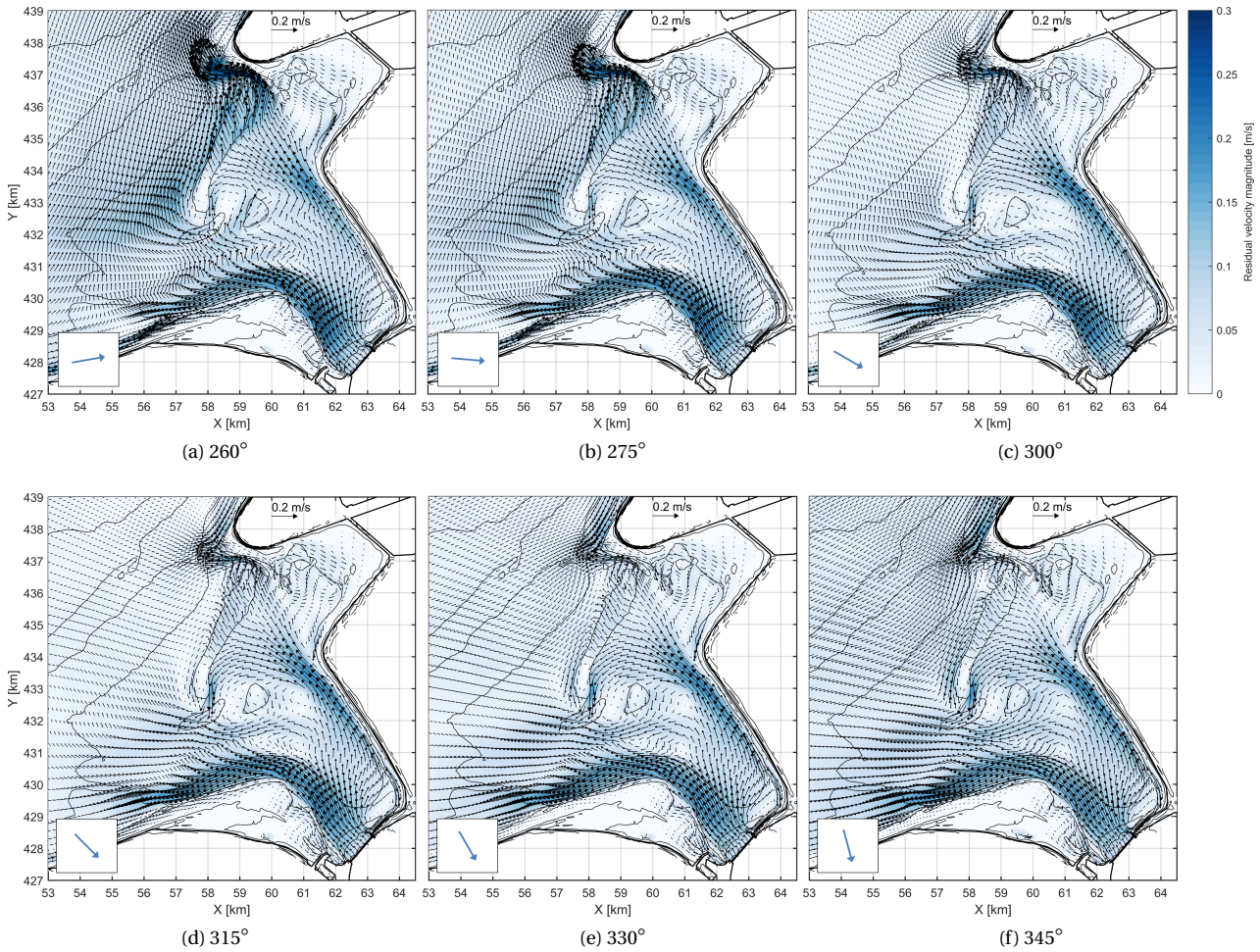

(a) 260° (b) 275° (c) 300°

(d) 315° (e) 330° (f) 345°

Figure 6.6: Residual currents in the Haringvliet ebb-tidal delta for wind speeds of 9.6m/s from various directions, simulation scenario D. The blue arrows indicate the wind direction.

6.2.3.2. WAVE-GENERATED CURRENTS

Figures 6.5 and 6.6 may suggest that residual flow velocities on top of the Hinderplaat always have an offshore direction (regardless of the imposed forcing direction) while this is certainly not true: although phenomenon is typically visible under calm and regular wave and wind conditions, for more energetic wave conditions we sometimes observe a remarkable change in the net flow patterns at the intertidal shoal. During high water, the Hinderplaat is completely flooded and a wave-induced water level gradient is found over the shoal. Apparently northwesterly breaking waves induce a higher water level along the seaside of the shoal that at the landside. This gradient causes cross-shore currents from east to west on top of the Hinderplaat.

Obliquely incident waves also induce longshore currents along the Hinderplaat as well as along the coasts of Goeree and the Slufter. These currents are generated by the dissipation of energy due to wave breaking. Cross-shore currents along the Hinderplaat are the strongest for normal incident waves (with respect to the shoal), whereas wave-generated longshore currents are stronger for slightly larger obliqueness. This corresponds with the longshore current theory, which states that maximum velocities occur for offshore wave angles of $\phi_0 = 45°$ (Bosboom and Stive, 2013). Besides, it also holds for the angle for which the longshore sediment transport reaches a maximum value (which is in correspondence with the S,ϕ-curve theory), but that is considered later on in this chapter.

Figure 6.7 shows the effect of NNW waves on the study area. In Figures 6.7a and 6.7b the instantaneous fraction of waves breaking is presented for high water and low water. It seems that waves break along the Slufterdam during the entire tidal cycle, whereas at the Hinderplaat and Kwade Hoek (along the coast of Go-

eree) they mostly break during low water. The reason behind this is that these areas are largely submerged during high water. As explained, longshore currents are generated by the wave forcing along the Slufter, Hinderplaat and at the coast of Goeree under NNW conditions (see Figure 6.7c). Cross-shore currents over the southern half of the Hinderplaat are also visible, although these currents are stronger for more perpendicular wave incidence (WNW conditions).

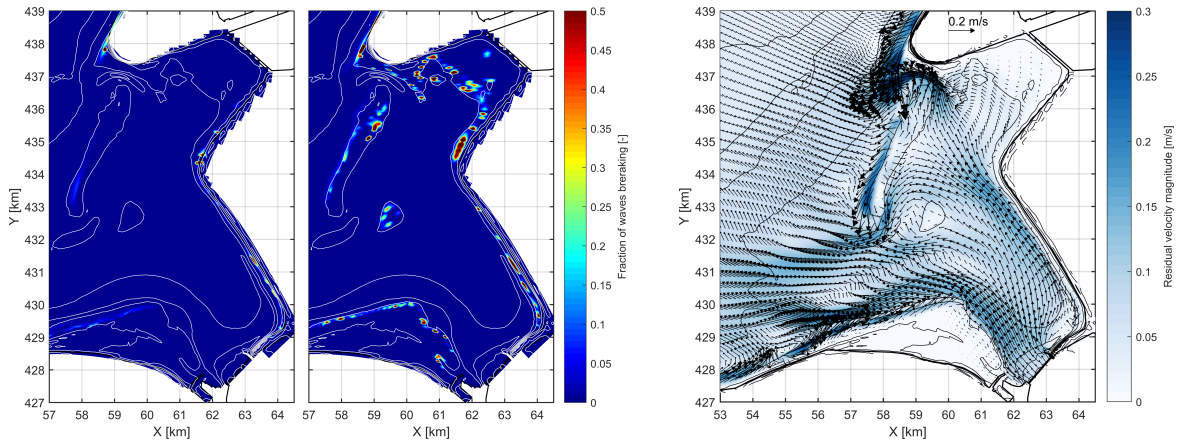

(a) Fraction breaking at HW

(b) Fraction breaking at LW

(c) Residual currents for scenario C: tide, discharge and wave forcing

Figure 6.7: Overview of the wave impact on the flow for medium NNW conditions

6.2.4. CURRENTS DURING AN EXTREME DISCHARGE EVENT

From January 29, 1995, until February 5, 1995, an extreme discharge event took place during spring tide. This event is modelled as realistic as possible (described in Sections 4.3 and 5.4) to gain insight into the morphodynamic response of the Haringvliet outer delta under such circumstances.

Figure 6.8 provides an overview of the typical flow conditions for very high discharges ($Q_{sluices} > 7000 m^3/s$). Under regular discharge conditions, both the Hinderplaat and the Garnalenplaat are exposed and the flow is guided through the surrounding channels. However, this is different for high river discharges: as shown in Figure 6.8a, the freshwater run-off is discharged over almost the entire outer delta and only the southern part of the Hinderplaat and the Slikken van Voorne (located south of the Slufter) remain exposed. Moreover, the flow velocities are significantly larger than under regular circumstances (with an order of magnitude of $1 m/s$). This has a direct impact on the residual flow, which then is strictly dominated by the river discharge instead of the wind and wave conditions, even on the Hinderplaat (see Figure 6.8b). Note the severe increase in flow velocities (instantaneous and residual) in comparison with the previously described scenarios in this chapter.

The upper plot of Figure 6.9 shows the flow through a cross-section along the Hinderplaat during the day with the highest river discharges (with a daily average value of $Q_{sluices} = 9015 m^3/s$). The dashed line represents the discharge through the shoal under the same wave- and wind conditions, but for an average discharge scenario ($Q_{sluices} = 897 m^3/s$). A positive discharge stands for an onshore directed flow. The lower plot shows the corresponding water levels at three locations: Hinder channel, Hinderplaat and the Haringvliet sluices. Under extreme discharges, the offshore flow volumes over the shoal are often twice as high during this event. Besides, the period of over which the flow is in offshore direction has almost doubled while the period of onshore directed flow is half as long. Furthermore, discharge values are never zero, which implies that there is always water flowing over the shoal.

However, the numerical model predicts what seems to be an unexpected discrepancy: not only the offshore directed discharges increase during the extreme event, but the onshore peak discharge is also significantly higher. Analyses of the model results have shown that this is caused by a translatory wave induced by the closure of the sluices. The sluices are closed around 08.00, after which the water level at the seaside of the sluices

rapidly decreases (see the blue line at the lower plot of Figure 6.9). This induces a translatory wave in onshore direction. This is most likely a hydrodynamic model artefact, that originates in the imposed boundary conditions. In the model simulations, opening and closing of the sluices takes about 30 minutes. A linear decrease in the river discharge is imposed as a strict boundary condition, that is independent of the exact water levels on both sides of the dam. In reality, opening and closing of the sluices is closely related to the water levels, as the sluices are automatically controlled by the pressure head across them. Therefore, discharge changes are less abrupt and it is less likely that translatory waves are generated. The effect of different closing scenarios of the sluices on the presence of translatory waves is out of the scope of this research.

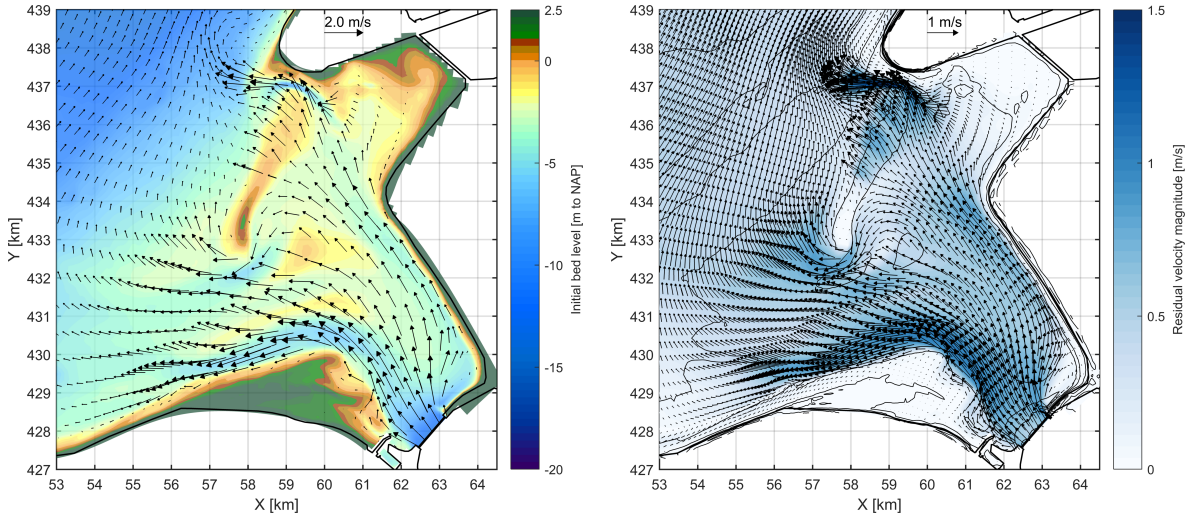

(a) Current patterns at low water

(b) Average residual currents during the event

Figure 6.8: Overview of the flow conditions due to an extreme discharge event

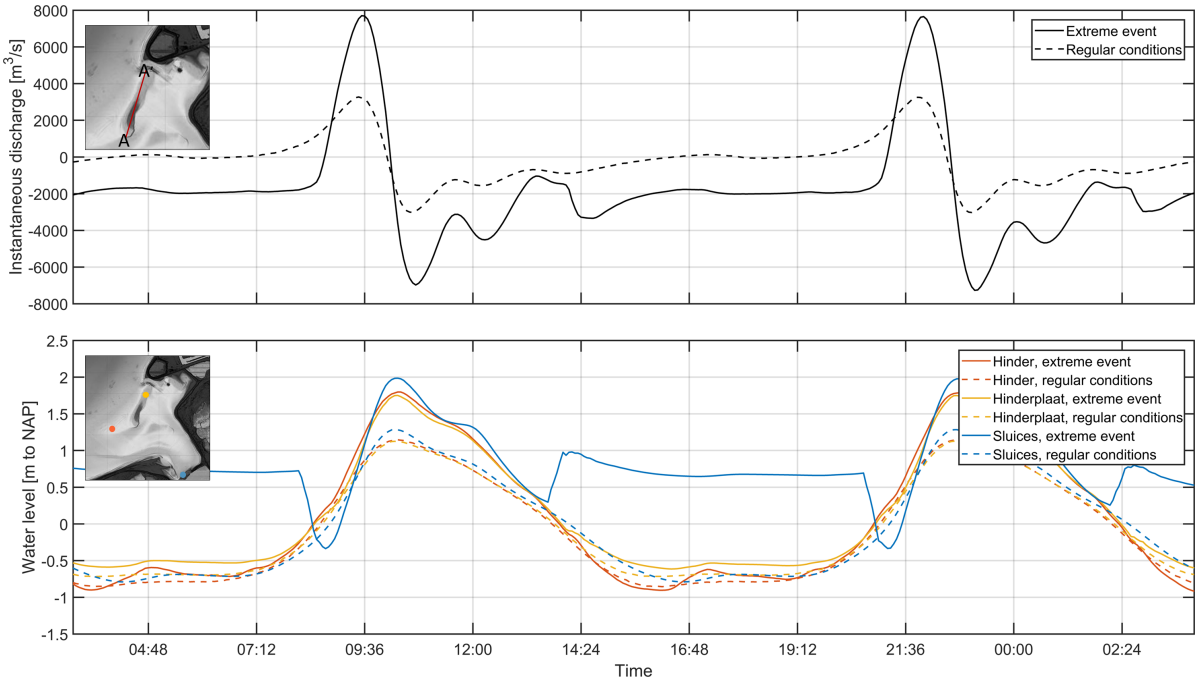

Figure 6.9: Instantaneous discharge through the Hinderplaat and corresponding water levels

6.3. SEDIMENT TRANSPORT AND MORPHOLOGICAL CHANGES

6.3.1. INITIAL BED LEVEL CHANGES

So far, the focus of this chapter has been on the hydrodynamics at the outer delta and on the relative importance of the processes for the residual flow. Yet to determine their link with the evolution of the Hinderplaat, their contribution to the transport rates and bed level changes is assessed. In this thesis, a top-down approach is adopted in which general patterns are observed first, before zooming in into the detailed transport patterns. Therefore, the initial bed level changes caused by the processes are considered first. Again, the focus is on two tides during which the imposed forcing remains constant.

Figure 6.10 shows the initial bed level changes for calm SW and NW conditions (all processes) as well as the observed bed level changes for the period of 1992-1995. The latter serves as a reference plot for all results of this section. The calculated values have been corrected for the prescribed MorFac (0.1) by multiplying the simulated net bed level change of each grid cell with a factor of 10. During calm conditions only very small bed level changes occur on top of the Hinderplaat, consisting of sedimentation at the seaward edge and erosion of the area behind it. Hindergat channel seems to erode, except for its seaward inlet, where sand is deposited. This is likely to be a consequence of the sudden decrease in velocities. It is striking that the sedimentation/erosion patterns are similar for SW and NW forcing (except for small magnitude deviations). An analysis of all simulations with calm conditions has shown that these patterns are even present for all prescribed wave directions. So, we may conclude that the patterns are mainly a consequence of the common factors between the various simulations: the tidal forcing and river discharge. However, (small) waves are necessary to stir up sediment and enable sediment transport, which is elaborated further on in this section.

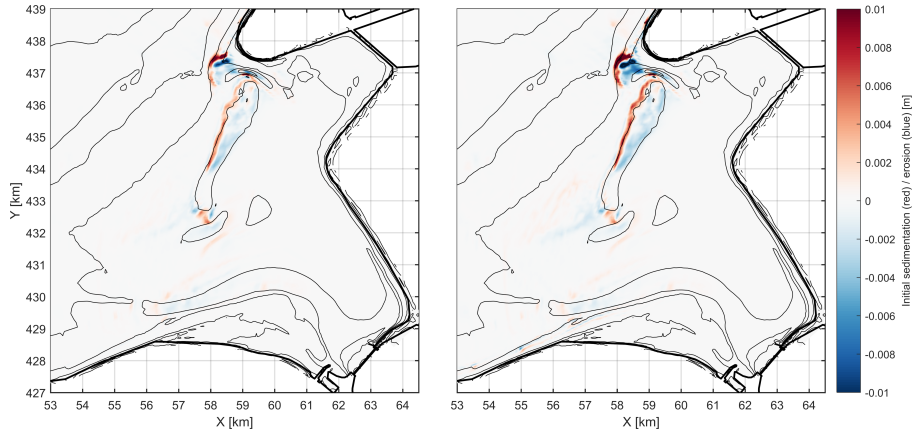

(a) simulated with SW wind and waves

(b) simulated with NW wind and waves

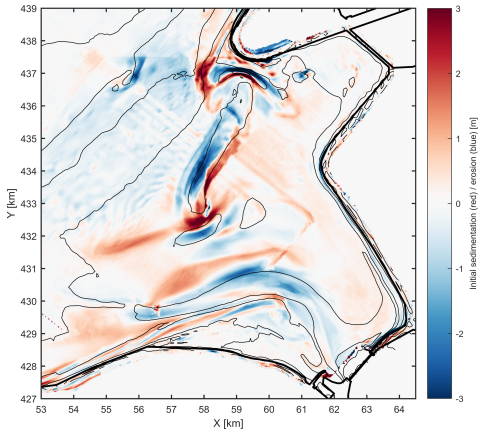

(c) observed rates for 1992-1995

Figure 6.10: Initial bed level changes for calm conditions after two tides and measured reference patterns

Simulations with regular conditions ($H_s = 1-2m$ and $U_{wind} \approx 9.5m/s$) show similar patterns as the previously discussed ones, with overall sedimentation of the seaward edge of the shoal, erosion of its landward area and no bed level changes at the southern tip (see Figure 6.11). However, westerly conditions (with SW to NW directions) show a patchy pattern on the shoal, with alternating sedimentation and erosion. This pattern is often seen as a consequence of the morphological spin-up of the numerical model. However, this is probably not the case as the calculations are performed with a (morphological) spin-up time of about three weeks and the imposed conditions are relatively mild.

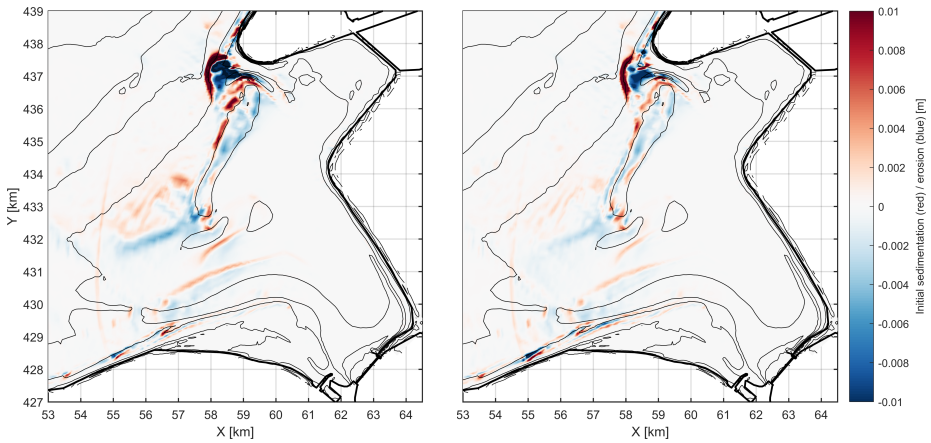

(a) simulated with WSW wind and waves (b) simulated with NNW wind and waves

Figure 6.11: Initial bed level changes for regular conditions after two tides

For an increasing intensity of the imposed forcing (i.e. larger values for H_s and U_{wind}) the patters for most directions remain similar and the sediment rates are generally larger for more energetic conditions. However, medium conditions and more energetic ones ($H_s > 2m$ and $U_{wind} > 10.5m/s$) from WNW to N directions show opposed patterns than milder conditions from these directions, as shown in Figure 6.12. The sedimentation/erosion patterns on top of the Hinderplaat generated under these conditions are very similar to the measured patterns indicated in Figure 6.10c: the simulations of Figure 6.12 correctly reproduce the landward migration of the shoal, as erosion is visible along the seaward side and sedimentation along the landward edge. Moreover, the shoal becomes longer as it spreads towards the south, which also matches the evolution that is analysed with the Vaklodingen dataset. The qualitative correspondence in sedimentation/ erosion patterns between these simulations and the observed patterns illustrate that WNW-N conditions play an essential role in the studied evolution of the Hinderplaat.

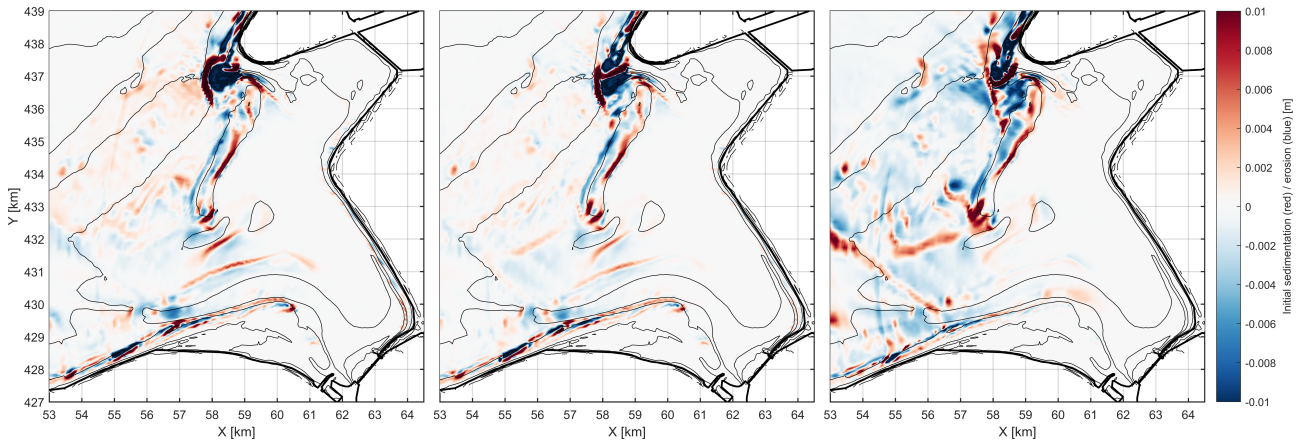

(a) medium WNW conditions (b) medium NNW conditions (c) medium-strong N waves and NE wind

Figure 6.12: Initial bed level changes for regular conditions after two tides

Stronger wave conditions with a more westerly orientation ($H_s > 3m$ and $U_{wind} > 13m/s$ from WSW-WNW direction) show similar patterns, although the strict division between erosion on the western edge and sedimentation on the eastern edge on the shoal is less pronounced, see Figure 6.13e. Furthermore, spreading of the Hinderplaat towards the south does not occur under these conditions. The sediment transport patterns that lead to these bed level changes are often even contrasting to the transport patterns generated under NW conditions. This will be elaborated further on in this chapter.

Strikingly, only simulations with medium-strong northern wave conditions combined with north-eastern wind speeds correctly reproduce the patterns on the Hinderplaat as well as the erosion of the upper shoreface. This is most likely not a correct representation of reality, as this wind condition is uncommon in the study area and an overall erosion of the shoreface has been observed in the considered period. It is probably an error of the numerical model, that underestimates the wave-asymmetry induced cross-shore transport. This is further elaborated in Appendix B.

6.3.2. THE FORCING MECHANISMS BEHIND MORPHOLOGICAL CHANGES

Flow results have shown that besides the tide and discharge flows through the sluices, wind-forcing forms an important mechanism when determining the residual patterns in the area of interest. However, this might be different for the sediment transport rates. To investigate the consequences of the hydrodynamic forcing mechanisms on the morphology, the impact of the various processes on the initial bed level changes is assessed in Figure 6.13.

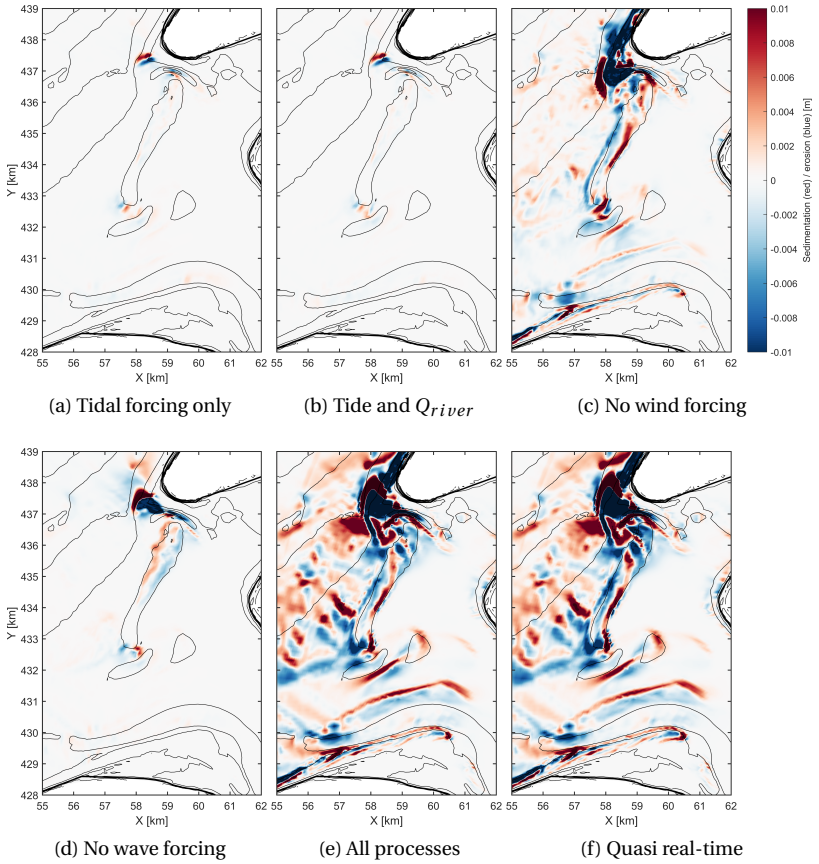

(a) Tidal forcing only (b) Tide and Q_{river} (c) No wind forcing

(d) No wave forcing (e) All processes (f) Quasi real-time

Figure 6.13: Initial bed level changes for all simulation scenarios, scenarios c-e are simulated with a medium-strong WSW condition

Tidal currents and discharge flows are hardly capable of generating sediment transport. If the wind forcing is disabled bed level changes are significantly smaller than when all processes are included. This is clearly visible at the shoreface, where changes are much smaller, but it also holds for the bed level changes on the Hinderplaat. For simulations without waves the bed level changes are several orders of magnitude smaller

on the entire area, which shows the essential importance of waves for sediment transport; they do not only induce the flow, but they also stir up the sediment and bring it into suspension. But this does not imply that other processes are irrelevant, as since both the wind forcing (as just explained) and the imposed surge levels enhance the magnitude of the changes. As defined in Chapter 4.3.1 the schematisation of the surge is limited to adapted water levels along the offshore boundaries. The modifications are uniform for the entire boundary, implying that water level gradients are not accounted. It are, however, the gradients that are likely to have an impact on the hydrodynamics of the area. Therefore, this analysis only shows the effect of a uniform surge level on the bed level changes, while the complete effect of the surge might be different. Nevertheless, Figure 6.13f already shows that a moderate increase of the water levels (surge levels of $0.3m$, already increase the sedimentation/erosion rates on the Hinderplaat.

6.3.3. SEDIMENT TRANSPORT PATTERNS

The sediment transport patterns that lead to the morphological changes of the previous section have been evaluated to gain understanding in the different responses of the system for varying wind- and wave-forcing directions. Figure 6.14 provides an impression of the residual sediment transport patterns and magnitudes on outer delta scale for a quasi-real-time simulation with medium NNW conditions (simulation D, wave condition 24). Under NW-N wave conditions, sediment transport from the Slufterdam towards the Hinderplaat takes place. This sediment is transported southwards along the seaward edge of the shoal, with the largest transport rates at its southern end. Likewise, the coastline of Goeree seems to be fed by sediment originating from the Bollen van den Ooster shoal in the Grevelingen outer delta. The modelled wave condition contains a wind direction of 302°, which is close to shore-normal. As shown in Figure 6.6c, residual currents in the foreshore tend to be minimal for these directions. This leads to relatively low sediment transport rates on the area in front of the Hinderplaat. Note that the largest transport rates are found in the shallow areas where waves break (*surf zone*).

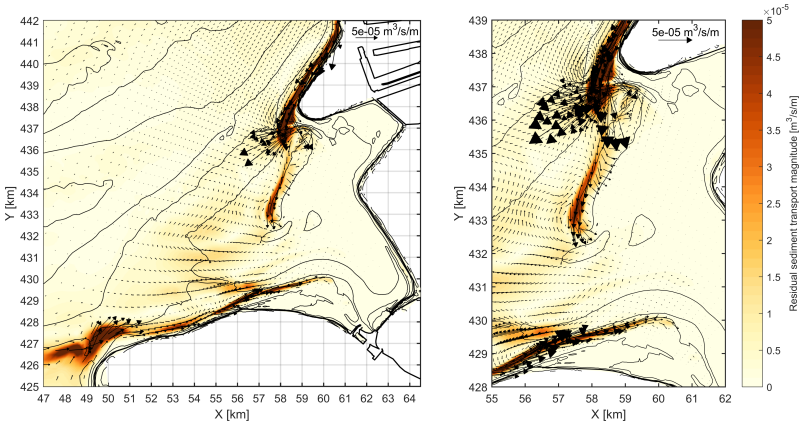

(a) Large-scale transports

(b) Detailed transports on the Hinderplaat

Figure 6.14: Residual sediment transport after two tides for NNW conditions

Several transport patterns can be distinguished on the Hinderplaat. Along its entire seaward edge southern directed transport takes place, with the largest transport rates at the southern end. This is probably the cause for the elongation of the shoal. At that location, the patterns are slightly deflected towards the SE, following the orientation of the Bokkegat channel. Over a major part of the shoal ESE directed transport occur, resulting in an overall landward migration. At the northern end, northwards directed transport occur, which acts as a sediment supply for the Hindergat channel that migrates towards the Slufter.

Figure 6.15 illustrates a time series of instantaneous sediment transports integrated over a cross-section along the Hinderplaat (from the northern to the southern end) for the same simulation as Figure 6.14. The red lines indicated the tidal phases, as previously defined. Sediment transport is apparently governed by the suspended load component due to the residual currents, as its values are often more than twenty times larger than the bed load component. A comparison of the time series with the velocity time series at Hinder channel of Figure 6.1 shows an expected positive correlation between the transport magnitudes at the Hinderplaat

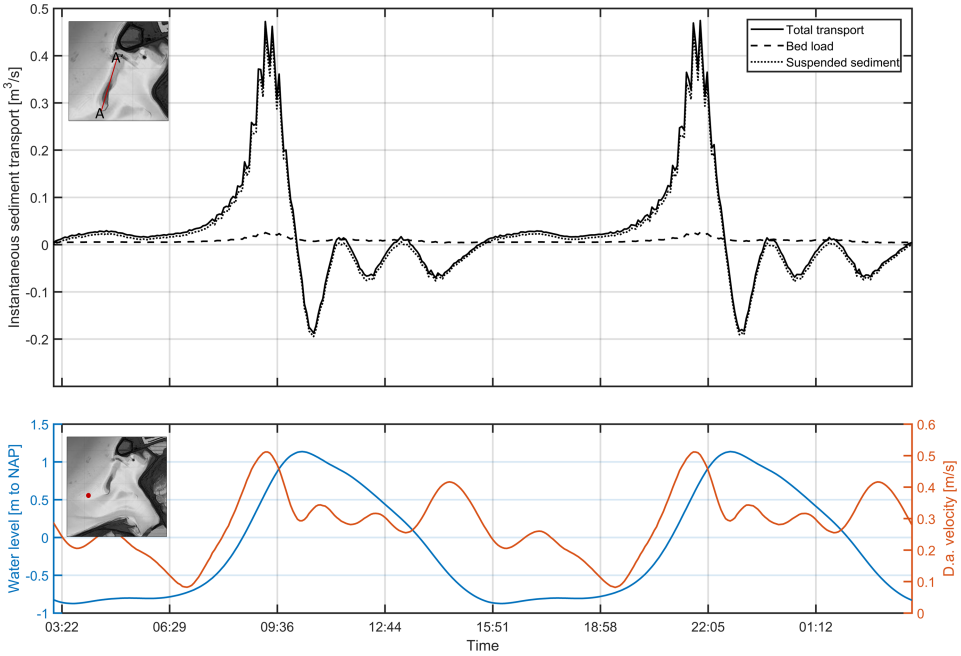

Figure 6.15: Instantaneous sediment transport integrated over a cross-section along the Hinderplaat for NW conditions during two tidal cycles

and the velocities at the channel in front of it. The largest transports occur just before high water, when the offshore flow is in flood direction and water flows both through the channels and over the Hinderplaat into the basin (see Figure C.7).

To illustrate the relative contribution of the hydrodynamic processes on the sediment transport rates during a tidal cycle, Figure 6.16 is presented: this figure shows the instantaneous transport rates for all simulation scenarios. Scenarios that include wind and/or wave forcing are simulated with the same NW condition as Figure 6.15.

A correlation is found between the sediment transports of scenarios A, B and D, which are all scenarios without wave-forcing, for which the transport rates are much smaller than for the other scenarios. From this one may once again conclude that wave forcing is crucial for morphodynamics. Apparently, neither the tides, the discharge flows or the wind-driven currents are capable of bringing sediment into suspension. This does not imply that they are not capable of transporting it, as it is shown that wind-driven residual currents may dominate over a large part of the study area (see Section 6.2.3). However, Figure 6.16 shows that under medium NW conditions wave-driven currents are the primary mechanism to determine the transport direction on top of the Hinderplaat, since simulations that exclude the wind-forcing are only slightly different. Surge levels act as moderate amplifiers of the sediment transport rates.

The correlation between the increase in bed load transport around 09.00 of Figure 6.15 and the increase in sediment transport for simulation scenarios A, B, and D of Figure 6.16 at that same time is remarkable. This may suggest that bed load transport is the dominant transport mechanism for these simulations. However, this is not the case: also for these scenarios most of the sediment is transported as suspended load.

As mentioned in Section 6.3.1, SW conditions usually lead to different sedimentation/erosion rates than NW conditions, although medium-strong conditions from WSW-WNW may cause initial bed level changes that are somehow similar to the changes induced by NW conditions. Yet, the sediment transport patterns show a great variation for different wave-incidence angles. Figure 6.17 presents the residual transport patterns for quasi-real-time simulations with southern to north-north-eastern conditions. Southern conditions hardly generate any transport as these waves can barely reach the area. Sediment transport patterns at the shoreface usually follow the wind-generated residual flow patterns. Here, the highest transport rates in front of the Hinderplaat are found for WSW conditions, although this is not necessarily the direction under which the max-

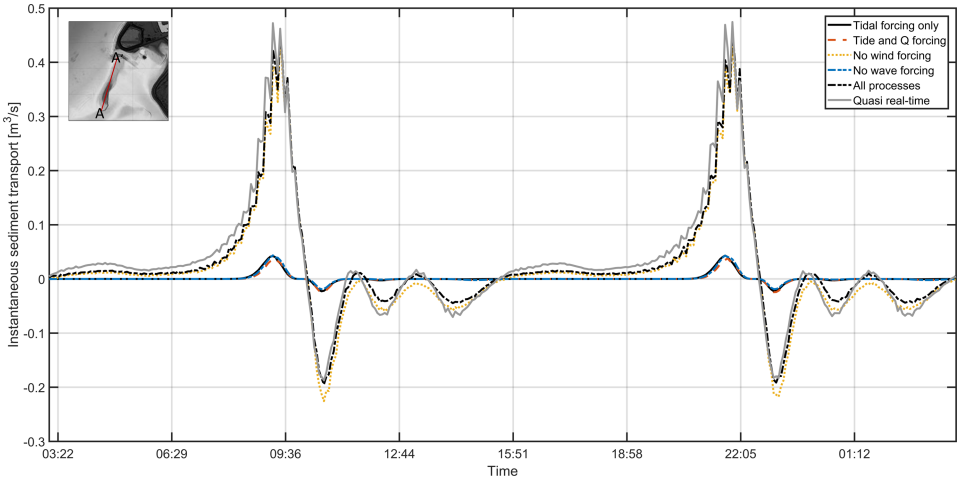

Figure 6.16: Instantaneous sediment transport integrated over a cross-section along the Hinderplaat for all simulation scenarios

imum rates on the shoal are generated. Landward directed transport of sediment on top of the shoal occurs mostly under WNW conditions, which is in correspondence with previous findings. Under WSW conditions the transport is partly landwards directed (southern side) and partly seawards (northern side). For SSW simulations the transports are mainly seaward directed and under S and NNE conditions hardly any transport is visible on top of the Hinderplaat.

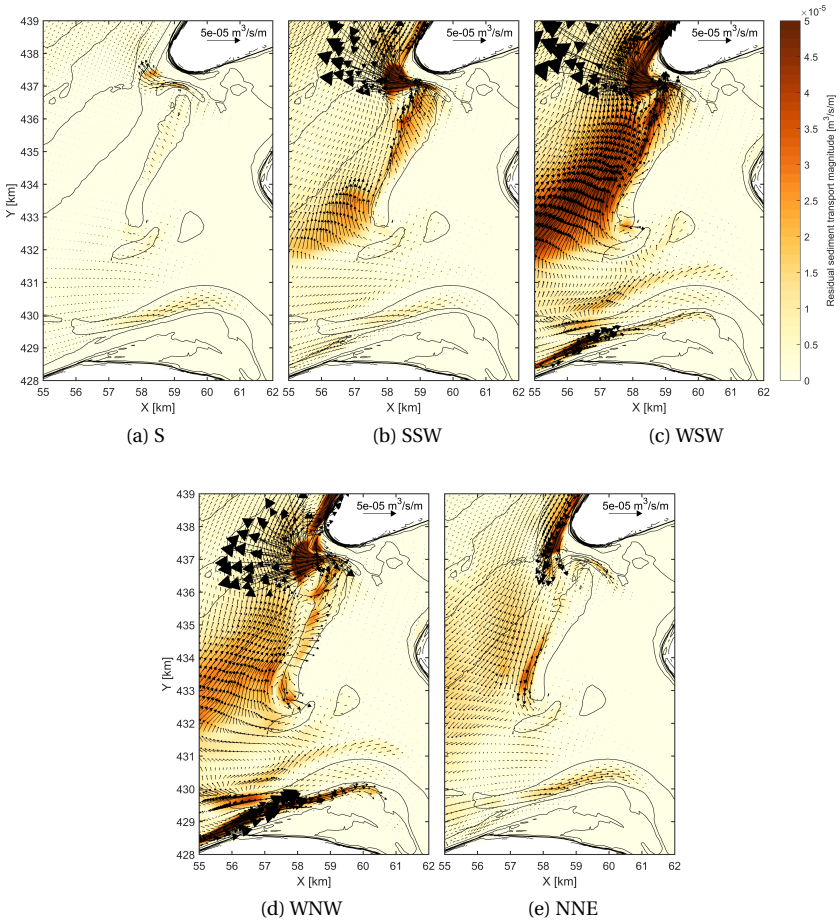

(a) S (b) SSW (c) WSW

(d) WNW (e) NNE

Figure 6.17: Residual sediment transport after two tides for different wave- and wind directions of medium strength-class

6.3.4. MORPHOLOGICAL IMPACT OF AN EXTREME DISCHARGE EVENT

The hypothesis has been formulated that the extreme discharge event of 1995 was the main cause for the breach in the Hinderplaat that was first observed in the bathymetry measurements of that same year. This bathymetry is shown in Figure 6.18a along with the initial model bathymetry (Figure 6.18b) and the calculated bathymetry after the hindcast simulation (Figure 6.18c). The bed level changes and sediment transport rates that lead to the bathymetric changes are presented in Figures 6.18d and 6.18e.

Three small initial breaches are created on top of the Hinderplaat; the largest one has the same location as the observed breach in the Vaklodingen data. Besides, they have the same orientation, which corresponds to the main flow direction on top of the shoal (see Figure 6.8). The channels Slijkgat, Bokkegat and Hindergat become deeper due to the event. The latter also shows a significant delta formation at the seaward side, due to a sudden decrease of flow velocities. On top of the Hinderplaat sediment is mainly transported across the shoal, towards the NW. This sediment is then deposited on the seaward edge of the shoal.

The presence of a translatory wave after closing the sluices, as described in Section 6.2.4, does not seem to have a big influence on the residual transport rates on the Hinderplaat: these are dominated by the offshore directed flow, caused by the water level gradients over the shoal. The same holds for the bed level changes on the shoal: the erosion rates on top of the shoal and the initial breaches are generated by the offshore directed discharges.

According to the model results, we can conclude that the extreme event of 1995 certainly had a crucial contribution to the breach at the Hinderplaat. Extreme river discharges led to high flow velocities over the shoal, resulting in an overall lowering of the bed with large erosion rates at the location of the initial breach. With this breach, a shallow channel was created on top of the shoal. It is very likely that the depth of the channel was increased later on by tidal flows (under regular conditions) after the event, leading to the channel formation observed in Figure 6.18a. But the question remains, why the initial breach occurred at that exact location.

Previous research has shown that the location of a breach is a very sensitive process, which is often not readily determined based on the geometry of the initial profile (De Vet, 2014). Aspects that may play a role in the exact location are for instance vegetation, spatially varying sediment and roughness characteristics and initial weaknesses in the soil. Surprisingly, the location of the breach is predicted correctly by the numerical model, which suggests that it has something to do with the imposed initial conditions. Figure 6.18b shows that the initial bathymetry of the location of the breach already showed a lower bed level that its surrounding areas, which explains the correct prediction by the model. This local lowering of the bed might have been caused by a previous storm or high discharge events. Moreover, it is likely that the geometry of the Hindergat contributed to the channel formation on the Hinderplaat. The construction of the Slufter and its sedimentation rates just north of the Hindergat have led to narrowing and sharp deflection of the channel inlet towards the SW, causing a stronger curvature of the tidal currents. This unnatural direction for the flow through the channel (especially in case of high discharges and strong currents) probably contributed in the process of breaching and channel formation.

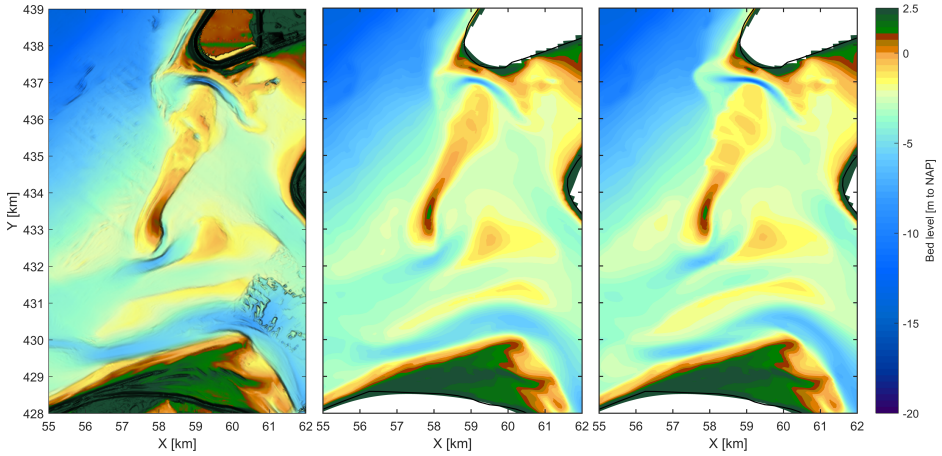

(a) Measured bathymetry 1995 (b) Initial model bathymetry (c) Calculated bathymetry after the event

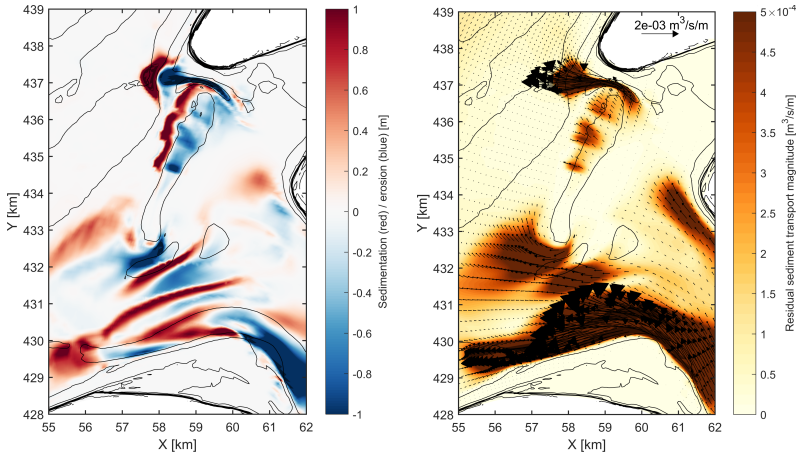

(d) Bed level changes due to the event (e) Mean total transport rates

Figure 6.18: Morphological impact of the high discharge event of 1995

7

CONCEPTUAL MODEL

7.1. INTRODUCTION

To synthesise and explain the results of this thesis as well as the findings of previous research (Aarninkhof and van Kessel, 1999, Elias and Van der Spek, 2014, Elias and van der Spek, 2016, Steijn et al., 2001, Van Holland, 1997, Van Vessem, 1998) a conceptual model is proposed to explain the morphological development of the Hinderplaat. This is presented in this chapter: firstly, the observed evolution is processed in Section 7.2 according to the evolutionary phases that are established in Section 3.4.6. Secondly, the modelling results regarding the mechanisms behind the degradation are processed in Section 7.3. Lastly, the model for the complete evolution since the closure of the Haringvliet is presented in Section 7.4.

7.2. EVOLUTION

Based on the findings of Chapter 3, a schematic overview of the morphological development of the Haringvliet outer delta is presented in Figure 7.1. The evolution has been divided into three characteristic phases, of which the last one consists of two parts. Figure 7.1 shows characteristic bathymetry maps for the considered stages. The main channels and shoals, which have undergone a significant transformation in time, are indicated by numbers. To show the shape of the shoals, these are represented in yellow. Moreover, the intertidal areas are visualised with an orange shading.

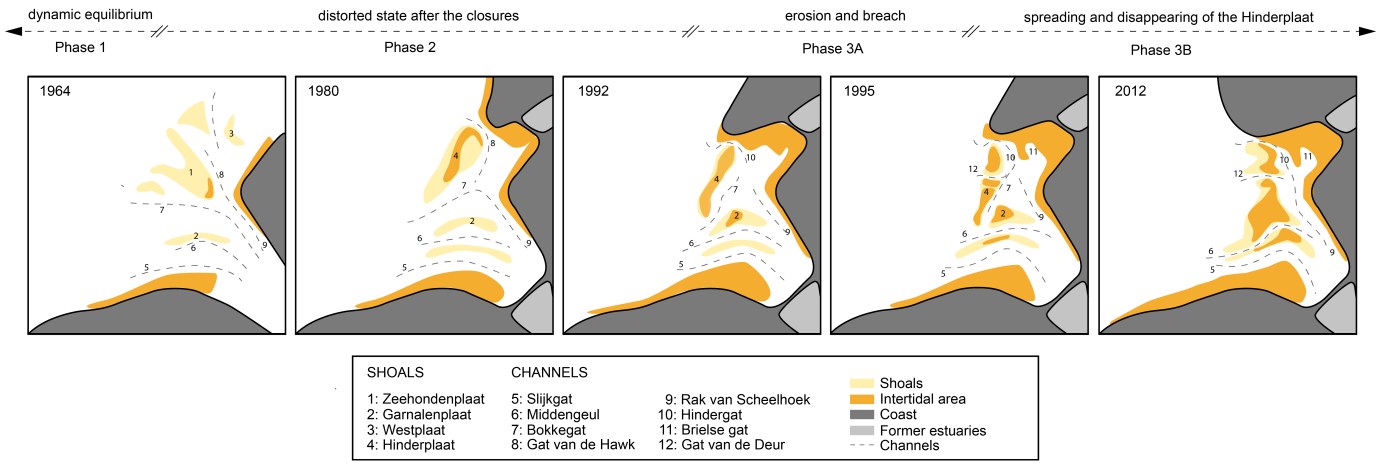

Figure 7.1: Schematic overview of the Haringvliet ebb-tidal delta development. Redrawn after original maps which are retrieved from the Vaklodingen dataset

7.3. MECHANISMS BEHIND THE DEGRADATION OF THE HINDERPLAAT

7.3.1. EVALUATION OF THE HYPOTHESES

To determine the mechanisms behind the morphological evolution of the Hinderplaat, first, the proposed hypotheses of Chapter 4 are evaluated below.

1. Current patterns in the Haringvliet ebb-tidal delta are strongly influenced by the wind forcing, considering the limited depth of the area.

This hypothesis is partly confirmed. Simulations with moderate wind forcing ($U \approx 9.5 m/s$) show that wind-driven currents are capable of changing the direction of the residual currents in the study area. However, this is most effective on the shoreface in front of the Hinderplaat, instead of at the intertidal areas of the outer delta. Wave-driven currents also have an impact on the residual flow, although their contribution is smaller than expected: they are not capable of altering the direction of the current patterns at the shoreface, but they do contribute to the net current speeds. Their influence on the currents on top of the Hinderplaat is however larger. Besides from the wind and waves, river discharge-forcing has a great impact on the residual currents, primarily where the main channels are located.

2. Wind effects are of major importance for the morphological evolution of the Hinderplaat and its surrounding channels.

This hypothesis is partly confirmed. It is true that wind effects are of vital importance for the residual currents surrounding the Hinderplaat, as the wind forcing is capable of fully altering the direction of the main flow. However, wind- and tidal-currents alone are not capable of inducing significant bed level changes: model results show that stirring up the sediment by waves is an essential mechanism for sediment transport in both alongshore and cross-shore direction. Thus, waves are indispensable for the morphological changes of the study area. Nevertheless, once the sediment is brought into suspension by the waves, the direction of the transport at the upper shoreface is mostly determined by the wind-driven currents. This does however not hold for sediment transport on the Hinderplaat itself: results have shown that transport rates on top of this shoal are mainly determined by wave-driven currents.

3. The landward migration of the Hinderplaat is part of its intrinsic behaviour under regular conditions, rather than a consequence of human activities and sporadic events

This hypothesis is confirmed. Model results show that regular forcing, without the contribution of extreme events nor human activities, is sufficient to explain the landward migration of the shoal. Wave conditions of medium-strength and more energetic ones ($H_s \geq 2.3 m$) from NW-N direction break in front of the Hinderplaat, stirring up sediment and generating cross-shore currents along the shoal (due to the water level gradient) that are responsible for the landward migration.

4. A reduction of the sediment availability of the foreshore combined with ongoing landward directed sediment transport in the back-barrier area caused the shift from an increase to a decrease in the height of the Hinderplaat in 1992

This hypothesis is mainly disproved. Lowering of the Hinderplaat bed levels mainly concerns the height decrease of the southern end of the shoal. This is a consequence of residual sediment transport from this area towards the south, which also caused the elongation of the shoal. This phenomenon occurs under WSW-NNE conditions, although the transport rates are strongest under NNW conditions. The link between the sediment availability originating from the shoreface, its transport towards the Hinderplaat and the height of the shoal could not be studied as the numerical model severely underestimates the cross-shore transport rates: previous research suggests that the shoreface erosion is a consequence of sediment transport caused by the deformation of short waves under the influence of decreasing water depth (wave-asymmetry). This type of transport is probably not reproduced well by the imposed transport formulation and is therefore underestimated. Thus, a correlation between these phenomena it is not entirely disproved. Besides, it should be noted that the increase in the height of the Hinderplaat mainly took place right after construction of the Slufter, which suggests that has been an essential temporal sediment source.

5. Longshore sediment transport rates induced by northern conditions play a key role in the existence of the Hinderplaat.

This hypothesis is confirmed. Model results showed that under NW to NE conditions large longshore transport rates are generated along the Slufterdam towards the Hinderplaat. These transports feed the sediment demand of the shoal and enable its extension in southern direction. This also explains the similarity in the orientations of the Slufter and the Hinderplaat.

6. Breaching of the Hinderplaat was a consequence of the high discharge event of February 1995.

This hypothesis is mainly confirmed. Model results show that the extreme event of 1995 certainly had a substantial contribution to the breach of the Hinderplaat. High discharges induced large water level gradients over the Hinderplaat, leading to fast offshore directed currents and sediment transport rates. This resulted in overall erosion rates on the northern part of the shoal and sediment deposition along its seaward edge. The morphological model predicts the formation of three small initial breaches; the largest has the same location and orientation as the observed breach in the bathymetric maps. It is expected that the depth of the channel was increased later on by tidal flows (under regular conditions) after the event, leading to channel formation.

7.3.2. CONCEPTUALISING THE DEGRADATION

In addition to the evaluated hypotheses, the main model findings are synthesised in Figure 7.2. The outer delta shows a considerable variation regarding which mechanisms are most dominant. Note that when we speak of dominant processes, we mean the processes that mainly determine the sediment transport patterns and rates (and thereby also the morphological changes), given the fact that the sediment is already brought into suspension. The reason for this is that waves are indispensable to mobilize the sediment from the bed in the study area. So in a way, waves always dominate the morphological changes. In Figure 7.2a only those areas have been marked that show an overruling dominance by a particular forcing mechanism. In other words: the residual patterns for areas that have not been marked show a great variation in dominant processes. Although a hydrodynamic process may be the prevailing mechanism at a morphological unit, this does not imply that the other processes are insignificant. Sediment transport patterns on top of the Hinderplaat are mainly determined by waves, but both wind and surge enhance the transport rates for instance. An

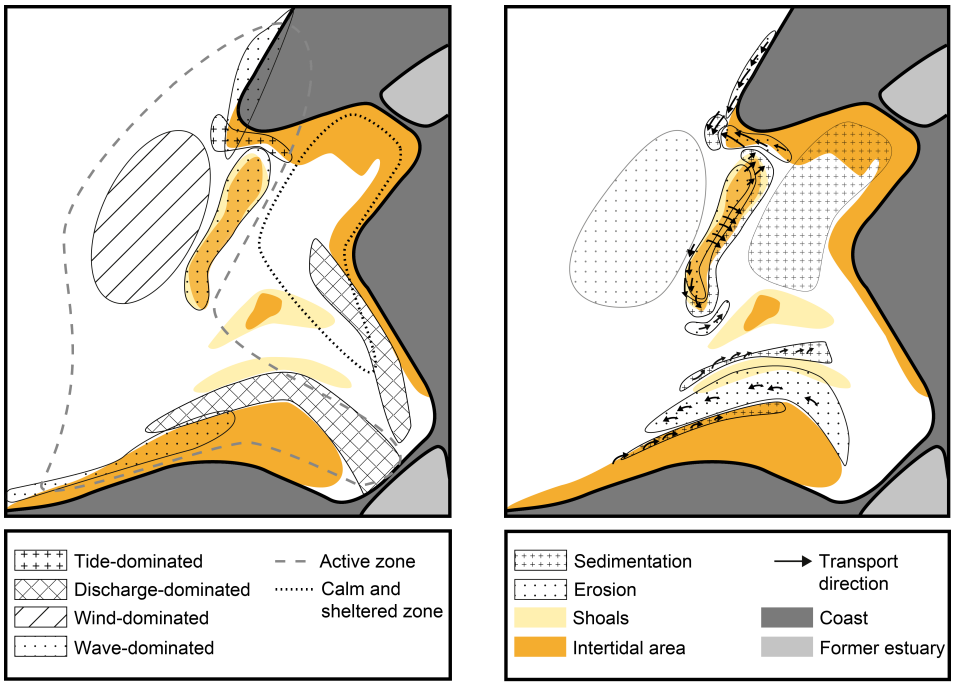

(a) The dominant mechanisms

(b) General transport and bed level changes

Figure 7.2: Conceptual description of the morphodynamic characteristics in 1992

active zone and a calm and sheltered zone have been defined. In the active region high flow velocities take place and large morphological activity is detected, whereas the calm zone shows much less hydrodynamic and morphological activity due to its sheltered location.

The findings of the data analysis and the morphological model have been combined to create a general overview of morphological development for the period right after 1992. This is presented in Figure 7.2b, which shows a conceptualised version of the sedimentation/erosion patterns and the underlying transport pathways. Note that the upper shoreface in front of the Hinderplaat and the sheltered area behind it are marked in grey since the bed level changes were less strong than at the other marked areas, but it is still noteworthy.

7.4. MECHANISMS BEHIND THE EVOLUTION

The findings of previous research and this study on the mechanisms behind the evolution of the Haringvliet outer delta have been combined and captured in Figure 7.3. This section describes each phase, grasping the entire evolution of the Hinderplaat, from its origin to its disappearing.

Phase 1: dynamic equilibrium prior to its existence
Before the closures of the Brielse Maas and the Haringvliet, the ebb-tidal delta was characterised by cross-shore channels and shoals which were a result of the balance between the cross-shore tidal currents and the wave action. Ebb currents transported sediment from the estuary mouth in offshore direction, which was deposited seaward where the flow velocities decreased beyond the transport value. The latter involved breaking waves on the generated sandbars, which caused landward directed sediment transport. Thereby it counteracted the continuous outbuilding of the ebb-tidal delta.

Phase 2: the origin of the Hinderplaat during the distorted state after the closures
Due to the closures, the cross-shore tidal flow disappeared while the wave-action remained the same, leading to a regime shift of the outer delta towards a wave-dominant environment. The tidal prism decreased, which forced the system to an equilibrium with a smaller ebb tidal delta. The dominance of the wave action caused significant erosion of the shoreface, transporting the sediment in eastern direction and creating the longshore sandbar Hinderplaat. After construction of the Slufter, its dam acted as a sediment source for the Hinderplaat. Breaking waves induced southward directed sediment transport both on the Slufter and on the intertidal bar, which facilitated the growth of the latter. On its landward side a sheltered back area was created, where the hydrodynamic conditions were mild enough for fine sediments to deposit.

Phase 3A: erosion and breaching of the Hinderplaat
As the longshore transport along the shoal continued, the Hinderplaat remained increasing in length by spreading in southern direction. High transport rates at its southern end under WSW-NNW wave conditions did not only contribute to its elongation, but they also induced a lowering of its highest point. In the meantime, waves generated a water level gradient along the sandbar which caused landward currents and sediment transport. As the outer edge of the shoal eroded the inner side accreted, resulting in a landward migration of the shoal. Surge levels and wind-generated currents enhanced the underlying sediment transport rates. An extreme discharge event in February 1995 caused very fast offshore directed flow on top of the bar that induced an initial breach. Tidal currents after the event contributed to the breaching process resulting in channel formation as the Gat van de Deur was created.

Phase 3B: spreading and disappearing of the Hinderplaat
After breaching the shoal destabilised and continuous channel formation and deformation has been observed. However, the channel formation was often limited to small-scale inlets which cannot be maintained by the limited tidal prisms through them. Infilling of the sheltered area continued, limiting the tidal circulation even more. Waves kept pushing the Hinderplaat in southern and landward direction, causing its merge with the Garnalenplaat. Meanwhile the channel Bokkegat, in between the shoals, had disappeared. The morphological changes in the outer delta have been so big, that the bathymetry is not likely to go back to its initial character (phase 1), even when fully opening the Haringvliet Sluices (Wijsman et al., 2018). Implementation of the Kierbesluit policy -which includes partial opening of the sluices during high water- will mainly influence the Slijkgat area.

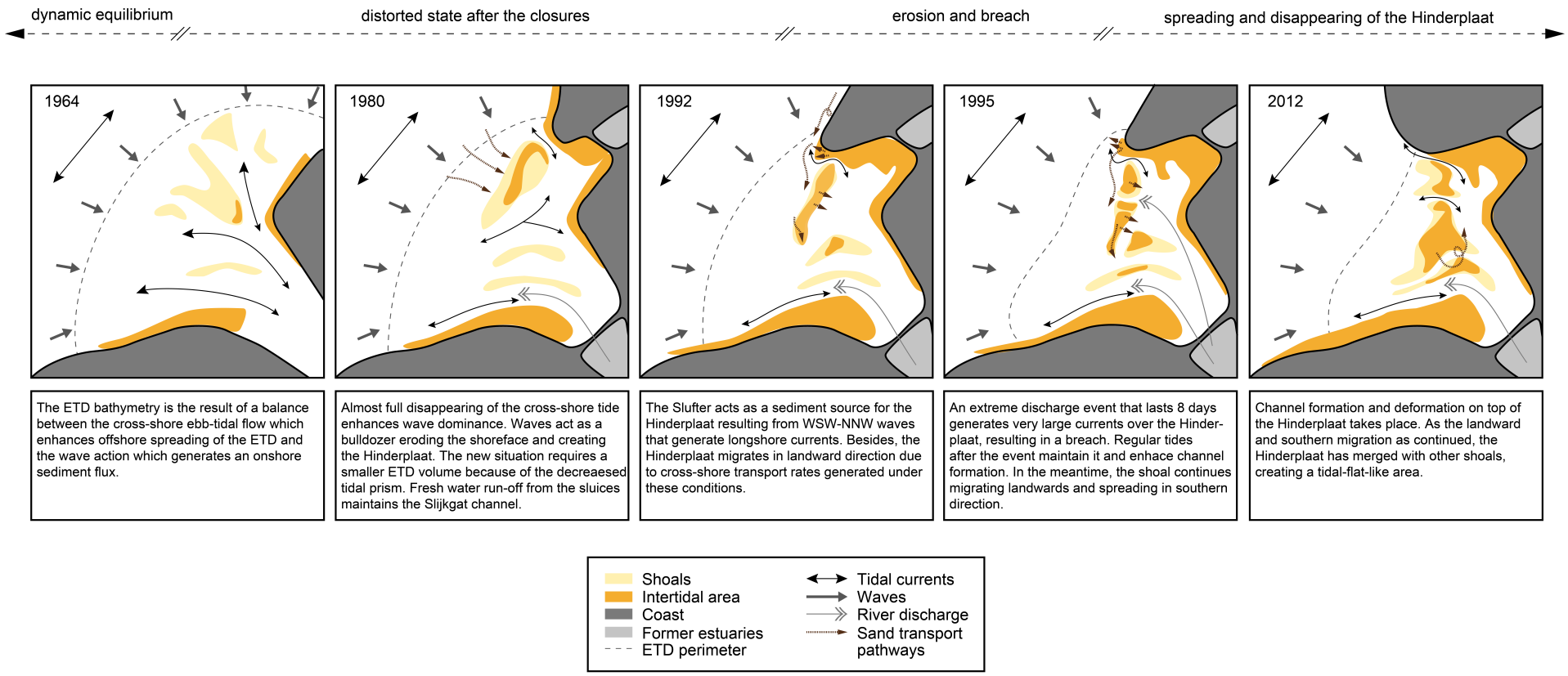

Figure 7.3: Conceptual model for the ebb-tidal delta evolution of the Haringvliet after a significant reduction in cross-shore flow

8

DISCUSSION

Before establishing the main conclusions that follow from the data analysis and modelling results, first a critical reflection is required on the conducted research. This chapter provides a discussion on the methods, results and generalisation of the research.

8.1. METHODOLOGY LIMITATIONS

The Vaklodingen dataset, which is used to study the bathymetric development of the Haringvliet outer delta, contains yearly measurements of the Dutch coast (covering the Delta-, Holland- and Wadden Sea Coast). However, not all areas are included in all yearly measurements, and the frequency of the measurements of the Haringvliet delta have varied over the years. This limits the bathymetric study, as only mid- to long-term trends can be identified. Besides, a comparison of trends between years has shown that sometimes errors are introduced during the data collection or processing. This leads directly to inaccuracies and uncertainties in the dataset since correction of these errors is hardly possible due to the unknown origin. Years with abnormal changes in the dataset are therefore excluded from the analysis.

Computational time restrictions in combination with a large number of simulations do not allow for three-dimensional computations with the Delft3D model. It was assumed that in the area of interest (Hinderplaat shoal) 3D-effects are of minor importance. Density-driven currents caused by the interaction of the fresh-water from upstream and the saline seawater will mainly influence the hydrodynamics of the area near the sluices and Slijkgat channel, especially under regular conditions. During extreme discharge events, the river discharge flows over the entire area. Density-driven currents may generate a landward directed undertow. Since the lower part of the water column contains higher sediment concentrations, this is likely to have a considerable effect on the net sediment transport rates. However, this will mainly take place at the channels. For this reason, this assumption is considered to be reasonable.

The tidal signal is simulated with a repeated morphological tide, which implies that variations in terms of spring-neap cycles are not accounted for. As a consequence, the model predicts less frequent inundation of the Hinderplaat shoal and the calculated residual tidal currents are probably smaller than in reality. This is not expected to have a significant influence on the sediment pathways, as wind and wave generated currents often overshadow the contribution of the tide on the residual currents on the Hinderplaat. Although the influence of the tide on the residual currents is limited, it does determine the water depth at the Hinderplaat. Including spring-neap variations in the model simulations might therefore change the predicted timescales of the bed level changes: these will probably become shorter. Moreover, a scenario with high wind speeds during spring-tide is very likely to have major impacts on the ebb-tidal bathymetry since the effect of the wind on the currents increases with decreasing depths. The implications for the Hinderplaat bathymetry of 1992 will however be small, considering that the shoal has fully emerged during low water.

The occurrence of a large-scale water level setup is accounted for by specifying the mean surge level of the concerning condition and adding it to the mean water level in the forcing at the alongshore offshore boundary. This implies that surge gradients in alongshore directions are not considered, while these gradients gen-

erate additional currents that are neglected in this thesis. Consequently, the obtained results on the effect of the surge are treated with care and it is stated that this effect is likely to be larger than suggested by these results. On the other hand, surge levels will be largest, and therefore most important, during (sporadic) extreme storm conditions with high wind speeds. These conditions are not within the scope of the modelling experiment, as it was the goal to investigate the development of the Hinderplaat under frequent forcing conditions.

8.2. IDENTIFYING THE MECHANISMS

By means of the data analysis, it was determined that the degradation of the Hinderplaat had been a gradual process, from which the hypothesis followed that it might have been a consequence of the natural behaviour under regular conditions. Modelling results have primarily confirmed this, although this does not imply that extreme storm events did not influence the study area. The impact of these events remains unstudied and further research is needed to understand the exact evolution fully. Yet it is shown that simulations with calm to strong conditions (thus excluding extreme storm events) are sufficient to explain the development of the shoal.

The breach of 1995, which lead to the formation of the channel Gat van de Deur, is proven to be a direct consequence of an extreme discharge event. However, a high river discharge is not the only mechanism that may lead to a breach. Breaching potential is achieved if the water level on one side of the shoal exceeds some critical elevation in relation to the crest of the barrier (Kraus et al., 2002). Duration of higher water level is also a contributing factor. Breaching from the seaward side of the Hinderplaat may occur during severe storm events through a combination of elevated water level by storm surges and large waves. Moreover, after a storm passes, the surge water that has piled up behind the Hinderplaat, surges back seaward generating an erosive current. This ebb surge can change the shape of existing inlets or even scour shallow initial breaches on top of the shoal (Pilkey et al., 1998, Tuan, 2007).

In this research, an attempt is made to discover the individual influence of the forcing mechanisms on the evolution of the Hinderplaat. One should consider that the studied processes are not entirely independent, as high wind speeds often coincide with energetic wave conditions and increased surge levels for instance. Moreover, even if a process is not capable of generating sediment transport itself, this does not mean that it does not contribute to the sediment transport rates. In fact, wind-forcing is hardly capable of bringing sediment into suspension, but when combined with waves it substantially increases the bed level changes. Besides, the relative contribution of the wind compared with the waves on the flow seems to be considerably larger for more energetic conditions, which suggests a non-linearity in the contribution of the different mechanisms.

This non-linearity makes it very difficult to provide quantitative results on effects of the different mechanisms. Besides, previous research has concluded that the morphological predictions of the model are not sufficiently accurate concerning net transport rates and bed level changes. Consequently, the presented results should be interpreted qualitatively instead of quantitatively.

The geometry of the outer delta has not been mentioned as a mechanism, as it does not exert a forcing on itself, while one should acknowledge that it does have a considerable influence on its own morphological development. A clear example for this is the observed breach through the Hinderplaat: although an extreme discharge event had a substantial contribution to the breach, the reason that the shoal breached at that exact location had to do with an already existing local lowering of the bed. Studying the morphological development of a coast requires morphodynamic research (i.e. research on the mutual adjustment of morphology and hydrodynamic processes involving sediment transport). Despite all, it was decided to conduct morphostatic simulations with the numerical model for three reasons. First of all, this research studies the short-term (two tidal cycles) response of the outer delta under various conditions. Flow patterns and initial sediment transport rates are good indicators to debate the reaction of the system to the modelled scenarios. Besides, longer-term morphological predictions of the model (that are obtained with morphodynamic simulations) show a broad uncertainty range (De Vries, 2007). Furthermore, time-wise it is not realistic to perform mid- nor long-term simulations, when considering the large number of required scenarios. Nevertheless, this implies that the feedback effect of the geometry on the hydrodynamics should be considered based on expert judgement.

Lastly, the effect of sea level rise on the evolution of the Haringvliet outer delta should not be overlooked. Although this is a slowly ongoing process, it will have a significant impact on the long-term morphodynamics (Passeri et al., 2015). For short-term simulations, it is acceptable to ignore its effect, while this certainly does not hold for (future) long-term studies. Unfortunately, the large observed changes since the closure of the Haringvliet make it highly complex to determine the effect of sea level rise on the evolution. Moreover, it is very likely that new human interferences will take place on the timescale over which sea level rise has an impact on the morphodynamics. This will once again add complexity to studies on this phenomenon.

8.3. GENERALISING THE RESULTS

This research assesses the relative contribution of several hydrodynamic drivers on the morphological evolution of the Haringvliet outer delta. However, for other outer deltas with different characteristics, the outcomes may be different. Even cases that at first sight seem to be very similar might have a different response to the local hydrodynamics.

A striking example of this is the Grevelingen outer delta, located south of the Haringvliet delta. After constructing the Grevelingendam and Brouwersdam, and thereby fully separating the Grevelingen from the North Sea, the outer delta showed a very similar evolution to the Haringvliet with the creation of the longshore intertidal bar Bollen van den Ooster (Elias et al., 2015). Differences in hydrodynamic forcing between the Haringvliet and the Grevelingen outer delta are relatively small: both former deltas no longer experience the cross-shore tide and the longshore tidal signal is very similar as well as the wind- and wave-forcing at their offshore boundaries. Despite all, the Bollen van den Ooster is still growing at the moment, while the degradation of the Hinderplaat started 25 years ago. This might either indicate that this outer delta has a slower adaptation, or that the equilibrium state is different. Differences in the morphological developments of the Hinderplaat and the Bollen van den Ooster might, for instance, be induced by the difference in orientation of the shoals. Either way, further research is necessary to provide a clear explanation.

With regard to the results of this research: these are now site specific and comparison with several other outer deltas is required to formulate general conclusions. The impact of wind-driven processes on shallow water areas, for instance, is far from understood (Wang et al., 2012) and fundamental research into this topic would benefit from a comparison between different case studies.

9

CONCLUSIONS

The objective of this research was to reveal the physical processes that are responsible for the degradation of the Hinderplaat and to define their link to the human interventions and extreme meteorological events. In this chapter, the research question is answered by presenting the answers and conclusions to the sub-questions as defined in Chapter 1.

1. What has been the morphological development of the Hinderplaat since the construction of the Delta Works in the Haringvliet estuary?

Before the closure of the Haringvliet estuary, shore-normal shoals and flats characterised the ebb-tidal delta, which was maintained by a combination of the tidal forcing in long- and cross-shore direction and the wave action. In 1968 the shore-normal Zeehondenplaat started to alter its orientation, eventually changing into the shore-parallel Hinderplaat, which obtained its pronounced spit-shaped geometry around 1976. Subsequently, the shoal migrated landwards and grew both in length and in height. This continued until 1992 when its degradation started. In general, the deterioration of the Hinderplaat can be divided in the following developments: a landward migration since its formation, lowering since 1992 and breaching in 1995. Erosion of the lower shoreface was observed approximately until the moment when the Hinderplaat started to decrease in height, although the upper shoreface on the seaward side of the Hinderplaat continued eroding. Additionally, a northward migration of the adjacent channel Hindergat took place until 2003.

2. What interventions have taken place in and around the Haringvliet outer delta and what meteorological events have occurred since the first closure?

Between 1950 and 1970 the Brielse Maas and the Haringvliet were dammed and subsequently the Brouwersdam was constructed in 1971. Moreover, the Port of Rotterdam has been extended several times, with the construction of Maasvlakte 1 & 2 and the Slufter. The coasts of Voorne and Goerree and the Slufterdam have regularly been nourished since 1969, whereas the Slijkgat has been dredged to maintain its navigability.

Two types of extreme events are considered: extremely high discharges through the Haringvliet Sluices and exceptionally strong storm events. Both in 1993 and 1995 unusually high daily values were observed for the water run-off through the sluices during several days. The highest discharge exceeded the value of $9000 m^3/s$. An extreme storm event in the Southwest Netherlands occurred on January 25^{th} 1990, with wind speeds of $30 m/s$ generating waves of over $6 m$ height offshore.

3. What are the characteristics of the water motion and which mechanisms are most dominant?

Closing off the estuary in 1970 caused a reduction of the tidal current velocities in the estuary, increasing the relative influence of the waves and thereby triggering a regime shift. Under calm conditions, the tidal flow patterns in the ebb-tidal delta are mainly determined by the tidal signal and the influence of the fresh-water outflow through the sluices. The latter is especially noticeable in the offshore flow direction and the increase in flow velocities at the main channels during low water. Residual currents on the Hinderplaat are offshore directed, as the shoal is only submerged during the part of the tidal cycle when the currents are in this direction. They have an overall magnitude of $0.10 m/s$, which is relatively large when considering that maximum

instantaneous velocities on the shoal are in the order of $0.5 m/s$.

For slightly more energetic conditions ($H_s > 1m$ and $U_{wind} > 7m/s$) wind- and wave-generated currents alter the residual flow patterns substantially. The flow at the upper shoreface on the western edge of the outer delta (seawards of the Hinderplaat) is then completely dominated by the wind. Depending on the wind direction, the resulting currents are in NE or SW direction. On higher-lying areas, like the Hinderplaat, the wind enhances the net flow velocities but it is not capable of determining the net flow direction. Wave-action generates currents on the Hinderplaat that may govern the residual currents over a tidal cycle. Northwesterly breaking waves induce a higher water level along the seaside of the shoal that at the landside. This gradient results in cross-shore currents from east to west. Obliquely incident waves also induce longshore currents along the Hinderplaat as well as along the coast of Goeree and the Slufter.

Extreme discharge events ($Q_{sluices} > 7000 m^3/s$) lead to a permanent submersion of the Hinderplaat, with flow velocities that are four times as high than under regular discharge scenarios. Moreover, the period over which the flow is in an offshore direction almost doubles while the period of onshore directed flow is half as long: this results in strong offshore directed currents on top of the shoal.

4. What are the characteristics of the sediment transports, which mechanisms are most dominant and how does this contribute to the observed morphological evolution of the Hinderplaat?

Analysis of the transport patterns and initial bed level changes simulated under various forcing scenarios shows that residual tidal currents contribute to offshore directed sediment transport, pushing the Hinderplaat in this direction. Yet this is readily counteracted by wave-forcing: medium wave conditions and more energetic ones ($H_s > 2m$) from WNW to N directions generate currents that transport sediment in an eastern direction across the shoal, inducing its landward migration. Besides, they cause longshore sediment transport towards the south along the Hinderplaat, which is the strongest at the southern end of the shoal. This leads to the decrease in the height of this part combined with an elongation in southern direction.

Waves are essential to enable sediment transport as tidal currents, discharge flows, surge levels and wind-driven currents are hardly capable of mobilising the sediment from the bed. Yet both the wind and the surge act as amplifiers for the sediment transport rates. The former mostly affects the lower shoreface, while the latter acts as an amplifier for the transport rates in the intertidal areas.

Non-frequent high discharge events provide a significant contribution to potential channel formation on the Hinderplaat by generating initial local breaches that may be maintained and enlarged by tidal flows under normal circumstances. The storm impact on the Hinderplaat is out of the scope of this research. However, it is expected that initial breaches may also be generated during extreme storm events with increased surge levels.

5. How are the mechanisms behind the degradation of the Hinderplaat related to the human interventions and meteorological events?

The formation and thereby existence of the Hinderplaat is a direct consequence of anthropogenic activities in the Haringvliet estuary. Nevertheless, the major part of its degradation (lowering, landward migration and further spreading) is a response of the system to the natural and regular hydrodynamic forcing, for which this evolution can be considered as part of the intrinsic behaviour of the shoal. In fact, the construction of the Slufterdam and its sand nourishments even contributed to the preservation of the shoal for several years, since model results indicated that it acted as a sediment source. This is also supported by the data analysis, which showed an increase in the height of the Hinderplaat directly after the realisation of the port extension. The only degradation process that is not considered to be a part of its intrinsic behaviour under regular conditions is the breaching process. This is concluded to be a direct consequence of the extreme discharge event of 1995. As a result, we conclude that the bathymetry of the Haringvliet characterised by the longshore Hinderplaat was not in an equilibrium state that was later on disturbed by human activities nor extreme meteorological events. Instead, it was an intermediate stage of the evolution, which was characterised by a distorted state of the bathymetry that was meant to change.

10

RECOMMENDATIONS

In this chapter recommendations for further research are presented, which either follow from the discussion or the conclusions of this research. First suggestions are given for further research on the Haringvliet case, regarding both the past as well as the future evolution of the outer delta. Herein also recommendations are given on the use of the Delft3D model. Subsequently, suggestions are given for further studies with the objective to contribute to generalised conclusions by comparison with other areas.

10.1. FURTHER RESEARCH ON THE HARINGVLIET

Morphological modelling goes hand in hand with a simplification of reality, which introduces limitations of the model. Due to several simplifications, three types of processes have not been accounted for in this study, while they could potentially be relevant for the morphological evolution of the outer delta and are, thereby, undoubtedly worthy of being studied.

- To start with, the effect of spring-neap variations of the tide on the delta morphodynamics is likely to be significant, when studying storm events that take place during low water at spring-tide. This can be implemented relatively easily in the Delft3D simulations with the model that has been used for this study, by adjusting the boundary forcing at the open sea boundaries.
- Secondly, further research is needed into the effect of the storm surge on the study area. This study only accounts for the surge as a general water level elevation, which is imposed uniformly over the offshore model boundary. However, it is mainly the gradient in the surge levels that is likely to generate additional currents that have not been considered in other studies. To process this in the morphological model and to derive the correct surge levels along the boundaries, the Haringvliet-Delft3D-model should be nested again into a bigger model (RIJMANO-model) according to the procedure described by Van Holland (1997).
- Lastly, model simulations should be performed in a three-dimensional mode to verify whether the depth-averaged assumption is valid. This is especially needed for studies on the Slijkgat channel and the muddy area of the Slikken van Voorne that include high discharge scenarios. Density effects are especially relevant in case of high discharges, when large volumes of freshwater flow over the saline seawater and gravitational circulation arises. Unfortunately, the adaptation of the model from 2DH- to 3D-mode is not trivial and such simulations are likely to be computationally demanding.

Some additional recommendations are given for future studies with the Haringvliet Delft3D model:

- Users of the model should consider that the model domain is relatively small, which makes it sensitive and may introduce errors when simulating highly energetic wave and wind conditions. A critical view is therefore required when analysing these results.
- Studies on the entire outer delta should consider including mud in the model. In the current model, mud can be implemented by assuming a constant mud concentration for every grid cell. Previous research has shown that this schematisation works fairly well for most parts of the outer delta, except for

the area around the Haringvliet Barrier (De Vries, 2007). However, to accurately simulate the relation between forcing scenarios and mud transport, it is recommended to compute mud in the advection-diffusion equation and to prescribe different concentrations of mud at the model boundaries depending on the wave conditions. Moreover, a sand-mud interaction model would contribute to a better representation of reality and might significantly change the model predictions, since the local presence of small volumes of mud may decrease the erosion rates of sand for instance (Stam et al., 2002).

- Implementing the river discharge through the Haringvliet sluices as a boundary condition consisting of a prescribed discharge time series, may induce translatory waves in case of high discharge scenarios. These waves are often a model artefact generated by the imposed conditions and they are not necessarily induced in reality. The discharge over the sluices is namely determined by the water levels on both sides of the dam. For studies on discharge- and closing- scenarios of the sluices the model should ideally be extended inside the Haringvliet. RTC-tools may then be used to simulate realistic closing scenarios depending on the water levels on both sides of the dam. Another approach is to obtain the realistic hydrodynamics by using models like SIMONA or WAQUA and to implement the output (time series of the discharge through the sluices) as boundary conditions in the Delft3D model.
- Mid- and long-term morphodynamic predictions still have a large uncertainty range. For recommendations on model settings and ideas for new calibrations runs to improve the predictive skill of the model is referred to De Vries (2007).

In the near future, the Kierbesluit-policy for the Haringvliet sluices will be implemented. This policy concerns the decision to leave the sluices partly open at high water to create a transition area from fresh to salt water and to enable that migratory fish such as salmon and sea trout can swim upstream past the sluices to their spawning grounds. It is expected that after implementation of this policy, the morphology of the outer delta will not go back to its initial state before the closure. Due to the current state of the delta, changes mainly will take place in and around the Slijkgat channel (Wijsman et al., 2018). New channel formation is also possible in the northern part of the ebb-tidal delta. Obtaining insights in the expected response of the system (e.g. in terms of hydrodynamic changes and sedimentation erosion patterns) requires a detailed analysis involving the use of a morphological model.

10.2. COMPARISON WITH OTHER INTERTIDAL AREAS

The findings of this research contribute to an understanding of the morphological evolution of the Haringvliet outer delta and the underlying mechanisms. A comparison between similar case-specific studies is required to establish a domain to which the findings on the contribution of independent hydrodynamic drivers can be generalised.

Model results revealed the significant impact of wind-driven currents on the flow patterns in this low lying area. The discovered turning points of this mechanisms are likely to be mainly depending on the orientation of the Hinderplaat. A comparison with similar cases, in which the wind dominance of shallow areas in front of elongated bars or coastlines is studied, could lead to the identification of correlations and a better understanding of the effect of this mechanism.

Moreover, a study on the Grevelingen outer delta is highly recommended for several reasons. First of all, it is remarkable that the intertidal shoal Bollen van den Ooster still exists, as discussed in Chapter 8. It would be very interesting to perform similar research on this shoal to find out what the key factors are for its preservation. The orientation of the shoal follows the alignment of the coast of Goeree. Thereby the shoal seems an extended surf-zone of the beach, just like in the Hinderplaat case. Considering the planned partial re-opening of the dam to build a tidal power plant in the Brouwersdam it is urgent to study what the equilibrium situation of the Grevelingen outer delta would be for the current situation and how this equilibrium might change as a consequence of the near future human intervention.

BIBLIOGRAPHY

Aarninkhof, S. G. J. and van Kessel, T. (1999). Data analyse Voordelta: grootschalige morfologische veranderingen 1960-1996. Technical report, WL Delft Hydraulics.

Bol, R. and Kraak, A. (1998). Section report: Hydrodynamics and density flow. Environmental Impact Assessment Management of the Haringvliet sluices. Technical report, Directorate-General of Public Works and Water Management.

Bosboom, J. and Stive, M. J. F. (2013). *Coastal Dynamics I. Lecture notes CIE4305*. VSSD, Delft, 2nd edition.

Boyd, R., Dalrymple, R., and Zaitlin, B. (1992). Classification of clastic coastal depositional environments. *Sedimentary Geology*, 80:139–150.

Burchard, H. and Baumert, H. (1998). The Formation of Estuarine Turbidity Maxima Due to Density Effects in the Salt Wedge. A Hydrodynamic Process Study. *Physical Oceanography*, 28:566–587.

Carter, R. W. G. (1988). *Coastal environments : an introduction to the physical, ecological, and cultural systems of coastlines*. Academic Press.

Cleveringa, J. (2008). Morphodynamics of the Delta coast (south-west Netherlands). Quantitative analysis and phenomenology of the morphological evolution 1964-2004. Technical report, Alkyon Hydraulic Consultancy & Research, Emmeloord.

Costanza, R., Arge, R., de Groot, R., Farberk, S., Grasso, M., Hannon, B., Limburg, K., Naeem, S., O'Neill, R., Paruelo, J., Raskin, R., Suttonkk, P., and van den Belt, M. (1997). The value of the world ' s ecosystem services and natural capital. *Nature*, 387(May):253–260.

Dalrymple, R., Zaitlin, B., and Boyd, R. (1992). Estuarine facies models: Conceptual basis and stratigraphic implications. *Journal of Sedimentary Petrology*, 62:1130–1146.

Davis, R. A. and Hayes, M. O. (1984). What is a Wave-Dominated Coast? *Developments in Sedimentology*, 39(C):313–329.

de Haas, T., Pierik, H. J., van der Spek, A. J., Cohen, K. M., van Maanen, B., and Kleinhans, M. G. (2017). Holocene evolution of tidal systems in The Netherlands: Effects of rivers, coastal boundary conditions, eco-engineering species, inherited relief and human interference. *Earth-Science Reviews*, 177(November):139–163.

De Vet, P. (2014). *Modelling sediment transport and morphology during overwash and breaching events*. Msc thesis, Delft University of Technology.

De Vriend, H. J. (1991). Mathematical modelling and large-scale coastal behaviour Part 1: Physical processes. *Journal of Hydraulic Research*, 29(6):727–740.

De Vriend, H. J. and Ribberink, J. S. (1996). Mathematical modelling of meso-tidal barrier island coasts. Part II: Process-based simulation models.

De Vries, M. J. (2007). *Morphological modelling of the Haringvlietmonding using Delft3D*. Msc thesis, Universiteit Twente.

De Winter, R. (2008). *Exploratory Research into the Maintenance of the Slijkgat*. Msc thesis, Delft University of Technology.

Deltares (2014a). Delft3D-FLOW user manual version 3.15, Simulation of multi-dimensional hydrodynamic flows and transport phenomena, including sediments. pages 1–684.

Deltares (2014b). Delft3D-WAVE user manual version 3.05, Simulation of short-crested waves with SWAN. pages 1–226.

Dissanayake, D. (2011). *Modelling Morphological Response of Large Tidal Inlet Systems to Sea Level Rise.* PhD thesis, UNESCO-IHE.

Dronkers, J. (1998). Morphodynamics of the Dutch Delta. In Dronkers, J. and Scheffers, M. B. A. M., editors, *Physics of Estuaries and Coastal Seas*, Rotterdam.

Dronkers, J. (2016). *Dynamics of Coastal Systems.* World Scientific Publishing Co Pte Ltd, Singapore, second edition.

Eelkema, M. (2013). *Eastern Scheldt inlet morphodynamics.* PhD thesis, Technische Universiteit Delft.

Eelkema, M., Wang, Z. B., Hibma, A., and Stive, M. J. F. (2013). Morphological Effects of the Eastern Scheldt Storm Surge Barrier on the Ebb-Tidal Delta. *Coastal Engineering Journal*, 55(03):26.

Elias, E. P. L. (2006). *Morphodynamics of Texel Inlet.* PhD thesis, Delft University of Technology.

Elias, E. P. L. and Van der Spek, A. J. F. (2014). Grootschalige morfologische veranderingen in de Voordelta. Technical report, Deltares.

Elias, E. P. L. and van der Spek, A. J. F. (2016). Large-scale morphological changes and sediment budget 1965-2013 of the Haringvliet ebb-tidal delta (SW Netherlands); Impacts of large-scale engineering. Technical report, Deltares, Delft.

Elias, E. P. L., van der Spek, A. J. F., and Lazar, M. (2015). The 'Voordelta', the contiguous ebb-tidal deltas in the SW Netherlands: Large-scale morphological changes and sediment budget 1965-2013 ; impacts of large-scale engineering. *Netherlands Journal of Geosciences.*

Eysink, W. (1990). Morphologic Response of Tidal Basins to Changes. *Coastal Engineering Proceedings*, 1(22):1948–1961.

Galappatti, G. and Vreugdenhil, C. B. (1985). A depth-integrated model for suspended sediment transport. *Journal of Hydraulic Research*, 23(4):359–377.

Galloway, W. E. (1975). Process Framework for Describing the Morphologic and Stratigraphic Evolution of Deltaic Depositional Systems. pages 87–98.

Giardino, A., Brière, C., and van der Werf, J. (2001). Morphological modelling of bar dynamics with Delft3D: the quest for optimal parameter settings. Technical report, Deltares.

Giardino, A., Den Heijer, K., and Santinelli, G. (2014). The state of the coast, case study: The South-Westerly Delta. Technical report, Deltares.

Hageman, B. (1969). Development of the western part of the Netherlands during the Holocene. *Geologie en Mijnbouw*, 48:373–388.

Hayes, M. O. (1979). Barrier island morphology as a function of tidal and wave regime. In Leatherman S.P. [ed.], Barrier Islands. Academic Press, New York, pp. 1–27. (July).

Hayes, M. O. (1980). General morphology and sediment patterns in tidal inlets. *Sedimentary Geology*, 26(1-3):139–156.

Holthuijsen, L. H. (2007). *Waves in Oceanic and Coastal Waters.* Cambridge University Press, New York, USA.

Jeuken, M. C. J. L., Wang, Z. B., Keiller, D., Townend, I. H., and Liek, G. A. (2003). Morphological Response of Estuaries To Nodal Tide Variation. *Proceedings of International Conference on Estuaries & Coasts (ICEC-2003)*, pages 166–173.

Kohsiek, L. (1988). Reworking of Former Ebb-Tidal Deltas into Large Longshore Bars Following the Artificial Closure of Tidal Inlets in the Southwest of the Netherlands.

Kragtwijk, N. G., Zitman, T. J., Stive, M. J., and Wang, Z. B. (2004). Morphological response of tidal basins to human interventions. *Coastal Engineering*, 51(3):207–221.

Kraus, N., Militello, A., and Todoroff, G. (2002). Barrier Breaching Processes and Barrier Spit Breach, Stone Lagoon, California. *Shore & Beach*, 70(4).

LeConte, L. J. (1905). Discussions of: Notes on the improvement of rivers and harbor outlets in the United States. *Transactions of American Soc. of Civil Engineers, P. A. WATTS,*, pages 306–308.

Lesser, G. (2009). *An Approach to Medium-term Coastal Morphological Modelling*. Phd, Delft University of Technology, UNESCO-IHE Institute for Water Education.

Marijs, K. and Parée, E. (2004). Nauwkeurigheid vaklodingen Westerschelde en -monding. Technical report, RIKZ.

Millennium Ecosystem Assessment (2005). *Ecosystems and Human Well-being: Current State and Trends*. Island Press, Washington.

Murray, N. J., Ma, Z., and Fuller, R. A. (2015). Tidal flats of the Yellow Sea: A review of ecosystem status and anthropogenic threats. *Austral Ecology*, 40(4):472–481.

Nienhuis, J. H., Ashton, A. D., Roos, P. C., Hulscher, S. J., and Giosan, L. (2013). Wave reworking of abandoned deltas. *Geophysical Research Letters*, 40(22):5899–5903.

O'Brien, M. P. (1931). Estuary tidal prisms related to entrance areas. *Civil Engineering*, 1:738–739.

O'Brien, M. P. (1969). Equilibrium flow areas of inlets and sandy coasts. *Journal of Waterways, Harbors, and Coastal Engineering*, 95:43–55.

Paalvast, P., Iedema, W., Ohm, M., and Posthoorn, R. (1998). MER Beheer Haringvlietsluizen: over de grens van zoet en zout, deelrapport ecologie en landschap.

Passeri, D. L., Hagen, S. C., Medeiros, S. C., Bilskie, M. V., Alizad, K., and Wang, D. (2015). The dynamic effects of sea level rise on low-gradient coastal landscapes: A review. *Earth's Future*, 3(3):159–181.

Perluka, R., Wiegmann, E., Jordans, R., and Swart, L. (2006). Opnametechnieken Waddenzee. Technical report, Rijkswaterstaat.

Piekhaar, R. and Kort, M. (1983). Haringvliet monding - Sedimentatieonderzoek 1970-1981. Technical report, Rijkswaterstaat Deltadienst, The Hague.

Pilkey, O., Neal, W., Riggs, S., Webb, C., Bush, D., Pilkey, D., Bullock, J., and Cowan, B. (1998). *The North Carolina shore and its barrier islands : restless ribbons of sand*. Duke University Press, Durham and London.

Rijksinstituut voor Kust en Zee (2007). Natuurcompensatie Maasvlakte Twee in de Voordelta. Technical report, Rijkswaterstaat.

Rijkswaterstaat (1973). Veranderingen in de mond van het Haringvliet sedert de afsluiting. Technical report, Driemaandelijks Bericht Deltawerken, 63, 146-163, The Hague.

Rijkswaterstaat (2014). Opzet Proef Slikken van Voorne: Natura 2000 Ontwerpbeheerplan Voordelta 2015-2021. Technical report, Rijkswaterstaat.

Rijkswaterstaat (2017a). Haringvliet: Haringvlietsluizen op een kier. https://www.rijkswaterstaat.nl/water/projectenoverzicht/haringvliet-haringvlietsluizen-op-een-kier/

Rijkswaterstaat (2017b). Waterbase. http://live.waterbase.nl

Rijkswaterstaat (2018). Matroos Helpdesk water: Multifunctional Access Tool foR Operational Oceandata Services.

Roelvink, J. A. (1999). Kleinschalig morfologisch onderzoek MV2 fase 1b: Gevoeligheidsonderzoek. Technical report, WL Delft Hydraulics.

Roelvink, J. A., van Holland, G., and Bosboom, J. (1998). Kleinschalig morfologisch onderzoek MV2: fase 1 Validatie. Technical report, WL Delft Hydraulics, Delft.

Sha, L. P. and Van den Berg, J. H. (1993). Variation in Ebb-tidal Delta Geometry along the coast of the Netherlands and the German Bight. *Coastal Research*, 9(3):730–746.

Stam, J. M. T., Groen, M., and Walburg, L. (2002). Haringvlietmonding : reconstructie van een afsluiting. Beschrijving, verklaring en modelaanpak van de effecten van de sluiting van de Haringvlietmonding 1970-2000. Technical Report november, RIKZ.

Steijn, R., Eysink, W., van Holland, G., and Van De Graaf, J. (2001). Bandbreedte morfologische Effectvoorspelling MV2: Een onderzoek ten behoeve van natuurtypering. Technical Report September, Alkyon, WL Delft Hydraulics, TUD.

Stive, M. J. F. and Wang, Z. B. (2003). Morphodynamic modelling of tidal basins and coastal inlets. *Elsevier Oceanography*, pages 367–392.

Terwindt, J. (1973). Sand movement in the in- and offshore tidal area of the SW part of the Netherlands. *Geologie en Mijnbouw*, 52(2):69–77.

Tönis, I. E., Stam, J. M. T., and Van De Graaf, J. (2002). Morphological changes of the Haringvliet estuary after closure in 1970. *Coastal Engineering*, 44(3):191–203.

Tuan, T. (2007). *Seasonal breaching of coastal barriers*. PhD thesis, UNESCO-IHE Delft.

Tung, T. T. (2011). *Morphodynamics of seasonally closed coastal inlets at the central coast of Vietnam*. PhD thesis, TU Delft.

Van der Kruif, H. (2017). Extreme weersomstandigheden en natuurgeweld sinds 1945.

Van der Spek, A. J. F. (1987). Inventariserend morfologisch onderzoek Voordelta; beschrijving van de ontwikkeling van de buitendelta's van Haringvliet en Grevelingen. Technical report, Rijkswaterstaat.

Van Holland, G. (1997). *Hydrodynamica en morfodynamica Haringvlietmonding*. Msc, Delft University of Technology.

Van Maren, D. (2004). *Morphodynamics of a cyclic prodrading delta: the Red River, Vietnam*. PhD thesis, Utrecht University.

van Rijn, L. C. and Walstra, D. J. R. (2003). Modelling of Sand Transport in DELFT3D. Technical Report November, WL Delft Hydraulics.

Van Vessem, P. (1998). Morfologie monding Haringvliet, verandering van een dynamisch onderwaterlandschap. Technical report, RIKZ-98.016.

Walstra, D., Van Ormondt, M., and Roelvink, J. (2004). Shoreface Nourishment Scenarios. Technical report, WL | Delft Hydraulics, Delft.

Walton, T. L. and Adams, W. D. (1977). Capacity of Inlet Outer Bars to Store Sand. In *Coastal Engineering 1976*, pages 1919–1937, New York, NY. American Society of Civil Engineers.

Wang, Z. B., Hoekstra, P., Burchard, H., Ridderinkhof, H., De Swart, H. E., and Stive, M. J. (2012). Morphodynamics of the Wadden Sea and its barrier island system. *Ocean and Coastal Management*, 68(October):39–57.

Wang, Z. B., Jeuken, C., and De Vriend, H. J. (1999). Tidal asymmetry and residual sediment transport in estuaries. Technical report, Deltares.

Wegman, C. (2015). *The erosion and redistribution of sediment from the Haringvliet delta after construction of the Haringvliet dam*. Msc thesis, Universiteit Utrecht.

Wegman, C., De Gelder, A., Dam, G., De Winter, W., and Raemakers, G. (2017). Onderzoeksgebied van wereldformaat.

Wiegmann, E., Perluka, R., Oude Elberink, S., and Vogelzang, J. (2005). Vaklodingen: de inwintechnieken en hun combinaties. Vergelijking tussen verschillende inwintechnieken en de combinaties ervan. page 47.

Wijsman, J., Escaravage, V., Huismans, Y., Nolte, A., van der Wijk, R., Wang, Z. B., and Tom Ysebaert, T. (2018). Potenties voor herstel getijdenatuur in het Haringvliet, Hollands Diep en de Biesbosch. Technical report, Wageningen University & Research, Wageningen.

NOMENCLATURE

LIST OF SYMBOLS

Symbol	*Unit*	*Meaning*
A_0	$[m]$	mean water level
A_{ch}	$[m^2]$	horizontal area covered by the channels
A_{eq}	$[m^2]$	minimum equilibrium cross-section of the entrance channel
A_f	$[m^2]$	flats area (the area above MSL)
A_i	$[m]$	local tidal amplitude of harmonic component i
A_{MSL}	$[m^2]$	minimum equilibrium flow area in a cross-section of the basin
C	$m^{\frac{1}{2}} s^{-1}$	Chezy coefficient
C	$[m^{2-3q}]$ ‘	coefficient
C_A	$[m^{2-3q}]$	coefficient
C_{od}	$[m^{-0.69}]$	empirical coefficient
C_V	$[m^{-3/2}]$	coefficient
D_c	$[m]$	characteristic channel depth
D_p	$[m]$	peak wave direction
H_m	$[m]$	mean tidal range
H_s	$[m]$	significant wave height
M_c	[%]	morphological impact of a wave condition
N_c	$[-]$	number of wave records per class
N_s	$[-]$	total number of wave records
P	$[m^3]$	tidal prism
Q	$[m^3 s^{-1}]$	discharge
T	$[years]$	adaptation timescale for morphological developments to take place
T_a	$[s]$	adaptation timescale for sedimentation or erosion
T_p	$[s]$	peak wave period
U_{wind}	$[ms^{-1}]$	wind velocity
V_C	$[m^3]$	equilibrium total channel volume, below MSL
V_{od}	$[m^3]$	sand volume stored in the outer delta
c	$[kgm^{-3}]$	depth averaged sediment concentration
c_e	$[kgm^{-3}]$	equilibrium depth averaged sediment concentration
f_i	$[s^{-1}]$	frequency of harmonic component i
p_c	$[-]$	probability of occurrence per wave condition
q	$[-]$	coefficient
u	$[ms^{-1}]$	flow velocity
w_s	$[ms^{-1}]$	settling velocity
α	$[m^{-1}]$	constant of proportionality
β	$[m^{-1}]$	constant of proportionality
φ_i	$[rad]$	phase of harmonic component i
ξ	$[m]$	water level elevation

LIST OF ACRONYMS

Abbreviation	*Meaning*
2DH	two-dimensional in the horizontal plane
2DV	two-dimensional in the vertical plane
3D	three-dimensinal
ADI	Alternating Direction Implicit (method)
d.a.	depth averaged
E	east
ETD	ebb-tidal delta
HAT	highest astronomical tide
ISE	initial sedimentation/erosion
JONSWAP	JOint North SeaWAve Project
LAT	lowest astronomical tide
MHHW	mean high high water
MHW	mean high water
MHWN	mean high water neap
MHWS	mean high water spring
MLLW	mean low low water
MLW	mean low water
MLWN	mean low water neap
MLWS	mean low water spring
MorFac	morphological acceleration factor
MSL	mean offshore sea level
N	north
NAP	Normaal Amsterdams Peil
S	south
W	west

LIST OF FIGURES

LIST OF TABLES

APPENDICES

A

BOUNDARY CONDITIONS

A.1. INTRODUCTION

This appendix elaborates on the boundary conditions of the morphological model that have been described in Section 5.4. This concerns the schematisation of the tidal signals, the processed wave and wind climates (under regular conditions as well as during the extreme discharge event) and the imposed discharge scenarios through the Haringvliet Sluices.

A.2. REPRESENTATIVE TIDAL SIGNALS

A morphological tide is implemented in the model to schematise the astronomic tidal signal. The use of a morphological tide implies that one single tide is chosen which is assumed to be normative for all transports that occur during a spring-neap cycle (De Vries, 2007). The schematisation is carried out by Van Holland (1997) with use of the RIJMANO-model (*Rijn-Maas-Mond*). To this end, the tidal signal of February 20, 1995 to March 1, 1995 is analysed.

The high discharge event of 1995 took place during spring-tide, see Figure A.1. The red arrow indicates the period of extreme discharge values. To include this in the model simulations, the amplitudes of the harmonic components of the morphological tidal signal are multiplied with a factor of 1.28. Note that the mean water level remains the same. The morphological tides that have been used in the Delft3D model are shown in Figure A.2.

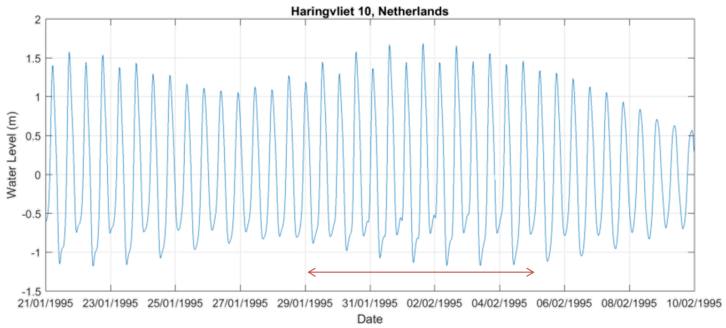

Figure A.1: Tidal signal of January and February 1995, retrieved from *Delft Dashboard*

A.3. GENERAL WAVE CLIMATE ANALYSIS

In general, many morphodynamic studies are performed to investigate the (future) net morphological changes of a system. This research has a descriptive character instead of a predictive one, trying to understand an observed evolution. Therefore, not only net transport rates, but also gross transports are relevant. Modelling the morphodynamic behaviour of the Haringvliet with a detailed wave climate provides essential information to

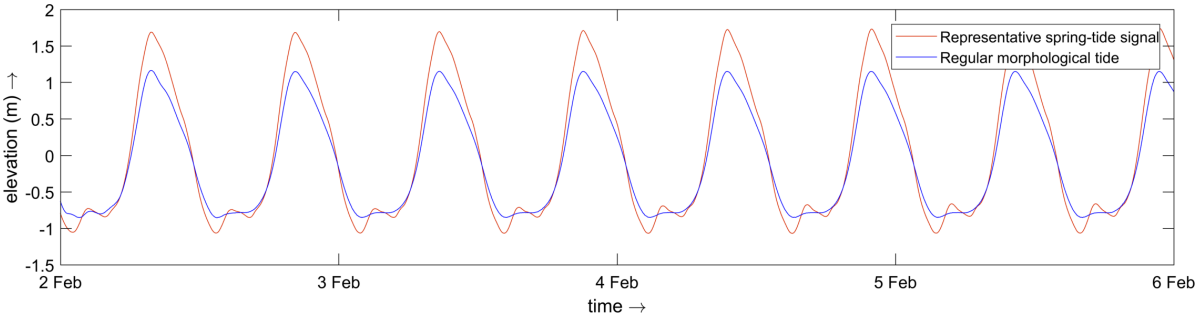

Figure A.2: Morphological tidal signal, just offshore of the ebb-tidal delta

understand the response of the system to the imposed forcing. Considering that every condition is also combined with varying forcing conditions (wind-forcing on/off, surge levels, etc.) this leads to a large amount of output data. To obtain a manageable output, the wave climate is analysed to determine which conditions should be analysed first.

Table 5.4 shows the wave climate that has been derived to investigate the natural morphodynamic response of the delta under various conditions. The overall conditions for each wave class are shown in Table A.1. Calm wave conditions have a higher probability of occurrence (p_c), but large waves have a larger impact on the morphology. To account for both parameters, the *morphological impact* (M_c) is specified (Lesser, 2009). This is estimated according to:

$$M_c = p_c H_{s,rep}^{2.5} = \frac{\sum_{i=1}^{N_c} H_{s,i}^{2.5}}{N_s} \tag{A.1}$$

Table A.1: Wave classes of the schematised wave climate

Wave class	$\boldsymbol{H_s}$ $[m]$	$\boldsymbol{p_c}$ [-]	$\boldsymbol{M_c}$ $[m^{2.5}]$
Calm	0-1	0.449	5.1
Regular	1-2	0.381	29.2
Medium	2-3	0.127	35.0
Medium-strong	3-4	0.035	22.0
Strong	4-5	0.006	7.0
Extreme	5-7	0.001	1.0

The Delft3D model is relatively small and seems to be quite sensitive when run with highly energetic conditions (rare and unrealistic patterns are observed near the model boundaries, which seem to penetrate through a large part of the model domain). This is not a problem since these conditions are not needed for the analyses; the aim is namely to study the evolution of the morphology under regular conditions, without the influence of extreme storms.

The Haringvliet outer delta is hardly influenced by wave conditions from east-north-eastern to southern directions. Simulations have been performed with these conditions for the completeness of the research and for future studies. However, the results are not treated in this thesis, since they seem to be irrelevant for the morphological evolution.

The greatest part of the results is obtained from simulations with the proposed wave climate. To investigate the turning points of the wind forcing effects additional wave conditions were required: to evaluate the effect of slight changes in wind direction, simulations have been performed with exactly the same wave conditions, wind velocities and surge levels for varying wind directions.

A.4. HINDCAST WAVE CLIMATE

The wave and wind conditions at measuring station Europlatform during the extreme discharge event of 1995 have been recorded by Rijkswaterstaat. The available dataset, containing measured values with a time step of three hours, has been implemented directly in the FLOW- and WAVE-modules of the morphological model. An overview of the prescribed conditions is presented in Tables A.2 and A.3. The time values indicate the simulation time, starting at the reference date of January 29, 1995.

Table A.2: List of wave and wind conditions during the 1995 extreme event, part 1

$Time$ [-]	H_s [m]	T_p [s]	D_p [°]	U_{wind} [m/s]	Dir_{wind} [°]
0	2.38	4.7	234	13.4	240
180	2.53	5.0	242	14.4	250
360	2.34	5.6	245	12.3	260
540	2.23	5.3	239	10.8	240
720	1.87	4.3	231	11.3	230
900	2.36	5.2	231	11.9	270
1080	1.78	5.6	233	6.2	270
1260	1.36	5.2	235	4.6	310
1440	1.41	4.3	317	9.5	340
1620	2.06	5.4	355	12.9	380
1800	2.26	5.1	0	10.3	380
1980	2.02	5.1	357	8.3	350
2160	1.94	5.5	352	8.8	350
2340	1.44	5.0	0	6.8	330
2520	1.45	4.7	351	6.8	330
2700	1.45	5.1	348	1.0	50
2880	1.62	6.0	340	4.1	180
3060	1.27	3.9	312	9.8	200
3240	1.87	4.3	208	13.9	190
3420	2.61	5.7	216	16.6	190
3600	3.16	5.2	216	17.6	200
3780	3.01	5.0	219	16.6	200
3960	2.60	5.0	223	15.5	210
4140	2.52	5.9	221	14.9	200
4320	3.18	5.5	225	16.0	210
4500	3.27	5.3	230	18.1	220
4680	3.33	5.6	228	17.6	230
4860	2.81	6.1	232	15.5	230
5040	3.02	5.7	230	14.9	230
5220	2.11	5.0	226	3.6	240
5400	1.56	5.1	227	5.1	250
5580	0.99	4.8	237	6.7	260
5760	0.95	3.5	271	8.8	320
5940	1.27	4.0	317	10.0	330
6120	1.45	4.4	332	7.8	330
6300	1.35	4.3	333	7.3	350
6480	1.42	4.8	343	4.6	350
6660	1.30	5.3	336	0.9	110
6840	0.97	5.0	352	3.1	210
7020	0.85	4.6	342	5.7	180
7200	1.09	4.4	263	9.3	190
7380	1.59	3.9	222	10.8	190
7560	1.47	3.7	205	11.8	190
7740	1.95	4.7	207	13.4	200

Table A.3: List of wave and wind conditions during the 1995 extreme event, part 2

$Time$ [-]	H_s [m]	T_p [s]	Dir_{wave} [deg]	U_{wind} [m/s]	Dir_{wind} [deg]
7920	2.20	5.3	215	13.0	210
8100	2.03	4.4	226	11.9	210
8280	1.96	4.4	226	11.9	210
8460	1.74	4.9	233	10.8	230
8640	1.74	5.0	229	10.3	230
8820	1.47	4.1	229	9.3	230
9000	1.21	3.7	232	9.3	230
9180	0.95	4.0	239	8.2	240
9360	0.92	4.0	244	6.7	270
9540	0.87	3.3	260	8.2	270
9720	0.81	3.5	275	6.7	270
9900	0.62	3.8	311	5.8	310
10080	0.71	3.9	319	5.1	280
10260	0.69	3.8	321	5.7	280
10440	0.59	3.6	321	4.1	250
10620	0.72	3.4	253	6.7	230
10800	1.08	4.3	229	9.3	210
10980	1.52	4.2	231	10.3	230
11160	1.42	3.9	237	10.8	240
11340	1.13	3.9	243	9.8	240

A.5. DISCHARGES

As described in Section 5.4, all model runs are performed with the *normal discharge scenario* (see Table 4.1) for the Haringvliet Sluices except for the hindcast, which is simulated with the daily mean values that were measured by Rijkswaterstaat. The former is implemented my means of harmonic components, while the latter is processed in the model as block values. For all cases holds that water is only discharged during low water. Figure A.3 provides an overview of the instantaneous discharge values for five consecutive days.

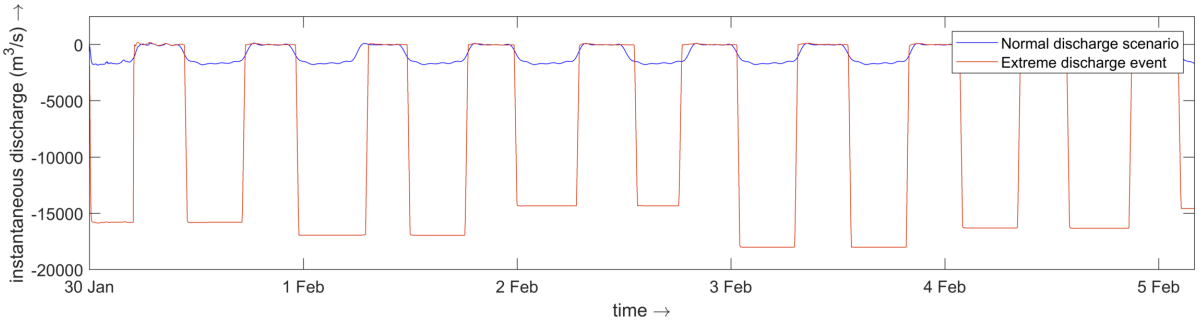

Figure A.3: Model discharges through the Haringvliet Sluices

B

SHOREFACE ERROR CALIBRATION

B.1. INTRODUCTION

Model results obtained in previous studies show significant differences of the predicted behaviour at the shoreface compared to the observed behaviour. Results of Van Holland (1997) and De Vries (2007) showed sedimentation in the shoreface in front of the Hinderplaat, while the Vaklodingen data indicate erosion patterns (see Figure B.1). This appendix treats the calibration of the model to potentially improve the predictive skill for this area.

B.2. ADAPTING THE MODEL SETTINGS

Van Holland suggested that the error could originate from the absence of wave-asymmetry transport in the simulations. Subsequently, De Vries concluded that application of the transport formulation TRANSPORT2004 (Van Rijn, including wave-asymmetry) led to a better reproduction of the development of the channels, sub tidal areas and flats. Nevertheless, the prediction over the entire area in front of the Hinderplaat remained erroneous. Also variation in the diffusivity coefficient did not lead to better representation of the sedimentation/erosion patterns.

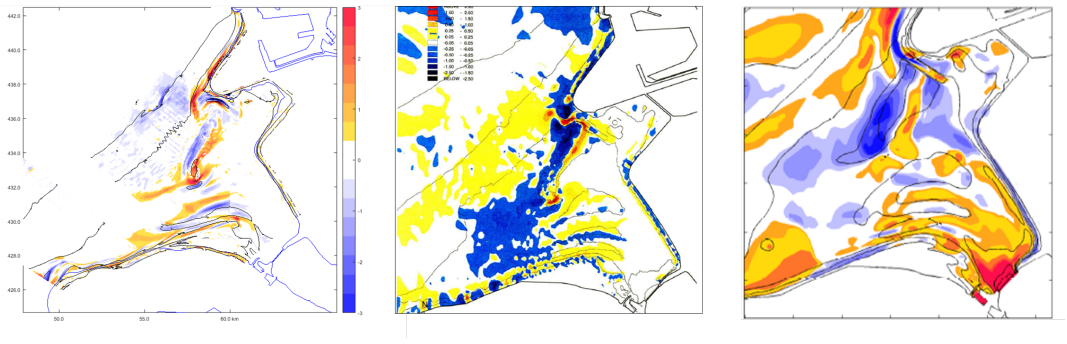

Figure B.1: Prediction error at the shoreface. Left: measured changes 1990-1995. Centre: modelled changes by Van Holland (1997) for 1990-1991. Right: modelled changes by De Vries (2007) ofr 1986-2000.

During this research calibrations runs have been performed with the following model parameters to investigate whether the prediction bed level changes at the shoreface could be improved:

- Sus, Bed, SuSW, BedW
- AlfaBs, AlfaBn
- FWFac
- D50

B.2.1. SUS, BED, SUSW, BEDW

Erosion on the shoreface is likely to be an effect of wave action on that location. Therefore it was tested whether relatively increasing the impact of the wave forcing on the morphology would lead to better results. This is done by testing numerous values for the parameters Sus, Bed, SusW and BedW, which represent current- and wave-related suspended and bedload sediment transport factors. By increasing the values of the latter three factors, the total wave related sediment transport should increase as this is computed by the model with the following formula (Deltares, 2014a):

$$S_{total} = Bed * S_{bedload\,current} + BedW * S_{bedload\,waves} + SusW * S_{suspended\,waves} \tag{B.1}$$

Figure B.2 shows the results for the calibration plots with these model parameters. The plot on the upper left is the reference case, in which the same settings are used as in other simulations of this research. The results of the other simulations show that adapting the values for the parameters Sus(W) and Bed(W) only changes the amount of sediment transport. Unfortunately, sedimentation of the shoreface is still predicted.

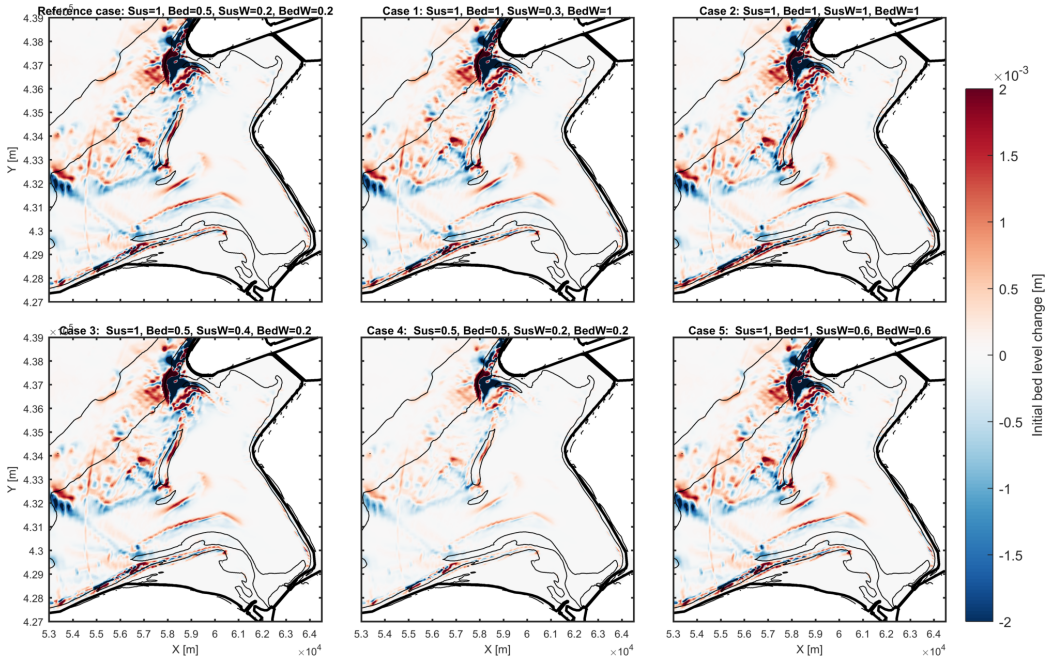

Figure B.2: Calibration runs with different values for Sus, Bed, SusW and BedW

.

B.2.2. ALFABS, ALFABN

Delft3D accounts for an adjustment of the bed-load transport for bed slope effects (Deltares, 2014a). Two bed slope directions are distinguished: the slope in the initial direction of the transport (the longitudinal bed slope) and the slope in the direction perpendicular to that (the transverse bed slope). The model parameters AlfaBs and AlfaBn are longitudinal and transverse bed gradient factors for bedload transport. Setting these values to 1 is closest to reality. However, sometimes model predictions become more realistic for other values.

Model simulations have been performed with a wide range of values for these parameters. Yet the results show exactly the same patterns for all model runs, see Figure B.3. The maximum difference in initial bed level changes between the scenarios is in the order of 10^{-5}.

B.2.3. FWFAC

The Longuet-Higgins streaming is a small current in the wave boundary layer in the direction of wave advance. This process can be important in the outer surf zone where limited wave breaking occurs. In the inner surf zone this effect is insignificant because the offshore directed flow induced by wave breaking and wave

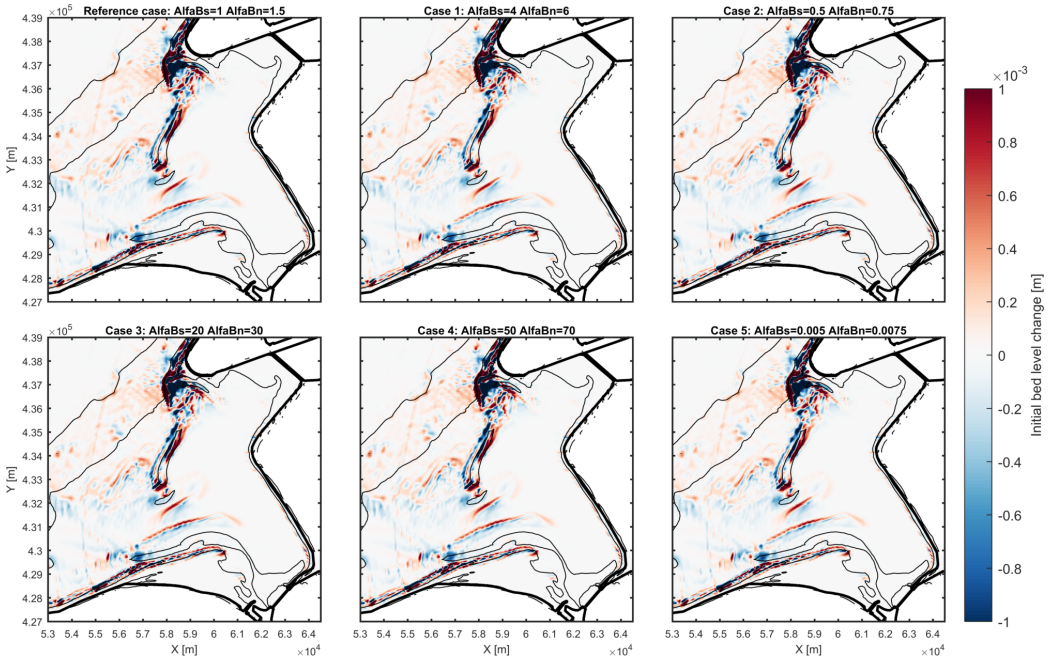

Figure B.3: Calibration runs with different values for AlfaBs and AlfaBn

.

mass transport are dominant (Giardino et al., 2001). Delft3D accounts for this streaming by including an additional shear stress in the wave propagation direction. It maximum is located at the bed and its value decreases linearly across the wave boundary layer to zero. By multiplying this with a factor of FWfac, the streaming effect can be scaled. Previous research has shown that with increasing streaming effects an increased erosion of the lower shoreface may occur (Walstra et al., 2004). However, model results of a simulation with medium waves from NW direction show that increasing or decreasing this value does not change the results for the initial bed level changes at the Haringvliet ebb-tidal delta. This is probably because wave breaking is already too dominant at its seaward edge.

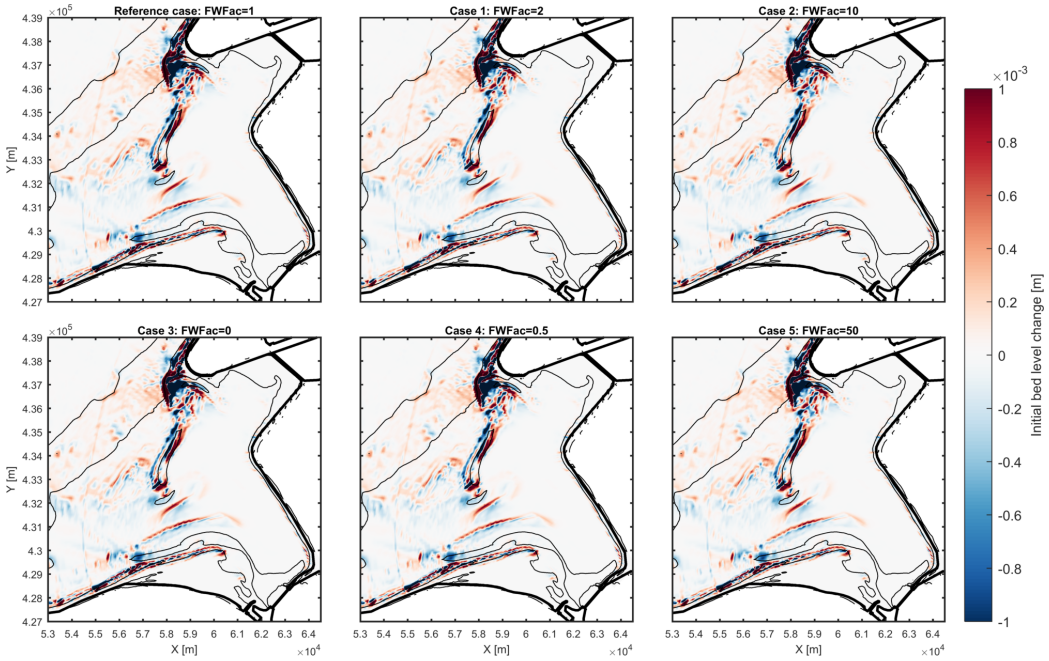

Figure B.4: Calibration runs with different values for FWFac

.

B.2.4. D50

Two additional model runs with different grain sizes are performed to study the effect of the median sediment diameter on the model predictions. The obtained model results are as expected: simulations with a smaller grain size show much more sediment transport and bed level changes, while simulations with a larger grain size show less activity of the seabed. Apart from the level of bed changes, the sedimentation/erosion patterns remain remarkably almost the same for all simulations. Therefore it is concluded that the prediction error at the shoreface is not directly a cause of the imposed grain size.

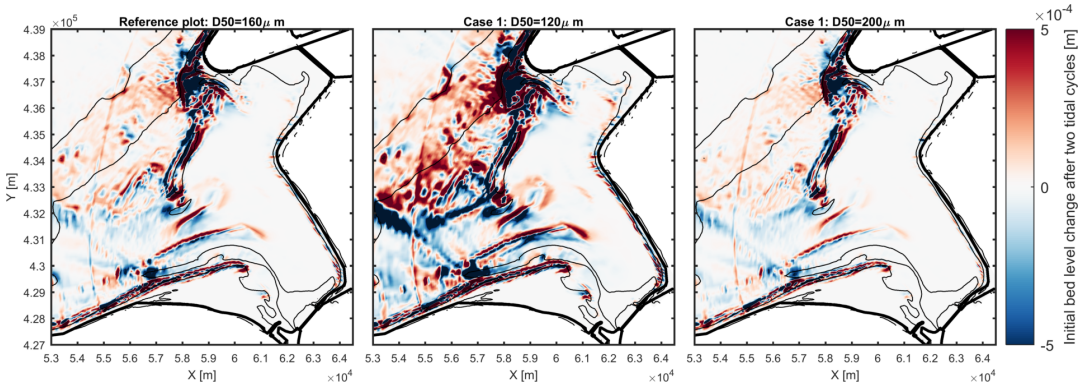

Figure B.5: Calibration runs with different grain size

.

B.3. THE ABSENCE OF SPRING-NEAP VARIATIONS IN THE TIDAL SIGNAL

By forcing the model with a representative morphological tide, variations of the water level amplitude due to for instance the daily inequality, spring-neap tidal cycles and the influence of the 18.6-year lunar nodal tidal cycle are not accounted for. Due to the absence of spring-tide in the simulations the residual currents may be smaller and the intertidal areas will be inundated less frequently. Especially the first implication may have an effect on the predicted evolution of the shoreface.

Situations with spring tide are simulated by implementing an increased tidal flow, see Figure A.2. This is combined with several wave conditions from different directions. In all cases the model still predicts sedimentation of the shoreface. Thus, it may be concluded that the preditive error is not a direct consequence of the absence of spring tide conditions.

B.4. SYNTHESIS AND CONCLUSION

It is concluded that the prediction error at the upper shoreface in front of the Hinderplaat can not be corrected by tuning the model with the parameters Sus(W), Bed(W), AlfaBs, AlfaBn and FWFac. Moreover the error is not a consequence of the prescribed median grain size. Model runs with an increased tidal flow show that the error is still introduced when simulating spring tide conditions.

Analysis of the residual transport direction in combination with the sedimentation/erosion patterns leads to new insights. Figure B.6 shows the initial bed level changes and the corresponding residual transport rates for four wave conditions of medium strength with different directions. At the seaward edge of the ebb-tidal delta, mostly longshore sediment transport is predicted. According to the model, conditions that generate southern directed net transport rates induce erosion, whereas northern directed net transports result in accretion of the shoreface. However, previous research explains the erosion of the shoreface as an effect of the wave action, which acts as a bulldozer mainly pushing the sediment in landward direction. The (almost) absence of cross-shore transport rates in the upper shoreface leads to the supposition that wave-asymmetry induced cross-shore transport is severely underestimated by the model, even after implementation of the van *Rijn 2007* transport formulation.

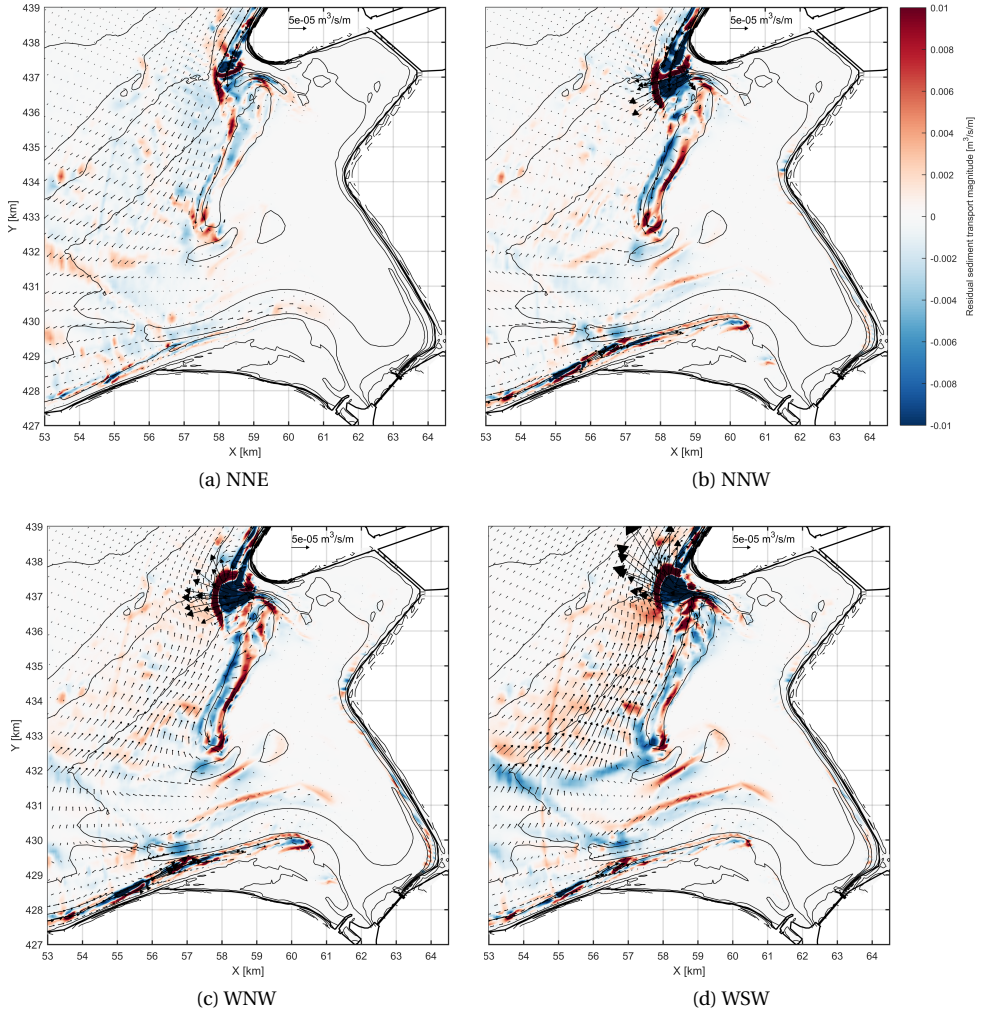

(a) NNE (b) NNW

(c) WNW (d) WSW

Figure B.6: Initial bed level changes and residual sediment transport for waves conditions from several directions

C

SUPPORTING SIMULATION RESULTS

C.1. INTRODUCTION

This appendix contains additional simulation results that support the results presented in Chapter 6. First, flow results are presented, after which additional sediment transport patterns are shown.

C.2. SIMULATED FLOW PATTERNS

In this section instantaneous flow patterns are presented for simulations with a tide only scenario, calm wave and wind conditions and for regular conditions. The results of these simulations are treated in Chapter 6 in terms of residual currents. Moreover, currents patterns during a tidal cycle of an extreme discharge event are presented.

Figure C.1 shows the current patterns for tidal forcing only (simulation scenario A). As discussed in Section 6.2, the patterns at phase 3 and 4 significantly deviate from the results of simulations that include a river discharge (simulation scenario B). During the first low water (phase 3) the flow patterns at all the channels of the outer delta are dominated by the river discharge. Its influence is visible up to the location of the Hinderplaat. During phase 4 the influence is limited to the channels Slijkgat en Rak van Scheelhoek.

Figures C.2 and C.3 show the flow patterns for calm conditions from WSW and NNW direction. Both conditions have a probability of occurrence of approximately 1%. No differences are detected between the flow patterns for these simulations and the simulation with tidal and Q_{river} forcing (Figure 6.1). Thus, it is concluded that calm wave conditions do not significantly alter the main flow patterns in the ebb-tidal delta.

In Section 6.2.3 it was explained that wind conditions of regular strength can substantially alter the flow patterns at phase 4 of the tidal cycle. However, the patters during the rest of the time remain more or less the same. This is supported by Figures C.4 and C.5, which show the patterns during a tidal cycle for regular WSW and NNW conditions.

To determine the influence of a high discharge event on the overall flow patterns during a tidal cycle, these patterns are presented in Figure C.6 for February 2 1995, which is the day when the highest discharge values occurred. The flow patters at phases 1 and 2 remain more or less the same, which is logical since the fresh water is only discharged during low water. Note that the slight increase in offshore velocities compared to the scenario with tidal and Q_{river} forcing is probably a consequence of the prevailing wind velocities (the daily average wind velocity is $6 m/s$). The patterns during phases 3 and 4 however, are completely altered by the discharge. Flow velocities are much higher than under regular conditions (note the different scale of the arrows) and water flows over the Hinderplaat in offshore direction.

Figure C.7 is presented to support the results on the sediment transport over the Hinderplaat, as shown in Figure 6.15. This snapshot shows the flow patterns at the moment when the largest transport rates over the shoal take place. The flow is clearly in flood direction over the entire ebb-tidal delta.

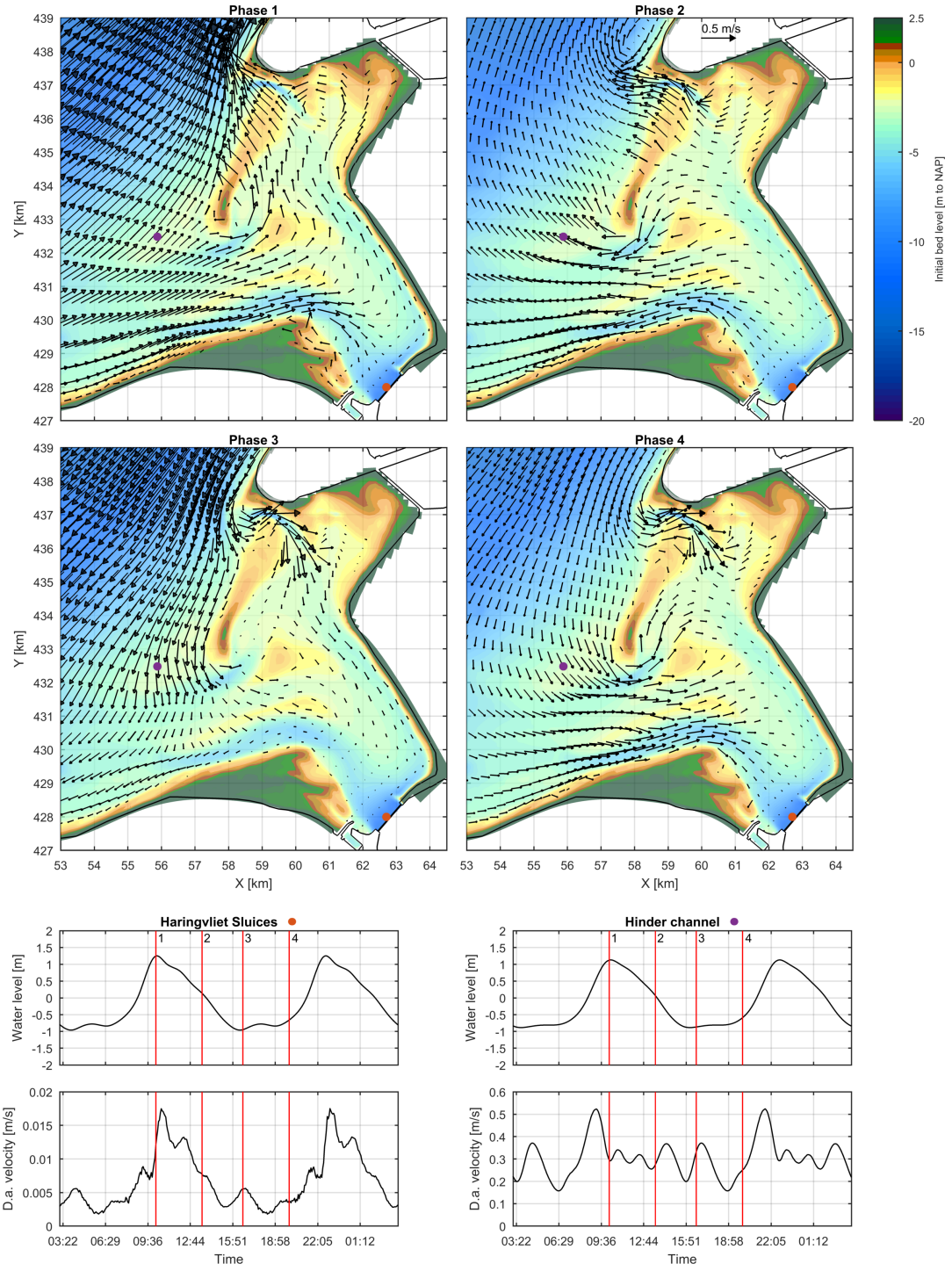

Figure C.1: Flow patters during a tidal cycle for tidal forcing only, simulation A from table 4.1

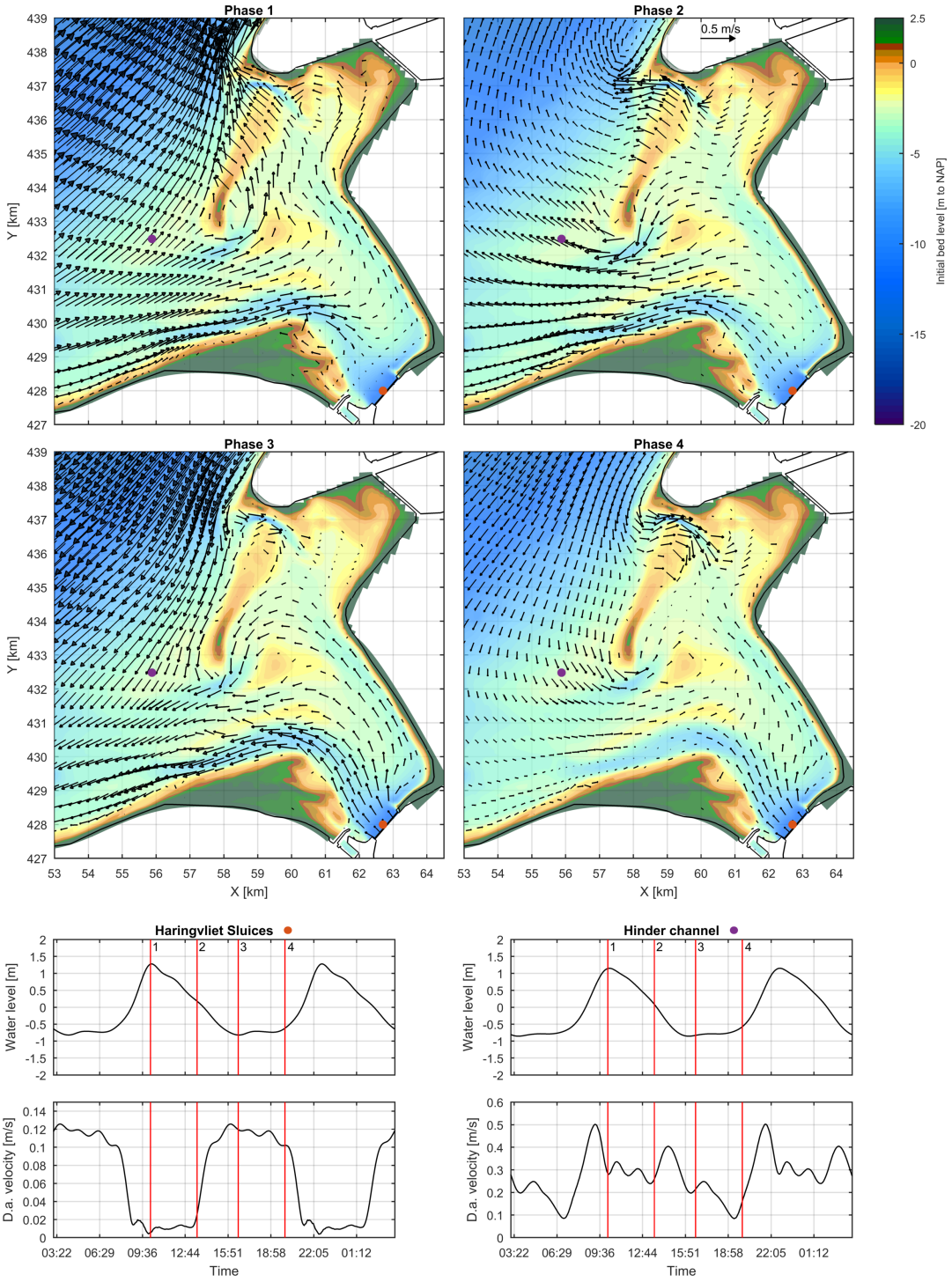

Figure C.2: Flow patters during a tidal cycle for WSW calm conditions, simulation E from table 4.1, wave condition 6 from table 5.4

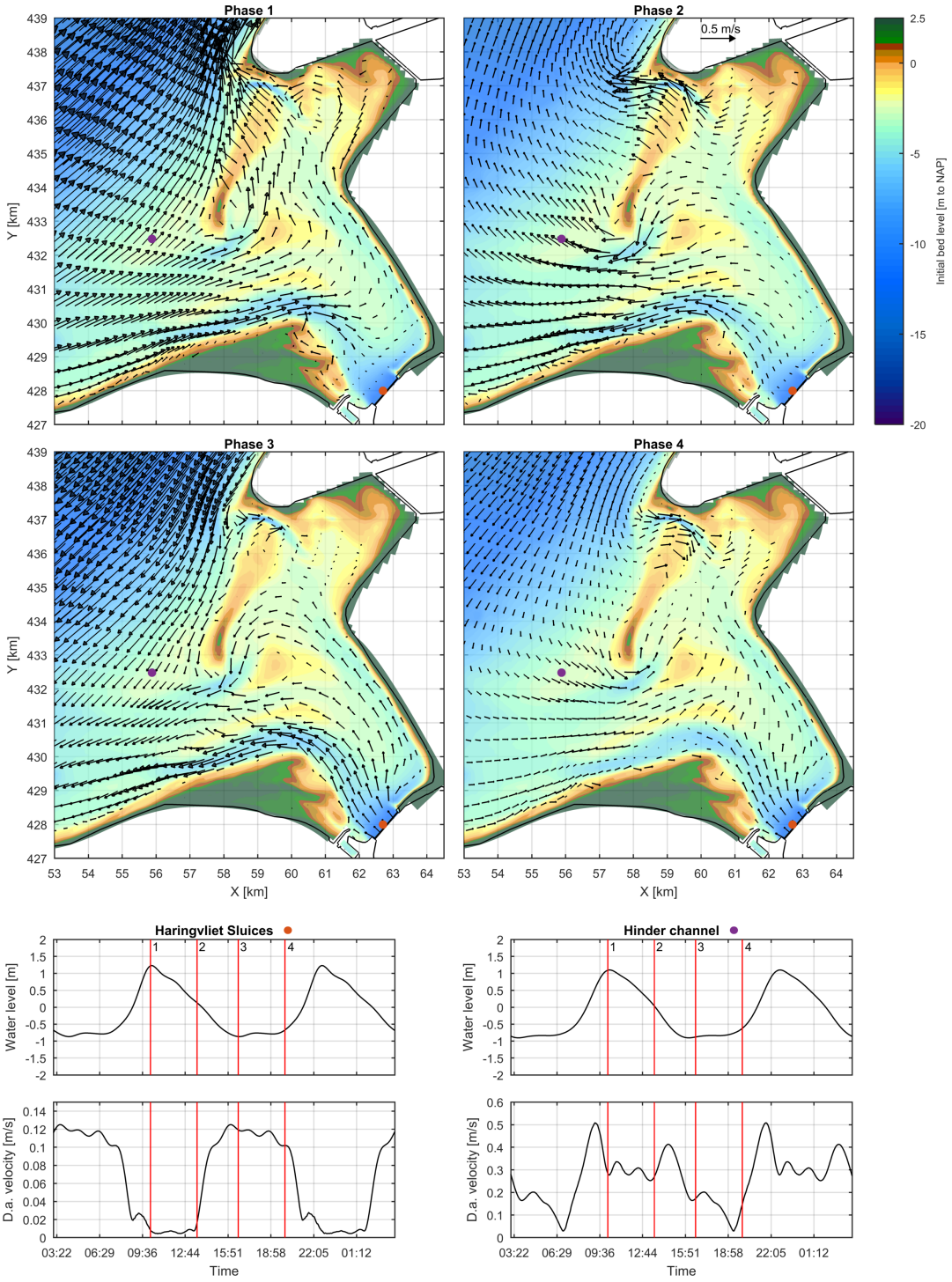

Figure C.3: Flow patters during a tidal cycle for NNW calm conditions, simulation E from table 4.1, wave condition 8 from table 5.4

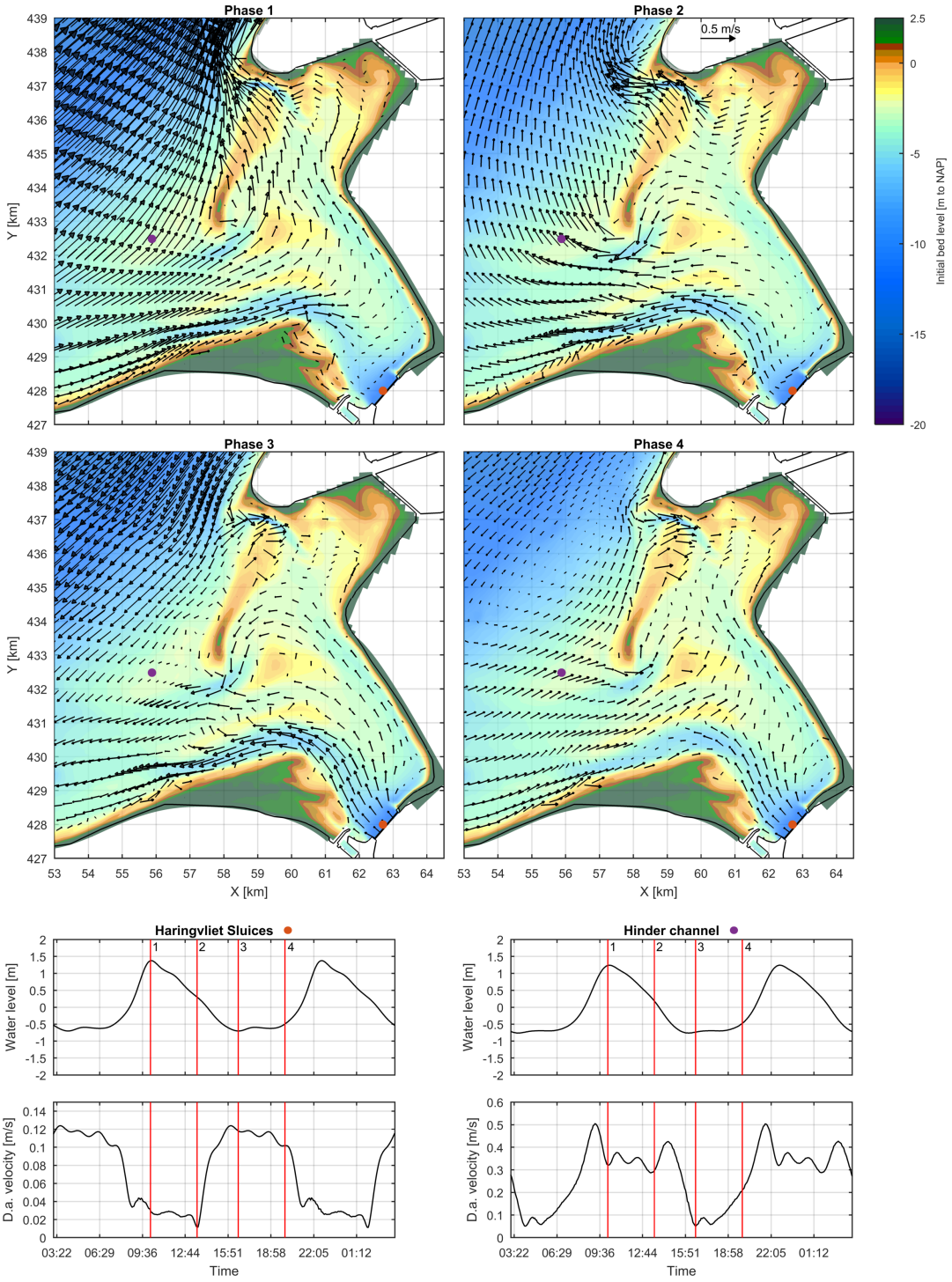

Figure C.4: Flow patters during a tidal cycle for WSW regular conditions, simulation E from table 4.1, wave condition 14 from table 5.4

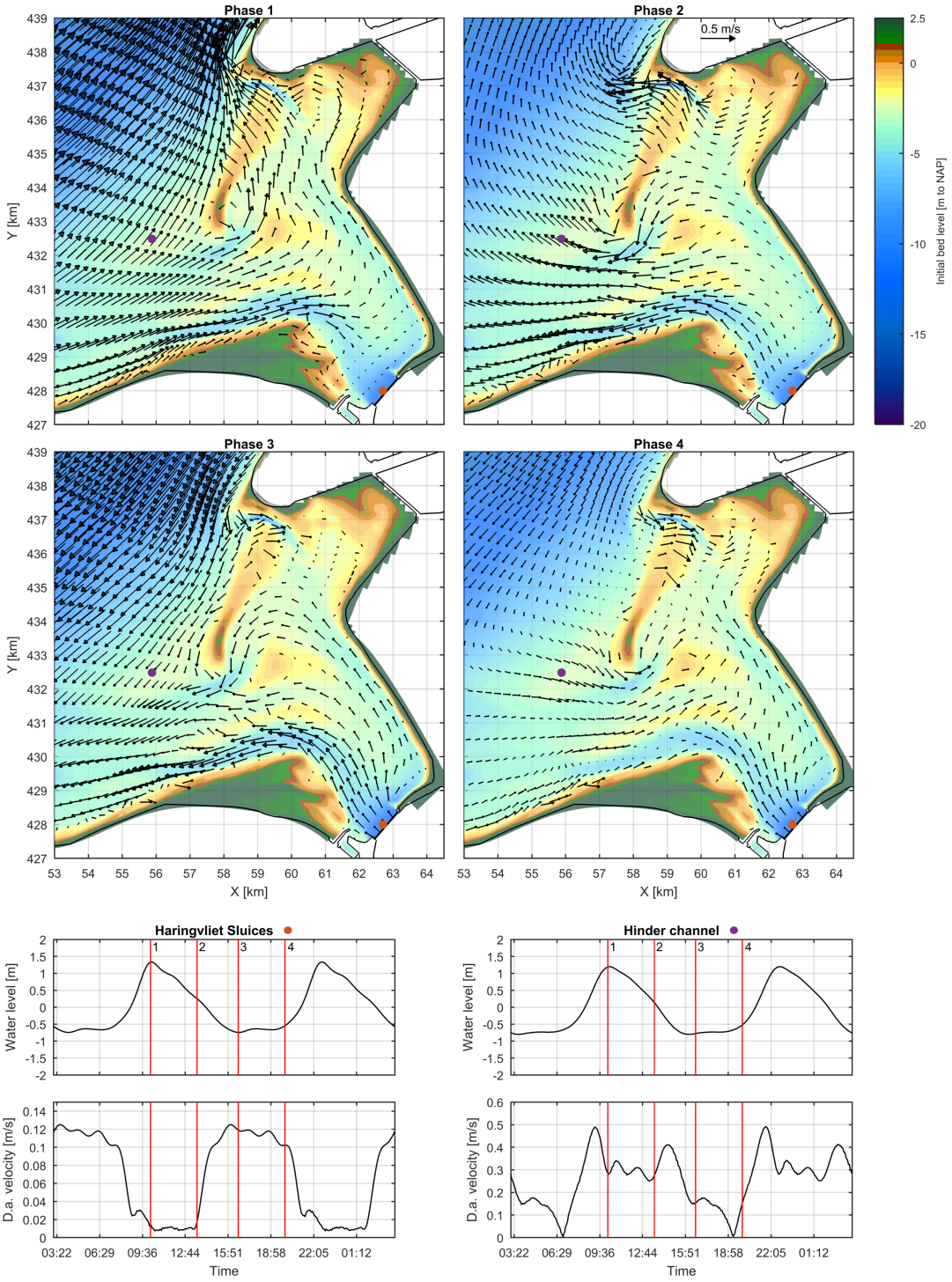

Figure C.5: Flow patters during a tidal cycle for NNW regular conditions, simulation E from table 4.1, wave condition 16 from table 5.4

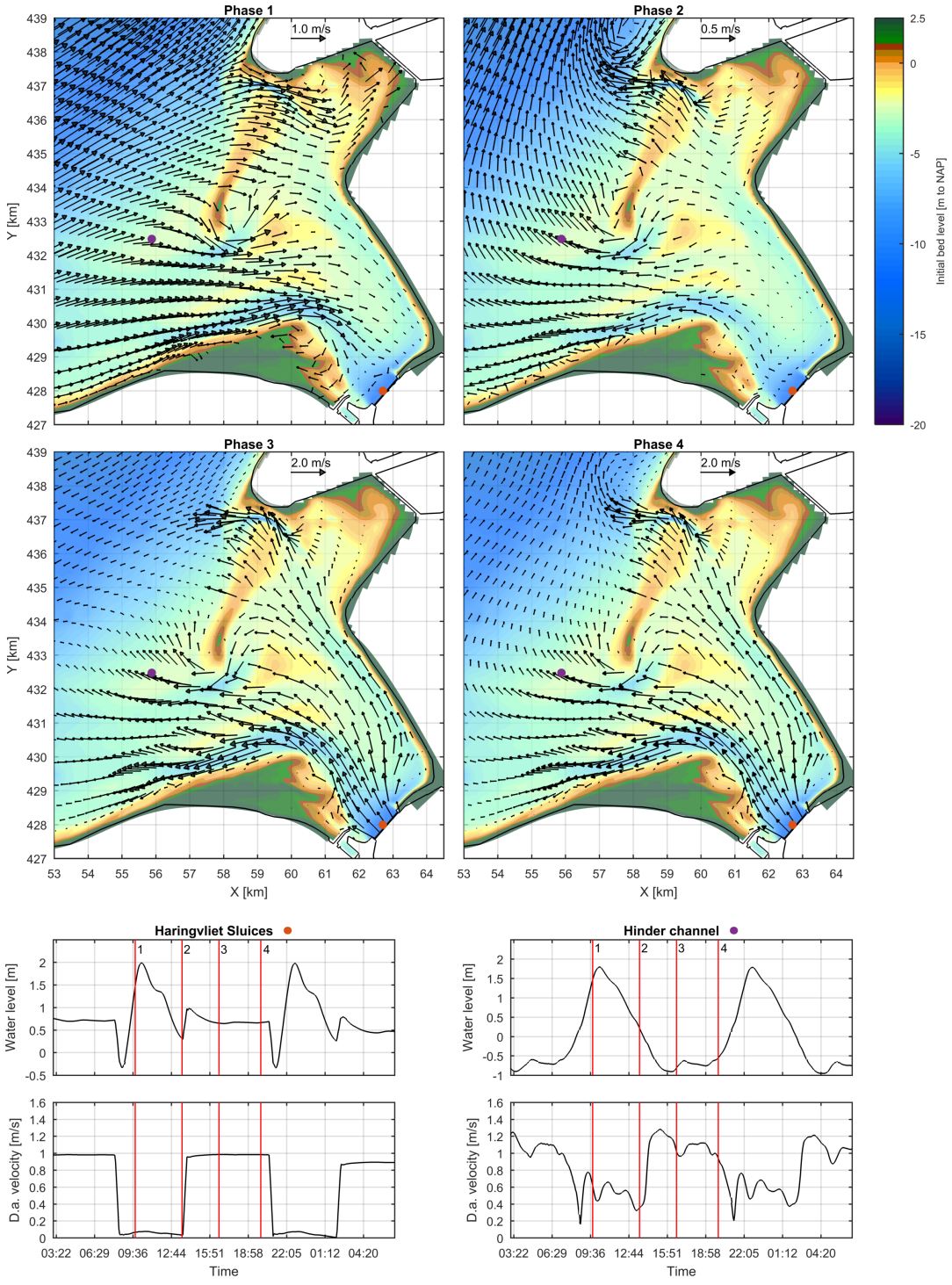

Figure C.6: Flow patters of a tidal cycle during the extreme discharge event of February 3 1995

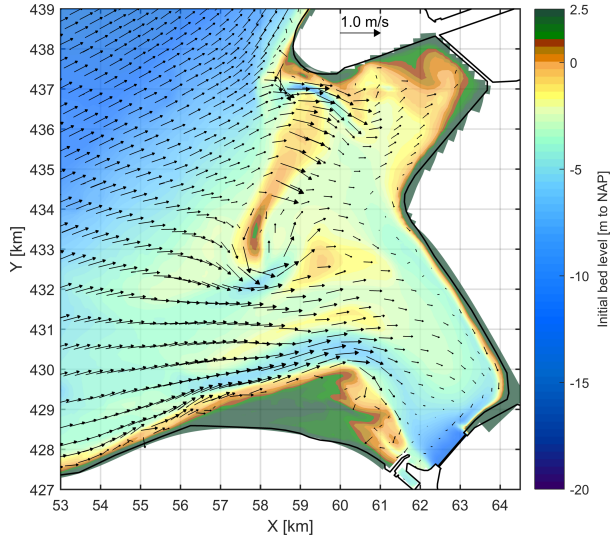

Figure C.7: Flow patters during maximum flood for a medium NW wave and wind condition. The arrows indicate the depth averaged velocities.

C.3. SEDIMENT TRANSPORT

Figure C.8 shows the residual sediment transport patterns for simulations with only tidal forcing and tidal and Q_{river} forcing, respectively. The corresponding initial bed level changes have been presented in Figure 6.13.

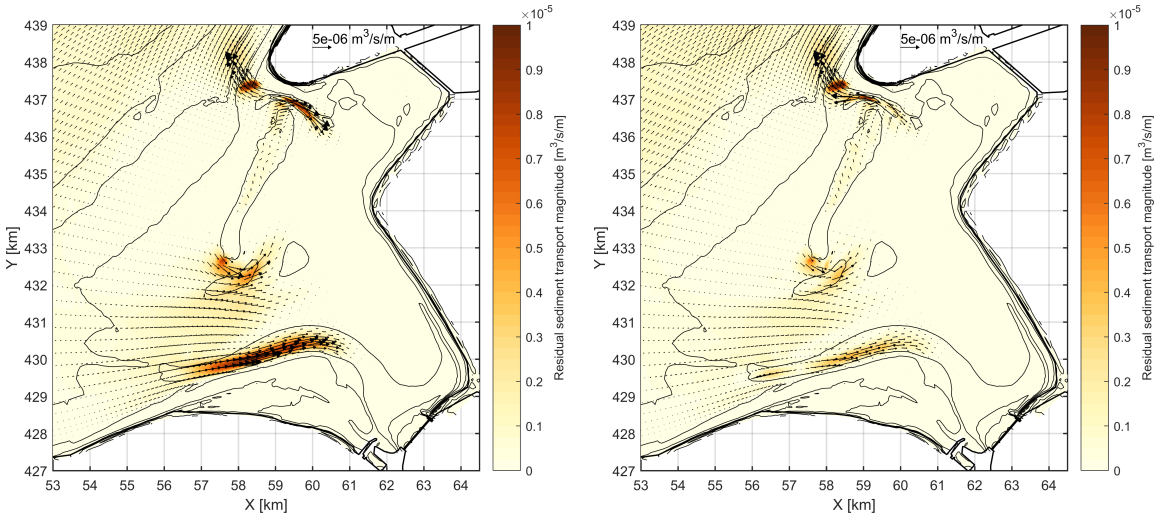

(a) Scenario A: tidal forcing

(b) Scenario B: tidal and Q_{river} forcing

Figure C.8: Residual sediment transport after two tidal cycles

Figures C.9 and C.10 show the mean total transport rates for calm and regular wave conditions. The corresponding bed level changes are presented in Section 6.3.1

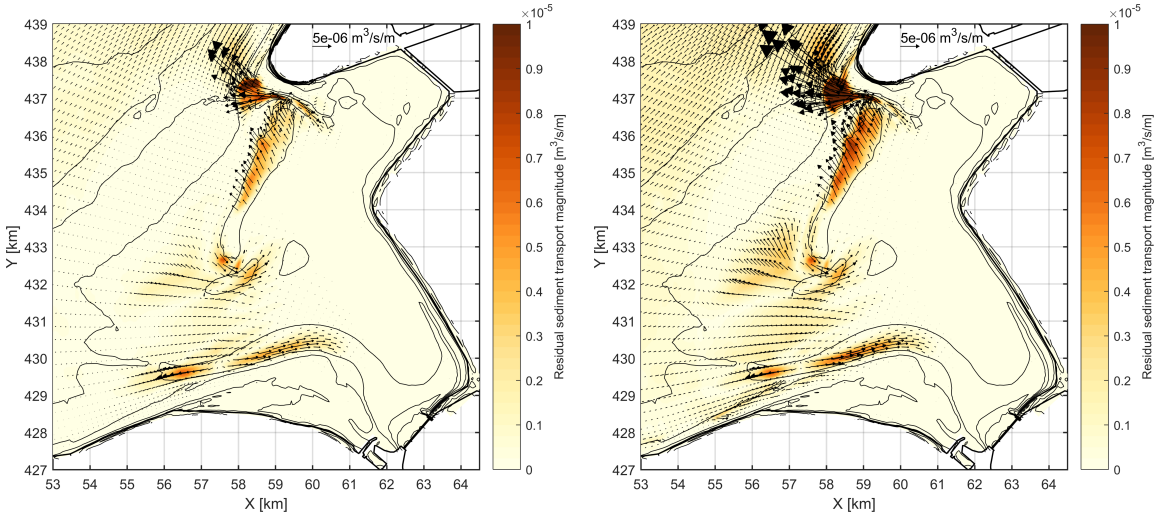

(a) WSW (b) NNW

Figure C.9: Residual sediment transport after two tidal cycles for calm conditions

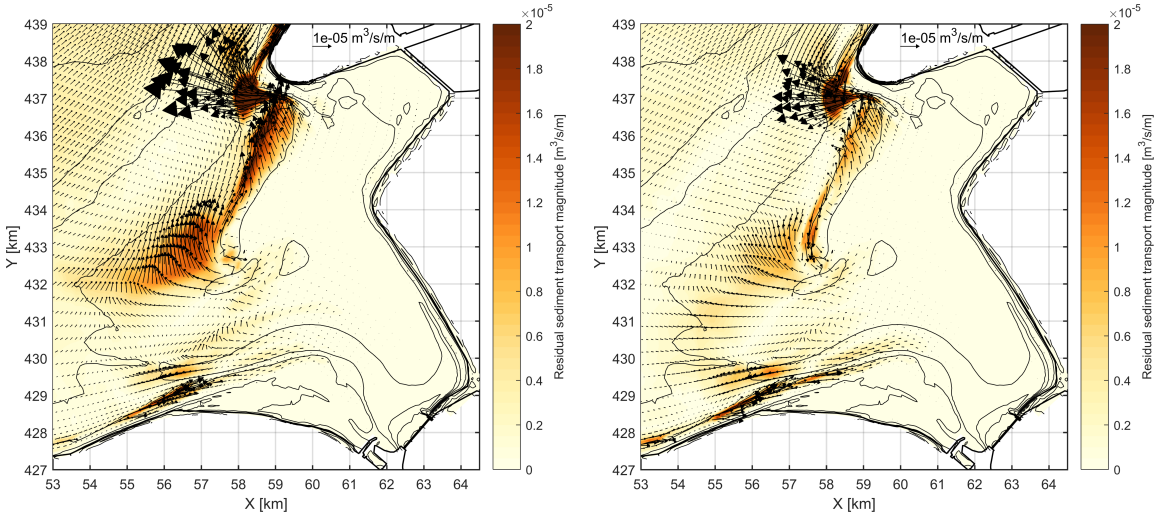

(a) WSW (b) NNW

Figure C.10: Residual sediment transport after two tidal cycles for regular conditions

D

ABSTRACT NCK-DAYS 2018

A part of this research was presented at the NCK-days of 2018, the annual conference of the Netherlands Centre for Coastal Research. The submitted abstract is shown in this appendix.

UNRAVELLING THE MECHANISMS BEHIND THE MORPHODYNAMIC EVOLUTION OF THE HARINGVLIET EBB-TIDAL DELTA

A. Colina Alonso[1,2]*, Z.B. Wang[1,2], B.C. van Prooijen[1], D.J.R. Walstra[1,2], P.K. Tonnon[2], P.L.M. de Vet[1,2]
[1] Delft University of Technology, [2] Deltares, * Ana.ColinaAlonso@deltares.nl

The morphology of ebb-tidal deltas (ETDs) evolves constantly under the influence of natural processes as well as anthropogenic activities. The Haringvliet ETD in the Southwest Netherlands is an extreme example of the latter: closing off the estuary in 1970 triggered a regime shift, completely altering the evolution of the ETD. Initially, the coast-normal sandy shoals evolved towards a narrow coast-parallel intertidal spit (the Hinderplaat). Subsequently, this tidal flat breached around 1995. Since then continuous erosion has been taking place, while ongoing sediment transport from the flat towards the coast has been observed.

Previous research with the aim to understand the morphological development of the Haringvliet ETD, has provided insights into the processes causing the large morphological changes directly after construction of the Haringvliet Barrier. The processes driving the observed ongoing erosion and flattening of the Hinderplaat are however still poorly studied and understood. In this research, we therefore investigate the underlying mechanisms and link these with former anthropogenic interferences and meteorological events.

A combination of data analysis and numerical simulations is applied. In our analysis of the *Vaklodingen* dataset, we separated the development of the subtidal shoreface and the intertidal area of the Hinderplaat. A clear correlation is found, showing that the erosion of the intertidal part of the Hinderplaat started when the shoreface stopped eroding. A 2DH Delft3D model is used to reveal the relative importance of the tidal-, wind-, surge- and wave-forcing driving the flow and sediment transport in the outer delta. Various simulations with a range of different forcings are performed. Tide-only simulations show hardly any transport on the Hinderplaat. Modelling results reveal that waves are essential to mobilize the sediment, yet the effects of waves are significantly enhanced by the wind-driven flow (see Figure 1).

Obtained knowledge on the importance of the hydrodynamic processes is crucial to understand the complex system of the Haringvliet ETD. This is not only necessary to explain the past evolution, but also to enable well thought-out decision making on future maintenance strategies. Moreover, the outcomes of this study on the development of the Hinderplaat are also a valuable benchmark for model concepts that are to be applied on other ETDs in the Netherlands and abroad.

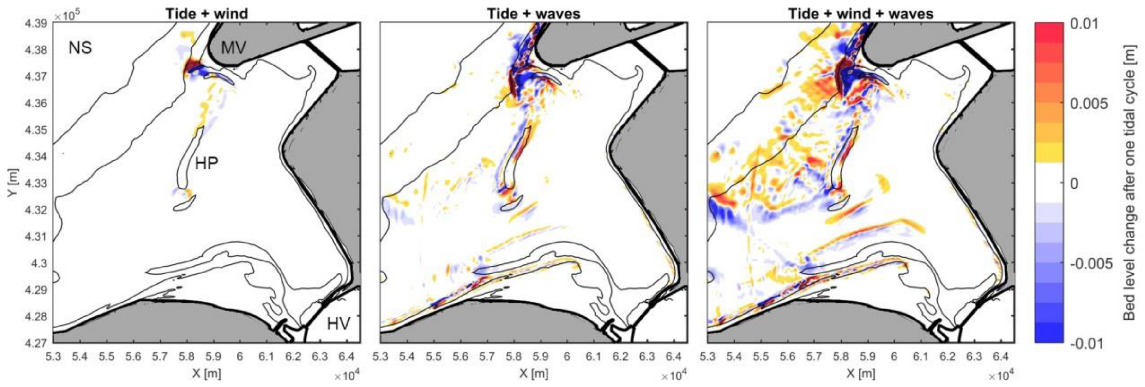

Figure 1: Initial bed level changes after one tidal cycle for 3 simulations, showing sedimentation (red) and erosion (blue) patterns. The left panel also indicates the locations of the North Sea (NS), Maasvlakte (MV), Hinderplaat (HP) and Haringvliet (HV).